TARGETING CD155 ON MYELOID DERIVED SUPPRESSOR CELLS TO PREVENT POSTOPERATIVE IMMUNOSUPPRESSION IN CANCER PATIENTS

André Bernard Martel, MD

Thesis submitted to the University of Ottawa
in partial Fulfillment of the requirements
for the degree of Master of Science in Microbiology and Immunology

Department of Biochemistry, Microbiology and Immunology
Faculty of Medicine
University of Ottawa

ABSTRACT

Surgery, although required to treat most solid cancers, can increase tumour seeding and metastases. We have previously shown that surgery-induced myeloid derived suppressor cells (Sx-MDSCs) play an important role in this process by directly suppressing NK cells. The Sx-MDSCs increase significantly immediately after surgery but the exact mechanism by which Sx-MDSCs suppress NK cells is still unknown. In this work, we have discovered that CD155 poliovirus receptor is significantly and specifically upregulated on Sx-MDSCs following surgical stress but is minimally expressed on other immune cells. We also demonstrate that blocking CD155 *in vivo* leads to an improved NK cell phenotype, measured by DNAM-1 and NKG2D, and increased NK cytotoxicity. Additionally, *ex vivo* CD155 blockade significantly decreases the suppressive effect of Sx-MDSCs in cancer patients. Expansion of CD155 on Sx-MDSCs could be responsible for the profound postoperative NK cell suppression, which makes it a very appealing perioperative target for immunotherapy.

ACKNOWLEDGEMENTS

As a surgical resident, deciding to hold residency training to pursue a Master's degree for two years is not a decision taken lightly, but I am very glad to have done so. The past two years have been some of the most challenging, yet motivating and fulfilling of my life. I am extremely grateful for the help and support of the following individuals. Without their help, I would not have been able to bring this project to completion.

First, I would like to thank my supervisor Dr. Rebecca Auer for her constant support and guidance during my years in the lab. Thank you for inspiring me to pursue this important work as a clinician-investigator and instilling in me a passion to ask the important questions, advance perioperative research and improve outcomes in cancer patients. I am also very appreciative of the tremendous support from senior research associate Dr. Michael Kennedy, who was instrumental in guiding me through my project, troubleshooting the several issues I initially faced and helping me stay motivated through it all.

I would also like to thank two special individuals who played major roles in the completion of my project. Christiano Tanese de Souza, thank you for your tremendous help planning and completing the animal experiments, for teaching me the humbling experience of operating on mice, and for your constantly positive attitude inside and out of work. Juliana Ng, I cannot thank you enough for your enormous help coordinating the recruitment and consenting of cancer patients, which often meant working at odd hours in the early morning or late at night.

To my lab mates Leonard Angka, Marisa Market, Oladunni Olanubi, Sarwat Khan, Gayashan Tennakoon, Dominique Boucher, and Marlena Scaffidi, thank you for your expertise and patience to teach me all the required skills to succeed in the lab. You are all exceptionally intelligent individuals and I am fortunate to have worked with you for two years. I would like

to also thank my Thesis Advisory Committee (TAC) members, Dr. Subash Sad and Dr. Michele Ardolino, for their guidance and expert opinion. You played important roles in shaping my project into the successful story it has become. I would like to acknowledge funding sources for this project, including the Division of General Surgery, the Clinician-Investigator Program (CIP), and Canadian Institutes of Health Research (CIHR).

To my general surgery residency program, thank you for believing in my project and allowing me to pursue the Surgeon-Scientist Program (SSP). I would like to particularly thank my program director Dr. Lara Williams for her constant guidance throughout my Master's. You somehow ensured a perfect balance between research productivity and clinical exposure to maintain my surgical skills. Also, I would like to acknowledge the guidance of my CIP program director Dr. Paul MacPherson, who ensured my research respected the milestones and advocated to have my time in the lab protected. Thank you to resident research leads Dr. Angel Arnaout and Dr. Reily Musselman for accepting me into the SSP and monitoring my progress.

Last but not least, I would like to thank very special individuals in my personal life. Brigitte, thank you for your constant love and support as I decided to pursue a Master's in the middle of my residency. It is clear that I would not have been able to undertake this project without you. My brother Eric, thank you for being my best friend all these years. To my parents Darlene and Alain, thank you for everything. I will be forever grateful for your dedication and sacrifices to ensure I reached my dreams. Without you, I would not have completed this Master's nor would I have become a caring, compassionate physician.

In these pages explaining my research thesis, while the words are my own, I hope you realize the work is from the combination of all these outstanding individuals.

TABLE OF CONTENTS

Abstract ……. ii

Acknowledgements …… iii

List of Abbreviations …… viii

List of Figures and Illustrations …….. xi

1. Introduction ……... 1

1.1. The Role of Natural Killer Cells in Cancer ……... 1

1.1.1. Natural Killer (NK) cell activity against tumours ……... 1

1.1.2. Tumour-induced dysfunction of NK cells ……... 4

1.2. Surgical Stress and NK cell Suppression …….. 6

1.2.1. Surgical stress …….. 6

1.2.2. Postoperative NK cell suppression …….. 12

1.3. Myeloid Derived Suppressor Cells ……. 14

1.3.1. Characterization of Myeloid Derived Suppressor Cells …….. 14

1.3.2. MDSCs in cancer and infection …….. 16

1.3.3. Surgery-induced MDSCs ……..……. 18

1.3.4. Sx-MDSC surface proteomic screen ……... 20

1.4. CD155 Poliovirus Receptor …… 23

1.4.1. CD155 poliovirus receptor and its ligands …….. 23

1.4.2. Cancer CD155 expression ……..…… 25

1.4.3. CD155 expression on myeloid cells …… 28

2. Rationale and Hypothesis …..……... 32

2.1. Rationale ……...……... 32

2.2. Hypothesis ……...……. 32

2.3. Research aims ……...……... 33

3. Methodology …...……... 33

3.1. Cell Lines …….. 33

3.2. Animals ……. 34

3.3. Cancer Surgery Patients ……. 34

3.4. Murine Model of Surgical Stress ……... 35

3.5. Immune Cell Phenotyping 39
3.5.1. Human samples 39
3.5.2. Murine samples 39
3.6. *Ex Vivo* Murine NK Cytotoxicity Assay 40
3.7. *In vivo* CD155 Blockade 41
3.8. *Ex Vivo* Human Suppression Assay 44
3.8.1. Cell preparation 44
3.8.2. *Ex vivo* CD155 blockade and plating 44
3.9. Statistical Analysis and Software 48
4. Results 49
4.1. Perioperative profiling of CD155 in cancer surgery patients 49
4.1.1. Clinical demographics of human cancer patients 49
4.1.2. Flow cytometry validation of perioperative human CD155 on Sx-MDSCs ... 51
4.1.3. Subgroup analyses of Sx-MDSC CD155 in cancer patients 54
4.2. MDSCs and granulocytes both expand postoperatively 58
4.3. Flow cytometry validation of cell populations in our murine model of surgical stress 61
4.3.1. Confirming CD155 expression in murine melanoma cell lines 61
4.3.2. Phenotyping of immune cell populations 64
4.4. Postoperative CD155 upregulation is specific to Sx-MDSCs in our murine model of surgical stress 67
4.5. Perioperative characterization of murine activating NK cell receptors 70
4.6. Targeting CD155 *in vivo* is sufficient to restore NK cell function and reduce metastases in our murine model of surgical stress 73
4.6.1. Titrating anti-CD155 blocking antibody *in vivo* 73
4.6.2. *In vivo* CD155 blockade improves NK cell phenotype and cytotoxicity 76
4.6.3. *In vivo* CD155 blockade decreases postoperative lung metastases 82
4.7. *Ex vivo* blockade of human CD155 improves NK cell cytotoxicity 85
4.7.1. Optimization of a novel human suppression assay 85
4.7.2. Clinical demographics for *ex vivo* CD155 blockade 91

4.7.3. *Ex vivo* CD155 blockade decreases Sx-MDSC suppression 93
5. Discussion 96
5.1. Surgical Stress 96
5.1.1. Surgical stress and NK cell suppression 96
5.1.2. Expansion of granulocytes and monocytes after surgery 96
5.1.3. Flow cytometry validation of postoperative immune populations 98
5.2. Perioperative Profiling of CD155 99
5.2.1. CD155 in human cancer patients 99
5.2.2. CD155 in the murine model of surgical stress 101
5.3. Perioperative Changes in Activating NK Cell Receptors 103
5.4. CD155 Blockade to Improve Postoperative NK Cell Function 104
5.4.1. *In vivo* blockade in the animal model of surgical stress 104
5.4.2. A novel *ex vivo* CD155 suppression assay 106
5.5. The Translational Potential of CD155 Blockade 108
5.6. Conclusion 109
6. References 111
7. Contributions of collaborators 127
8. Appendix 128
Appendix A: Antibody Table 128
Appendix B: Human CD155 Antibody Selection 130
Appendix C: Detailed Flow Cytometry Gating of Human Sx-MDSC 131
Appendix D: Non-cancer Sx-MDSC CD155 132
Appendix E: Flow Cytometry Gating for Human *Ex Vivo* Suppression Assay ... 133
9. Curriculum Vitae 134

LIST OF ABBREVIATIONS

α-CD155	–	Purified anti-CD155 antibody
ACK	–	Ammonia Chloride Potassium
ACVS	–	Animal Care and Veterinary Services
ADCC	–	Antibody-Dependent Cellular Cytotoxicity
Arg-1	–	Arginase-1
ATCC	–	American Type Culture Collection
B16F10	–	Melanoma line, wild-type
BL	–	Baseline
BM	–	Bone Marrow
BSA	–	Bovine Serum Albumin
BV	–	Brilliant Violet
CD	–	Cluster of Differentiation
CD96	–	Cluster of Differentiation 96, also known as Tactile
CD155	–	Poliovirus receptor
CP450	–	Cell Proliferation Dye 450
CO_2	–	Carbon Dioxide
DAMP	–	Damage-associated molecular pattern
DC	–	Dendritic Cell
DFS	–	Disease-Free Survival
DMEM	–	Dulbecco's Modified Eagle's Media
DNAM-1	–	DNAX Accessory Molecule-1, also known as CD226
DTH	–	Delayed-Type Hypersensitivity
EDTA	–	Ethylenediaminetetraacetic Acid
EGF	–	Epidermal Growth Factor
E:T	–	Effector-to-Target Ratio
EthD-1	–	Ethidium Homodimer-1, also known as Propidium Iodide (PI)
FBS	–	Fetal Bovine Serum
FSC	–	Forward Scatter
GI	–	Gastrointestinal
GM-CSF	–	Granulocyte-Monocyte Colony Stimulating Factor
GR1	–	Granulocytic Marker 1
GU	–	Genitourinary
G-MDSC	–	Granulocytic-MDSC
HC	–	Hemocytometer
HCV	–	Hepatitis C Virus
HD	–	Healthy Donor; High Density
IHC	–	Immunohistochemistry
IL	–	Interleukin
IFN-γ	–	Interferon-Gamma

IMC	–	Immature Myeloid Cell
iNOS	–	Inducible Nitric Oxide Synthase
IP	–	Intraperitoneal
ITAM	–	Immunoreceptor Tyrosine-Based Activating Motif
ITIM	–	Immunoreceptor Tyrosine-Based Inhibitory Motif
IV	–	Intravenous
K562	–	Human Leukemia target cell
KIR	–	Killer Cell Immunoglobulin-Like Receptor
KLRG1	–	Killer Cell Lectin-Like Receptor 1
KO	–	Knock out
LD	–	Low-Density
LILR	–	Leukocyte Immunoglobulin-Like Receptor
Lin	–	Lineage Markers
Ly6C	–	Lymphocyte Antigen 6 Complex, Locus C1
Ly6G	–	Lymphocyte Antigen 6 Complex, Locus G6D
MDSC	–	Myeloid Derived Suppressor Cell
MFI	–	Mean Fluorescence Intensity
MHC	–	Major Histocompatibility Complex
MIC	–	MHC-Class I-chain related antigens (MIC-A, MIC-B)
MIS	–	Minimally Invasive Surgery
M-MDSC	–	Monocytic-MDSC
MMP9	–	Matrix Metallopeptidase-9
MPC	–	Myeloid Progenitor Cell
MRD	–	Minimal Residual Disease
NCR	–	Natural Cytotoxicity Receptor
Necl	–	Nectin-Like
NFκB	–	Nuclear Factor κ-B
NK	–	Natural Killer Cell
NKA	–	NK Activity
NKC	–	NK Cytotoxicity
NK92	–	Natural Killer-92 Cell Line
NKG2D	–	Natural Killer Group 2 D Receptor
NO	–	Nitric Oxide
OS	–	Overall Survival
PBMC	–	Peripheral Blood Mononuclear Cell
PBS	–	Phosphate-Buffered Saline
PDGF	–	Platelet-Derived Growth Factor
Pen-Strep	–	Penicillin-Streptomycin
PGE2	–	Prostaglandin E2
PFA	–	Paraformaldehyde Fixation
PHBSP	–	Perioperative Human Blood and Tissue Collection Program

POD	–	Postoperative Day
PVR	–	Poliovirus Receptor
RAE-1ε	–	Retinoic Acid Early Inducible 1 ε
RCT	–	Randomized Controlled Trial
RPMI	–	Roswell Park Memorial Institute Media
RN	–	Registered Nurse
ROS	–	Reactive Oxygen Species
sCD155	–	Soluble CD155
sgRNA	–	Single Guide RNA
siRNA	–	Small Interfering RNA
SD	–	Standard Deviation
SDCU	–	Surgical Day Care Unit
SSC	–	Side Scatter
Sx	–	Surgery
Sx-MDSC	–	Surgery-Induced Myeloid Derived Suppressor Cell
TGF-β	–	Transforming Growth Factor-Beta
TIGIT	–	T Cell Immunoreceptor with Ig and ITIM Domains
TIL	–	Tumour-Infiltrating Lymphocyte
TIMC	–	Tumour-Infiltrating Myeloid Cell
TME	–	Tumour Microenvironment
TNF-α	–	Tumour Necrosis Factor-Alpha
U	–	Unit
ULBP	–	UL16-Binding Proteins (ULBP1, ULBP2, ULBP3, ULBP4)
VEGF	–	Vascular Endothelial Growth Factor
WBGE	–	Whole Blood Gene Expression
WT	–	Wild-Type
YAC-1	–	Murine Leukemia target cell

LIST OF FIGURES AND TABLES

Figure 1. The Ebb and Flow phases of surgical stress ……... 11
Table 1. Surgery-induced MDSC (Sx-MDSC) Surface Proteomic Screen …… 22
Figure 2. Tipping the balance: Proposed Mechanism of Surgery-Induced MDSC (Sx-MDSC) CD155 Suppression Following Surgical Stress ……. 31
Figure 3. Animal Model of Surgical Stress to Examine Perioperative CD155 Expression ……... 37
Figure 4. Modified Animal Model of Surgical Stress with *In Vivo* CD155 Blockade ... 43
Figure 5. Representative Diagram of a Novel Human CD155 Suppression Assay ….... 47
Table 2. Clinical Demographics of CD155 Profiling in Cancer Patients ……... 50
Figure 6. Flow Phenotyping of Surgery-Induced MDSC (Sx-MDSC) CD155 in Human Cancer Patients ……... 53
Figure 7. Perioperative Sx-MDSC CD155 Profiling in Human Cancer Patients ……... 57
Figure 8. Surgery-Induced Myeloid-Derived Suppressor Cells (Sx-MDSCs) and Granulocytes Expand Following Surgical Stress …… 60
Figure 9. Validation of CD155 Expression in Murine B16F10 Melanoma Cells …….. 63
Figure 10. Flow Cytometry Gating of Postoperative Murine Immune Cell Populations 66
Figure 11. Postoperative CD155 is Specific to Sx-MDSCs ……... 69
Figure 12. Activating NK Cell Receptor Changes Following Surgical Stress ……... 72
Figure 13. *In Vivo* Titration of α-CD155 in our Animal Model of Surgical Stress ….... 75
Figure 14. *In vivo* CD155 Blockade Improves the Postoperative NK Cell Phenotype 78
Figure 15. NK Cytotoxicity Following *In Vivo* CD155 Blockade ……..... 81
Figure 16. *In Vivo* CD155 Blockade Leads to Reduced B16F10 Lung Metastases ….. 84
Figure 17. Optimization of a Novel *Ex Vivo* CD155 Human Suppression Assay …..... 87
Figure 18. Anti-CD155 Blocking Antibody is Stably Bound to Surface CD155 on Human Sx-MDSCs ……..... 90
Table 3. Clinical demographics of cancer patients for *ex vivo* CD155 Suppression Assay ……... 92
Figure 19. *Ex vivo* CD155 Blockade Decreases the Suppressive Effect of Sx-MDSC .. 95

1. INTRODUCTION

1.1. The Role of Natural Killer Cells in Cancer

1.1.1. Natural Killer (NK) cell activity against tumours

First discovered in 1975 by Kiessling *et al.* (1), Natural Killer (NK) cells are lymphocytes of the innate immune system that play a key role in the first-line of immune response to pathogens and tumours (1–6). They are derived from the bone marrow and circulate in the blood, comprising between 5 to 15% of peripheral blood lymphocytes (3, 5, 7). The NK cell phenotype is characterized by the absence of T cell receptor CD3 and presence of lineage marker CD56 (8, 9). There are two main functional categories of NK cells, depending on their relative expression of CD56 and CD16, either $CD56^{bright}CD16^{-}$ or $CD56^{dim}CD16^{+}$ (8, 10, 11). More than 90 percent of human NK cells are $CD56^{dim}CD16^{+}$ and these are responsible for the majority of cytotoxicity against target cells in the resting state (8, 12–14). However, the $CD56^{bright}CD16^{-}$ NK cells produce significantly greater amounts of cytokines when stimulated, including interferon-γ (IFN-γ), Tumor Necrosis Factor-α (TNF-α), Granulocyte-Macrophage Colony Stimulating Factor (GM-CSF), interleukin-10 (IL-10) and IL-13 (8, 14, 15).

As part of the innate immune response, NK cells can be rapidly stimulated by circulating cytokines such as IL-2 and IFN-γ without requiring prior sensitization to target cells (3, 16). Major histocompatibility complex (MHC) class-I is constitutively expressed on all healthy cells, but frequently impaired or absent in virally-infected cells or tumours (7, 17). As initially described in the "missing-self hypothesis" of the innate NK cell response, loss of MHC class-I on infected or transformed cells leads to NK cell activation, which results in direct cell lysis via perforin and granzymes, and release of inflammatory cytokines including IFN-γ and TNF-

α (7, 18). NK cells also play an important role in the adaptive response to anti-tumour immunity (19–21). Once thought to be a feature unique to T cells and B cells, it is now known that activated NK cells can have improved long-term effector functions and enhanced responses to re-stimulation (20). O'Leary *et al.* discovered that severe combined immunodeficiency (SCID) mice deficient in lymphocytes (T cells, B cells, and NK cells) were unable to mount a hapten-induced delayed type hypersensitivity (DTH) response (21). However, adoptive transfer of only NK cells from sensitized donor mice resulted in normal DTH, confirming the ability of NK cells to mount an adaptive immune response (21).

NK cell activity was initially thought to be simply from recognizing MHC-absent cells as "non-self", triggering cytotoxic activity (4, 7, 22). However, their effect on target cells is more delicate and depends on specialized and complex signaling pathways from a combination of activating and inhibitory receptors, cytokines, chemokines and adhesion molecules (2–4). Key human inhibitory receptors, such as killer cell immunoglobulin-like receptors (KIRs), Natural Killer Group 2 A (NKG2A, or CD159), killer cell lectin-like receptor 1 (KLRG1) and leukocyte immunoglobulin-like receptor (LILR), have an immunoreceptor tyrosine-based inhibitory motif (ITIM) in the cytoplasmic domain and they recognize various MHC class-I ligands (3, 5, 15). Activating NK cell receptors, on the other hand, contain the immunoreceptor tyrosine-based activating motif (ITAM) and, once bound, trigger increased cytotoxic activity marked by downstream degranulation and cytokine production (5). Notable human activating receptors include DNAX Accessory Molecule-1 (DNAM-1), NKG2D, CD16, the natural cytotoxicity receptor (NCR) family (NKp30, NKp44, NKp46, NKp80) and select KIRs. Most of these trigger the Src homology 2 domain-containing kinases (ZAP70 or Syk) signalling pathways, but NKG2D utilizes phosphatidylinositol 3-kinase (PI3K) (3, 5, 15). Murine NK cell receptors have some degree of overlap with humans. Inhibitory murine receptors include

Ly49A, Ly49C, KLRG1, LILR, and NKG2A, while activating receptors are Ly49D, Ly49H, CD16, CD244, NCRs, NKG2D and DNAM-1 (3, 5).

DNAM-1, also known as CD226, is an activating receptor expressed on most NK cells and has the ability to bind two known ligands, CD155 and CD112 (5, 23–25). The DNAM-1-CD155 relationship will be discussed in detail further (section 1.4) but in brief, the two DNAM-1 ligands CD155 and CD112 can be overexpressed on several tumours, highlighting a key anti-tumour role for this NK cell receptor. In fact, binding of DNAM-1 with its ligand triggers direct NK cell cytotoxicity and increased IFN-γ production (26–28).

NKG2D is also an activating receptor found on NK cells and T cells that plays an integral role in tumour immune surveillance (5, 29, 30). There are various known stress-induced NKG2D ligands that have some homology to MHC class-I ligands, including the MHC-class I-chain (MIC) related A and B antigens (MIC-A, MIC-B) and UL16-binding proteins (ULBP1, ULBP2, ULBP3, ULBP4) in humans, and retinoic acid early inducible 1 (RAE-1) in mice. These ligands are all expressed at low levels under normal conditions but are significantly upregulated in times of stress (3, 25, 29, 30). Additionally, they are overexpressed in several tumours including breast, lung, kidney, prostate and colon cancers (17, 30). Key *in vitro* studies have confirmed the anti-tumour role of NKG2D by transfecting NKG2D ligands into various target tumour cells. NK cells exhibited enhance5muld cytotoxicity against MICA-transfected Daudi lymphoma cells but blockade of either MICA (clone 2C10) or NKG2D (clone 1D11) significantly decreased NK-mediated killing by twofold and tenfold, respectively (17).

Importantly, some tumours can overexpress either DNAM-1 or NKG2D ligands, but not both, and presence of either DNAM-1 or NKG2D on NK cells is needed for NK-mediated cytotoxicity of tumour cells (31, 32). El-Sherbiny *et al.* studied these two receptors on NK cells of multiple myeloma patients. By performing cytotoxicity assays of isolated NK cells

cultured with multiple myeloma cell lines, they noted that blocking DNAM-1 or NKG2D with a monoclonal antibody led to impaired cytotoxicity only if the tumour overexpressed the associated ligands (31). Similarly, Gilfillan *et al.* developed DNAM-1$^{-/-}$ mice and saw that *ex vivo* NK cytotoxicity was relatively preserved in DNAM-1$^{-/-}$ mice if tumours overexpressed NKG2D ligands, such as YAC-1 cells, but killing was significantly impaired by more than tenfold if tumours lacked NKG2D ligands, like B16F10 cells. Interestingly, NK cells from wild type (WT) mice with normal DNAM-1 expression did not have an impaired killing ability, regardless of ligand expression on target cells, suggesting the presence of only one receptor, NKG2D or DNAM-1, is sufficient to preserve NK-mediated killing of tumours (32). Given the fact that NK cells require NKG2D and DNAM-1 to maintain effective anti-tumour immune surveillance, it is no surprise that tumours have developed several escape mechanisms, including inhibition of these activating NK cell receptors.

1.1.2. Tumour-induced dysfunction of NK cells

NK cells play a central role in tumour surveillance, but several cancers have developed mechanisms to subvert the NK immune response either by directly suppressing NK cells or avoiding their detection (25, 33–35). This concept of immune escape is critical for tumour survival and can be accomplished through various pathways, including modifying tumour antigens, increasing inhibitory molecules such as programmed death-ligand 1 (PD-L1) or cytotoxic T-lymphocyte-associated protein 4 (CTLA-4), and/or inducing a suppressive tumour microenvironment (TME) with regulatory T cells (Tregs) and, as discussed in more detail in 1.3, Myeloid Derived Suppressor Cells (MDSCs) (25, 33, 34).

At a certain point during cancer progression, the rate of tumour growth surpasses vascularization, transitioning the TME to a hypoxic state (36–38). Hypoxia in the TME seems

to be the main trigger that induces immunosuppressive changes, first by releasing reactive oxygen species (ROS), anti-inflammatory cytokines such as transforming growth factor-β (TGF-β) and growth factors including vascular endothelial growth factor (VEGF) (39, 40). Hypoxic changes in the TME can also cause downregulation of activating NK cell receptors including some NCRs (NKp30, NKp44, NKp46) and NKG2D, leading to impaired cytotoxicity (35, 40, 41). Balsamo *et al.* studied the NK cell phenotype under hypoxic conditions. After culturing healthy isolated NK cells in a hypoxic anaerobic incubator, they noted a significant downregulation of NKp30, NKp44, NKp46, and NKG2D, as well as impaired NK function measured by CD107a degranulation and chromium 51 (^{51}Cr)-release cytotoxicity when co-cultured with melanoma target cells (41). Interestingly, the hypoxic stress can cause some tumours to shed surface NKG2D ligands, which appears to downregulate and antagonize NKG2D receptors on NK cells and T cells (30, 40, 42).

Furthermore, certain tumours are able to escape the immune response by downregulating the NKG2D and DNAM-1 pathways specifically (25). Studies have shown that NKG2D and DNAM-1 both play important anti-tumour roles *in vivo* (29, 43) and targeting these two activating receptors may be a promising approach to cancer immunotherapy (25). In fact, murine models lacking either NKG2D or DNAM-1 had significantly higher tumour growth and metastases compared to WT mice (29, 43). DNAM-1$^{-/-}$ mice receiving subcutaneous (SC) MethA fibrosarcoma injections had much larger tumours and decreased overall survival (OS) compared to WT mice (10% vs 80% at 50 days) (43). Additionally, *ex vivo* NK cytotoxicity from DNAM-1$^{-/-}$ mice was markedly impaired against various murine lymphoma target cells (43). In another study, NKG2D deficient transgenic adenocarcinoma of mouse prostate (TRAMP) murine model (Klrk1$^{-/-}$ TRAMP), Guerra *et al.* showed that lack of NKG2D function caused a significant increase in tumour growth and earlier onset of disease (29).

Another key mechanism of NKG2D downregulation is through tumour production of suppressive cytokines, most notably TGF-β (44, 45). Lee *et al.* cultured fresh healthy NK cells with plasma isolated from cancer patients and noted, similar to unpublished results from our laboratory, a significant downregulation of NKG2D and decrease in NK cytotoxicity of target CEM leukemia cells. However, when blocking with anti-TGF-β1 antibody, NKG2D levels and NK cytotoxicity both normalized (44). Interestingly, there is a direct correlation between NK cell function and levels of activating receptors on tumour-infiltrating NK cells, including DNAM-1 and NKG2D (46). Mamessier *et al.* measured these activating receptors on NK cells isolated from the TME of 139 breast cancer patients undergoing surgical resection. DNAM-1 and NKG2D levels decreased progressively with cancer stage and this correlated with lower CD107a degranulation and IFN-γ production (46). While there are several studies on cancer models supporting the central role of NK cells in anti-tumour immune surveillance, another, less well studied mediator of devastating suppression of NK cells, to a degree much greater than the TME, is immediately following surgical stress.

1.2. Surgical Stress and NK Cell Suppression

1.2.1 Surgical stress

Surgery is well known as the only curative treatment modality for most solid malignancies, and it is particularly important to ensure negative surgical margins of the cancer specimen (47–51). While surgical resection of tumours has clear benefits, the stress on the immune system can cause increased tumour growth and spreading (48, 52–55). However, this concept is not new. It has been known for over 100 years that the stress induced by surgery can aggravate postoperative metastases (56, 57). In animal models, this effect was much more pronounced if

primary tumours were not completely excised (56, 57). With surgical resection of a tumour, there is the possibility of leaving a small amount of occult or microscopic neoplastic cells at the surgical margin, which is also known as minimal residual disease (MRD) (53, 58). Surgery can in fact cause accelerated growth of MRD, ultimately leading to decreased disease-free survival (DFS) and overall survival (OS) (53, 54, 58).

The tissue trauma during surgery causes an immediate release of stress-induced hormones such as glucocorticoids and catecholamines, resulting from stimulation of the autonomic nervous system and hypothalamo-pituitary-adrenal axis (48, 59, 60). Additionally, endothelial injury triggers activation of platelets and release of alarmins, or damage-associated molecular patterns (DAMPs), and together these stimulate the release of growth factors including epidermal growth factor (EGF), platelet-derived growth factor (PDGF) and VEGF (51, 61–64). These growth factors are released during the early inflammatory phase of wound healing but they also negatively influence tumorigenesis by increasing tumour invasion, proliferation and angiogenesis (61, 65, 66).

In response to tissue injury and DAMPs, immune cells are recruited to the site of injury, first neutrophils followed shortly afterwards by monocytes (51, 61, 67, 68). Importantly, monocytes have cell surface pattern recognition receptors (PRRs), such as toll-like receptors (TLRs), C-type lectin receptors (CLRs) and NOD-like receptors (NLRs), that can detect DAMPs and trigger the Nuclear Factor κ-B (NFκB) pathway (63, 64). This monocyte activation causes a massive yet short-lived release of pro-inflammatory cytokines, including IL-1, IL-6, TNF-α, IFN-γ and GM-CSF (59, 62, 63, 69–71). Importantly, the expansion in these pro-inflammatory cytokines is proportional to the degree of surgical stress (62, 63, 72, 73). In 2013, Narita *et al.* evaluated cytokine levels of 165 prostate cancer patients undergoing surgery. Interestingly, pro-inflammatory cytokines IL-1, IL-6, and TNF-α were all significantly elevated less than

one hour following surgery and this was notably higher in the open laparotomy group compared to minimally invasive laparoscopy (72). In a randomized control trial (RCT) comparing laparoscopic to open colon resections, Veenhof *et al.* showed that IL-6 was nearly threefold higher in the open surgery group at 1 and 2 hours after surgery but the difference was lost at 24 hours postoperatively (74). Therefore, if the stress of surgery is profound enough, a systemic inflammatory immune response ensues which is proportional to the severity of tissue damage (67, 69, 75, 76). In various animal models of surgery, the length and severity of surgical stress correlates with postoperative tumour burden (62, 76–79). Certain groups were able to show that mice undergoing less invasive laparoscopic surgery had significantly less tumour growth and lung metastases compared to laparotomy (62, 76).

Furthermore, monocyte-derived IL-6 appears to be the major pro-inflammatory cytokine in the immediate postoperative period and has a negative feedback effect on TNF-α and IL-1 to halt the pro-inflammatory phase and transition into the anti-inflammatory response (63, 64). As detailed in Figure 1 outlining the ebb and flow of surgical stress, the intense albeit short pro-inflammatory phase in the 24 hours after surgery triggers a sustained anti-inflammatory phase, which can last up to several weeks (64, 68). The latter is thought to be from an adaptive response to limit excessive inflammatory damage (68, 80). The immunosuppressive phase includes several components: release of anti-inflammatory cytokines (TGF-β, IL-4, IL-5, IL-10, IL-13), prostaglandin E2 (PGE2), and impaired cellular immunity by direct suppression of NK cells and T cells (48, 63, 81–83). Additionally, this suppressive phase is marked by decreased lymphocyte proliferation (63, 82) and loss of T helper type-1 (Th1) cytokine response (70, 81). Interestingly, the Th1/Th2 balance appears to shift towards Th2 in various gastrointestinal (GI) surgeries (63, 81, 84) and this is particularly important because Th2 is mainly responsible for producing anti-inflammatory cytokines (63, 84, 85).

In the relatively short perioperative period, these significant pro-metastatic and suppressive changes occur, which enables tumour cells to evade the immune response (54, 67). In 2003, Coffey highlighted the perioperative period as a critical window of opportunity for immunotherapies (53). But surprisingly, the perioperative window of opportunity has mostly been ignored for the development of potential immunotherapies (54, 86). In fact, less than 1% of registered cancer trials are interventions in the perioperative period (87). One key innate immune population to target in this critical window are the NK cells, which undergo profound and devastating suppressive changes in the postoperative period. As discussed in the next sections, postoperative NK cell suppression correlates with accumulation of anti-inflammatory cytokines and surgery-induced MDSCs (summarized in Figure 1).

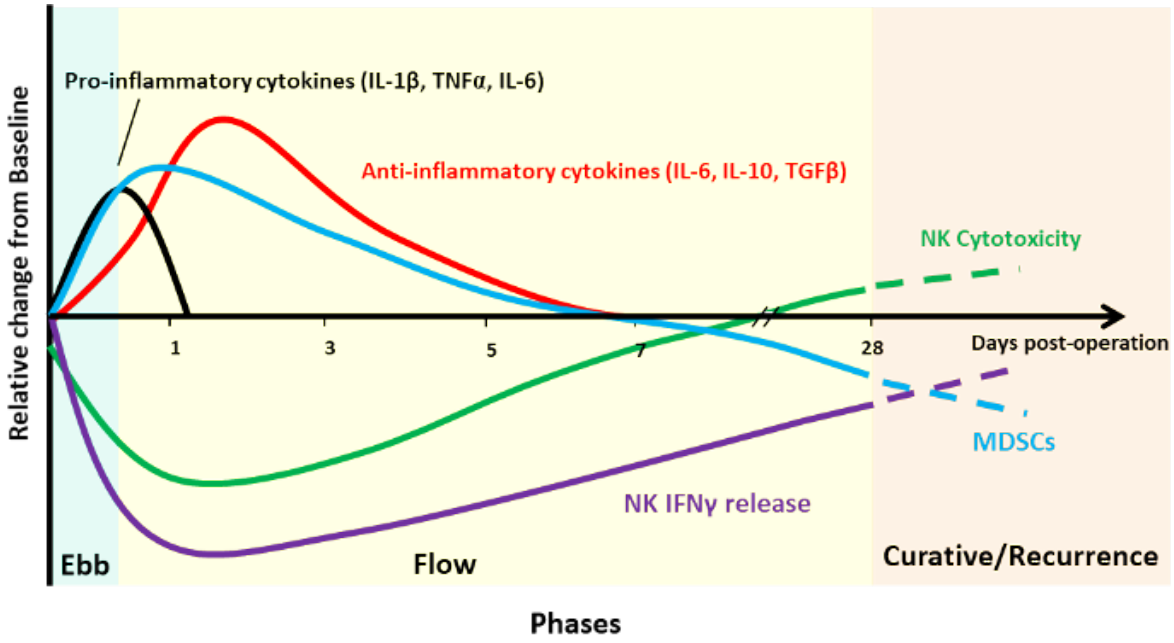
Relative change from Baseline
Pro-inflammatory cytokines (IL-1β, TNFα, IL-6)
Anti-inflammatory cytokines (IL-6, IL-10, TGFβ)
NK Cytotoxicity
1
3
5
7
28
Days post-operation
MDSCs
NK IFNγ release
Ebb
Flow
Curative/Recurrence
Phases

Figure 1. The Ebb and Flow phases of surgical stress.
Surgical stress leads to an immediate but short ebb phase for 24 hours including the release of pro-inflammatory cytokines in black (IL1-β, TNF-α, IL-6), DAMPs and growth factors. On POD1, the flow phase begins, marked by anti-inflammatory cytokines in red (IL-6, IL-10, TGF-β), upregulation of surgery-induced MDSCs in blue (Sx-MDSCs) and profound NK cell suppression (cytotoxicity in green and IFN-γ release in purple). The sustained flow phase can persist for up to several weeks.
Reproduced with permission from Dr. Rebecca Auer and adapted from Angka et al. (64)

1.2.2. Postoperative NK cell suppression

NK cells play a critical anti-tumour role perioperatively, as they are one of the main innate immune cells responsible for clearing MRD by direct tumour lysis without requiring antigen presentation (49, 71, 88–90). This function, however, is significantly impaired following surgical stress (49, 83, 89–92). In 1991, Pollock *et al*. were the first to discover impaired *ex vivo* NK cytotoxicity after surgery. They measured killing by ^{51}Cr-release assay of K562 target cells at baseline and on postoperative day 1 (POD1) for 34 cancer patients and noted a significant decrease in all patients (90). In their follow-up study of 85 cancer patients, they detected impaired NK-mediaed killing as early as 18 hours postoperatively (55). Importantly, NK cell frequencies were still normal at that time point, suggesting the suppression was due to direct impairment in tumour-lysis rather than a decrease in NK cell numbers (55). Results from Whole Blood Gene Expression (WBGE) performed by Watt *et al.* helped confirm these findings. They measured WBGE for 6 colorectal cancer patients at baseline and POD1, and their analysis revealed over 300 significantly differentially expressed genes on POD1 compared to baseline (93). Interestingly, one of their top hits in terms of downregulated fold change was a cluster corresponding to NK cell cytotoxic activity, Granzyme-B and IFN-γ encoding genes, while the genes significantly upregulated on POD1 included growth factors (EGF, VEGF) and pro-inflammatory cytokines (IL-1, IL-6, TNF-α) (93).

The degree of surgical stress also appears to correlate with the amount of NK cell suppression (88, 94). Leung *et al.* found that, while still significantly decreased in both groups, impairment in *ex vivo* NK cytotoxicity was much less pronounced in laparoscopic colon resections compared to laparotomy (94). Ramirez *et al.* identified significantly impaired NK cytotoxicity following surgery in various cancer resections including mastectomies, thoracotomies, and

liver resections (88). This highlights a key concept, that postoperative suppression of NK function is present regardless of cancer type or surgical approach. In various preclinical animal models, our group and others have shown that the degree of postoperative NK cell suppression is directly linked to increased tumour seeding and metastases (83, 91, 92, 95). By performing adoptive NK transfers into NK-deficient mice, we have previously shown that NK cells are the main immune population responsible for controlling postoperative metastases (91, 95). Surgically stressed NK cells resulted in significantly more lung metastases (91, 95) and their ability to kill target cells *ex vivo* was markedly reduced compared to non-stressed NK cells (91).

While the postoperative NK function is significantly impaired, several studies have also shown that absolute NK cell numbers are decreased (68, 71, 73, 81, 91). In a prospective study of elective GI surgeries, Decker *et al.* discovered that NK cells are significantly lower on POD1 and POD2 compared to baseline (81). In other studies, NK cell numbers were significantly decreased up until POD4 and POD5 (68, 71). Ng *et al.* saw similar effects in lung cancer patients. They measured lymphocyte populations at different postoperative time points (POD1, POD3, POD7) and patients undergoing thoracotomy had significantly less NK cells until POD7, but they did not measure beyond one week (73). Importantly, our group and others have recently discovered that NK activity is impaired for much longer than initially anticipated, up to one month after the date of surgery (14, 49, 96). In fact, Brochner *et al.* measured NK cytotoxicity by ^{51}Cr-release assay in ovarian cancer patients, and NK-mediated killing was still impaired on POD21 (96). Similarly, in a study of 42 colorectal cancer patients, we measured NK activity (NKA) by IFN-γ release at various perioperative time points and over 65% of patients still had suppressed NKA by POD28 (14). Despite clearly characterizing the extent and duration of NK cell dysfunction following surgery, surprisingly most of these

studies were unable to confidently determine the exact underlying mechanism of suppression. This changed with the discovery of one key suppressive population that expands significantly postoperatively, the Surgery-Induced Myeloid Derived Suppressor Cells (Sx-MDSCs).

1.3. Myeloid-Derived Suppressor Cells (MDSCs)

1.3.1. Characterization of Myeloid-Derived Suppressor Cells

It has been known for several years that tumour-infiltrating lymphocytes (TILs) can be inhibited by suppressive myeloid cells in the TME (97, 98). First described in 1987, Young reported a suppressive myeloid cell produced from the bone marrow that could strongly suppress T cells in a murine model of Lewis lung carcinoma (97). This suppressive population was thought to be stimulated by tumour production of colony stimulating factor (CSF) in the TME. However, it was not until nearly 20 years later that the Myeloid Derived Suppressor Cells (MDSCs) were properly described as a distinct population. MDSCs are very heterogeneous and can have varying levels of granularity, but they are all by definition immature myeloid cells (IMCs), including progenitors of macrophages, granulocytes and dendritic cells (DCs) (99–101). Most of the MDSC research has been in cancer models, but several other pathological conditions can stimulate production of IMCs, including sepsis, chronic inflammation and trauma (99, 102–104). As highlighted initially by Gabrilovich and Nagaraj, the three original common features of MDSCs are: immaturity, myeloid origin and a strong ability to suppress T cells (99).

Phenotyping studies have discovered important cell surface markers to identify the MDSCs. In mice, MDSCs are characterized by the presence of granulocytic marker GR1 and myeloid lineage marker CD11b ($GR1^+/CD11b^+$) (99, 105). This population represents only 2 to 4% of

naïve spleens but increases significantly in cancer up to 30 to 40% (99, 100, 106). Murine MDSC subtypes can be separated based on the two molecules that form the GR1 receptor, Lymphocyte antigen 6 complex locus G6D (Ly6G) and locus C1 (Ly6C) (99, 101, 102). Monocytic MDSCs (M-MDSCs) express Ly6C only while polymorphonuclear MDSCs (PMN-MDSCs) express Ly6G with minimal Ly6C (99, 101). Further phenotyping can therefore characterize murine M-MDSCs as $CD11b^{+}/GR1^{Int}/Ly6G^{-}/Ly6C^{+}$ and PMN-MDSCs as $CD11b^{+}/GR1^{Hi}/Ly6G^{+}/Ly6C^{Lo}$ (102). While phenotypically similar, these two subtypes are quite different morphologically. N1, (107).

In humans, lack of the GR1 surface marker makes their characterization more difficult (103, 108). Human MDSCs are generally identified by the absence of lymphocyte lineage (Lin) markers (CD3, CD19, CD56) and presence of common myeloid lineage markers CD33 and/or CD11b (102, 106). Bronte *et al.* reported that CD33 can confidently be used as the sole myeloid marker to characterize human MDSCs (102). Therefore, it is now accepted that the human equivalent of M-MDSC can be identified as $Lin^{-}/CD33^{+}/CD14^{+}/CD15^{Lo}$ while the PMN-MDSC as $Lin^{-}/CD33^{+}/CD14^{-}/CD15^{+}$. Importantly, the human high-density (HD) neutrophils are removed in the high-density layer during Ficoll gradient separation. The fraction of remaining neutrophils, low-density (LD) neutrophils, are therefore considered PMN-MDSCs during flow phenotyping as gated on $Lin^{-}/CD33^{+}/CD14^{-}/CD15^{+}$ (102). As stated by Bronte, Ficoll gradient separation is the only known method to separate human HD neutrophils from PMN-MDSCs (102). However, such processing is not feasible for murine functional assays as the volume of blood is often not sufficient (data not shown). Therefore, for murine phenotyping both HD neutrophils and PMN-MDSCs are included in the granulocyte population.

M-MDSCs have much stronger suppressive activity than PMN-MDSCs, the latter being relatively weakly suppressive (105). M-MDSCs inhibit cells in part by utilizing two key

arginine pathways; inducible nitric oxide synthase (iNOS) to oxidize L-arginine into nitric oxide (NO) and citrulline, as well as Arginase-1 (Arg-1), which converts L-arginine into urea and ornithine (99, 103, 108). Additionally, TGF-β plays an important role in the suppressive effect of M-MDSCs. In murine cancer models, exposing the $CD11b^{+}/GR1^{Int}$ M-MDSCs to fibrosarcoma 15-12RM and 18Neo cells (109) or CT26 colon cancer cells (110) activated the production of TGF-β, but this effect was not seen with the $CD11b^{+}/GR1^{Hi}$ PMN-MDSCs (109). The inhibition pathway by PMN-MDSCs is therefore different, as they don't appear to produce TGF-β upon stimulation. Furthermore, they mainly produce reactive oxygen species (ROS) through nicotinamide adenine dinucleotide phosphate (NADPH) oxidase (99, 108). Interestingly, ROS from MDSCs not only have the ability to directly inhibit cells but they can also limit the differentiation potential of IMCs (100, 103, 111). In a murine C3 sarcoma model, Kusmartsev was able to show that IMCs isolated from tumour-bearing mice had a significant delay to differentiate into DCs and macrophages *in vitro*, while this process remained normal in IMCs from naïve mice. Additionally, ROS levels were significantly higher in the IMCs from tumour-bearing mice (100, 111) and endogenous hydrogen peroxide is thought to play the main role in the PMN-MDSC suppressive effect (111).

1.3.2. MDSCs in cancer and infection

Levels of MDSCs also correlate strongly with cancer stage and prognosis (112–115). Diaz-Montero *et al.* measured MDSCs from peripheral blood mononuclear cells (PBMCs) of 106 cancer patients and both absolute MDSC numbers (MDSC/µl of blood) and percentage increased progressively with cancer stage. These were highest in stage IV cancer patients, almost twofold greater than early stage cancers (3.77% vs 1.26% of whole blood) (113). Additionally, MDSC percentage was predictive of overall survival (OS) in metastatic breast

cancer, where a high MDSC percentage was associated with a significantly lower OS (6.8 months vs 19.6 months) (114). In 40 gastric cancer patients, high levels of MDSCs in blood correlated with advanced cancer stages III-IV and decreased OS (less than 60% vs 90% at 2 years) (115).

MDSCs appear to have a close reciprocal relationship with tumour cells of the TME. Firstly, they are stimulated by various factors produced by the TME, including growth factors (VEGF and GM-CSF), cytokines (IL-1β, IL-6, IL-10, IL13, and TNF-α), as well as COX-2 and PGE2 (106, 107, 116, 117). In a murine model, injecting IL-1β-secreting fibrosarcoma tumours resulted in a significant increase in blood and spleen MDSCs compared to tumours without IL-1β production. Resecting the IL-1β-secreting tumours then normalized MDSC levels within 7 to 10 days (116). PGE2, produced by conversion of arachidonic acid by COX-2, is another key inflammatory mediator produced by several tumours and stimulates MDSCs (116–118). In fact, blocking PGE2 in a murine 4T1 breast cancer model, through knockout mice and COX-2 inhibition, led to decreased MSDC numbers and significantly delayed tumour growth (118). While MDSCs can be stimulated by TME factors, on the other hand MDSCs can infiltrate tumours and remodel the TME into a more suppressive environment (117, 119). MDSCs produce several important pro-metastatic and pro-angiogenic mediators including VEGF, matrix metallopeptidase-9 (MMP-9) and TGF-β (105, 117, 119–121). In fact, TGF-β production from tumour-infiltrating M-MDSCs likely represents the main source of TGF-β in the TME (120). In a MC26 colon cancer model, co-injection of MC26 with $CD11b^{+}/GR1^{+}$ MDSCs led to significantly higher tumour growth and angiogenesis compared to tumours alone (121).

While most of the research on MDSCs has been related to cancer models or the TME, these cells are also known to play a key role in suppressing lymphocytes during various acute and

chronic viral infections including Hepatitis C Virus (HCV), Human Immunodeficiency Virus (HIV), Vesicular Stomatitis Virus (VSV), and adenovirus (103, 122). Goh *et al.* studied MDSCs in HCV patients and upon co-culture of HCV-induced MDSCs with NK cells, there was significantly decreased NK-secreted IFN-γ production (122). Interestingly, NK function was normalized when blocking Arg-1 and restored in a dose-dependent manner when supplementing the culture with L-arginine, suggesting the suppression of NK cells is dependent on MDSC Arg-1 expression (122). Additionally, MDSC levels increase significantly in sepsis patients with a nearly tenfold increase in gram negative sepsis compared to healthy controls (104). A large amount of work has improved understanding of the role of MDSCs in cancer, infections and sepsis, but one specific area that has not gained much attention thus far is the critical perioperative window of immunosuppression.

1.3.3. Surgery-Induced MDSCs

Under normal conditions, even with a small amount of circulating myeloid progenitor cells thy(MPCs) there are up to 1 $x10^{11}$ granulocytes produced daily (123, 124). During times of intense stress, such as trauma, severe infections or surgery, the bone marrow (BM) is stimulated to produce an even higher amount of granulocytes, mainly neutrophils, as the first-line of the inflammatory response (124–126). This process of intense *de novo* production of myeloid cells is defined as emergency myelopoiesis (124–126). Since MDSCs are a subset of IMCs that are significantly upregulated in times of stress, one would expect MDSCs to also be increased during emergency myelopoiesis, specifically following surgical stress. Additionally, key pro-inflammatory cytokines that are strong mediators of emergency myelopoiesis, such as IL-6 and G-CSF, are also significantly increased postoperatively (62, 72, 125). Surprisingly, there are few studies examining the effects of surgical stress on MDSCs and even fewer

characterizing the suppressive effect of surgery-induced MDSCs (Sx-MDSCs) on the innate immune response (112, 127–129). In 1982 Uchida *et al.* studied 21 early-stage breast cancer patients and detected a significant decrease in postoperative NK cytotoxicity (130). Interestingly, this 40 to 50% suppression was thought to be dependent on "suppressor monocytes", as the cytotoxicity improved significantly when depleting monocytes from postoperative PBMCs (130). Although unknown at the time, these cells were likely Sx-MDSCs. Yuan *et al.* examined MDSCs perioperatively for 64 rectal cancer patients and postoperative Sx-MDSC levels were significantly greater than at baseline, but their earliest time point measured was POD7 and they did not assess suppressive function (128). They did, however, by multivariate analysis discover an association between high baseline MDSC levels, defined as greater than 3.87% of whole blood, and increased risk of local recurrence (128). Similarly, Jones *et al.* detected a twofold increase in intermediate monocytes on POD1 for 40 lung cancer patients (127).

Compared to baseline, Sx-MDSCs appear to have a much more suppressive phenotype. Human postoperative MDSCs isolated on POD1 following thoracotomy for 76 lung cancer patients had higher levels of MMP-9 and VEGF, as well as greater angiogenesis and tumour growth in an allograft tumour model (112, 129). Sx-MDSCs isolated on POD1, POD3 and POD7 following thoracotomy also demonstrated higher levels of T-cell suppression in co-culture suppression assays, with POD1 Sx-MDSCs having the strongest suppression (112). Additionally, in a murine Lewis lung carcinoma experimental metastasis model of surgery, consisting of laparotomy and left hepatectomy, blocking $CD11b^{+}/GR1^{+}$ MDSCs *in vivo* led to a significantly lower number of postoperative lung metastases (112, 129).

Using experimental (B16F10-LacZ melanoma) and spontaneous (4T1 orthotopic breast cancer) murine models of surgical stress, we have previously shown that the percentage of

$CD11b^+/GR1^+$ MDSC increases significantly in the spleen following surgery but decreases in the bone marrow (131), reinforcing the concept of postoperative emergency myelopoiesis. When measuring the PMN-MDSC percentage of 9 colorectal cancer patients undergoing surgical resection, POD1 was more than twofold greater than baseline. Additionally, murine and human POD1 Sx-MDSCs were greatly suppressive of NK cells in *ex vivo* co-culture cytotoxicity assays, much more than baseline MDSCs (131). These studies suggest that Sx-MDSCs play a key role in the critical perioperative window. While phenotypically similar to MDSCs from the TME, the acute stimulation following surgical trauma and resulting emergency myelopoiesis appears to induce stronger suppressive and pro-metastatic properties, although there are no known studies directly comparing TME MDSCs to Sx-MDSCs. We have previously performed flow phenotyping studies of POD1 Sx-MDSCs for humans and murine models (manuscript in preparation). The postoperative human Sx-MDSC population consists mainly of M-MDSCs, identified by $Lin^-/CD33^+/HLA\text{-}DR^{Lo}/CD14^+/CD15^-$, while murine Sx-MDSCs were identified as $CD45^+/CD11b^+/GR1^+/Ly6G^-/Ly6C^+$. In an attempt to identify unique surface markers on human Sx-MDSCs, we decided to analyze its cell surface receptors by proteomic screen.

1.3.4. Sx-MDSC surface proteomic screen

In order to better characterize the Sx-MDSC population, we previously ran a proteomic screen of N-glycosylated cell surface markers developed by our collaborator Dr. Kislinger (132). $CD33^+$ myeloid cells were isolated from cancer patients at baseline and POD1, and N-glycosylated surface proteins were analyzed by Liquid Chromatography-Mass Spectrometry (LC/MS). Of the 1,176 peptides discovered, 127 were Cluster of Differentiation (CD) molecules with 5 surface proteins detected at high intensities on POD1 while being

undetectable at baseline. Listed in table 1, most of these proteins are known to be involved in the suppressive mechanism of MDSCs, including IL-10 receptor, TNF receptor, and ADAM17 which is a metalloprotease that cleaves IL-6 and TNF-α into their mature forms (133). However, one particular surface protein of interest was unexpectedly discovered, the CD155 Poliovirus receptor (PVR). As discussed in the next section, CD155 may play a critical role in the Sx-MDSC suppressive phenotype.

Table 1. Surgery-induced MDSC (Sx-MDSC) Surface Proteomic Screen

Predicted CD33 Subset	Protein Name	Accession	CD33+ Fraction		
			Baseline	POD1	
			#1	#1	#2
CD33-	CD3	P04234	ND	ND	ND
CD33-/+	CD11b	P11215	1.63E+08	5.02E+08	5.99E+08
CD33-/+	CD14	P08571	5.18E+07	6.53E+07	1.32E+08
POD1	IL10Rb	Q08334	ND	2.70E+07	2.22E+07
POD1	TNFR1	P19438	ND	1.29E+07	2.38E+07
POD1	ADAM17	P78536	ND	1.29E+07	1.30E+07
POD1	CD82	P27701	ND	2.25E+06	7.43E+06
POD1	PVR	P15151	ND	2.41E+06	2.41E+06

POD1 – Postoperative day 1, ND – not discovered, IL10Rb – IL-10 Receptor b, TNFR1 – Tumor necrosis factor receptor 1, ADAM17 – ADAM metallopeptidase domain 17, PVR – Poliovirus receptor

Reproduced with permission from Dr. Rebecca Auer, unpublished data.

1.4. CD155 Poliovirus Receptor

1.4.1. CD155 Poliovirus receptor and its ligands

First discovered in 1989, CD155, also known as poliovirus receptor (PVR) or Nectin-Like (Necl)-5, is a 70 kD trans-membrane protein belonging to the immunoglobulin superfamily (24, 134–136). While its expression is very low in normal human tissue, it is overexpressed in several transformed cells (137–139) and is involved in cell adhesion, movement and proliferation (24, 139). Necl receptors are responsible for cell to cell adhesion by forming tight junctions between epithelial cells (24, 139). In normal conditions, cell to cell adhesion leads to contact inhibition during which there is a halt in cell migration (24, 140, 141). This concept of contact inhibition is particularly important to ensure controlled epithelial wound healing following injury (24, 142). However, in transformed or malignant cells, there can be loss of contact inhibition which leads to uncontrolled proliferation (24). CD155 is known to colocalize with integrin at the leading edge of migrating cells (139). Through activators and inhibitors of integrin and CD155-knock out (KO) fibroblast cell lines, Ikeda *et al.* confirmed that CD155 and integrin are both required for directional cell migration and loss of either one greatly reduces cell motility (138, 139). Importantly, by using an *in vitro* cell density assay of NIH3T3 adherent fibroblast cells, Fujito *et al.* showed that binding of CD155 with Nectin-3 during cell adhesion led to a significant downregulation of CD155, which limited NIH3T3 cell movement and proliferation (143). The lack of contact-initiated downregulation of CD155 may be one key mechanism of uncontrolled proliferation in transformed cells. CD155 also greatly influences cell proliferation by shortening the G0/G1 rest phase and enhancing growth factor-induced cell movement (136–138).

The CD155 receptor has three known ligands on NK and T cells, including DNAM-1, T-cell Immunoreceptor with Ig and ITIM domains (TIGIT) and CD96 (T-cell activated increased late expression, or TACTILE) (24, 26, 28, 134, 144). DNAM-1 is a transmembrane glycoprotein of the immunoglobulin superfamily expressed on the majority of lymphocytes including NK cells and T cells (23, 24, 145). DNAM-1 is the only immune-activating receptor that, when bound, stimulates cytotoxicity of NK cells and T cells, and increases IFN-γ production (26, 27, 144, 146). In fact, cytotoxicity and production of GM-CSF and TNF-α were greatly reduced against colorectal and ovarian tumour cells *in vitro* when blocking DNAM-1 with the DX11 monoclonal antibody (27). Oppositely, TIGIT is inhibitory in nature (26, 28, 134, 136) and binding of CD155 with TIGIT directly decreases NK cytotoxicity and IFN-γ production (147, 148). Staniestky *et al.* performed murine and human NK cytotoxicity assays and showed that both NK cytotoxicity and IFN-γ release were significantly greater when blocking TIGIT with various monoclonal antibodies (147, 148). Chan *et al.* were the first to discover that CD96 shares a similar inhibitory function as TIGIT by directly inhibiting NK cells (28). They studied $CD96^{-/-}$ mice and saw that the presence of CD96 expression in WT mice limited IFN-γ production in response to lipopolysaccharide (LPS) stimulation. Additionally, both TIGIT and CD96 have a greater affinity for CD155 compared to DNAM-1 (28, 147, 149).

While initially thought to constitutively enhance cytotoxicity (23), it is now known that the downstream effect of CD155 binding with DNAM-1 is not so simple. Ultimately, the effect of CD155 on NK cells or T cells depends on the relative ratio of DNAM-1 to TIGIT/CD96 (134, 136, 150). Expression of DNAM-1 greater than TIGIT/CD96 enhances effector cell function and improves cytotoxicity but the opposite occurs when TIGIT/CD96 expression prevails, resulting in strong NK and T cell suppression (134, 136, 149). CD155 also causes downregulation of DNAM-1 on NK and T cells (10, 150, 151). Seth *et al.* determined that lack

of host CD155, through knockout mice ($CD155^{-/-}$) and a monoclonal antibody (clone 3F1), led to a significantly higher expression of DNAM-1 on T cells (151). However, following adoptive T cell transfers into WT mice with normal CD155 expression, DNAM-1 levels decreased back to baseline (151). Importantly, CD15co5 has much greater affinity for TIGIT and CD96 than DNAM-1 (28, 147). These changes induced by CD155 all lead to a general suppressive state and appear to also play a central role in tumour immune evasion.

1.4.2. Cancer CD155 expression

CD155 is expressed at low levels in normal human tissue but is upregulated in several different types of cancer (136, 152–155). Sloan *et al.* noted an absence of CD155 expression by immunohistochemistry (IHC) in most organs, including brain, heart, pancreas, intestine, skeletal muscle and others (152). However, expression is significantly increased in various cancers, such as prostate, kidney, colorectal, pancreatic, non-small cell lung (NSCL), ovarian and breast cancers, as well as more rare tumours such as glioblastoma and fibrosarcoma (152–160).

The first key step in the sequence of cancer metastasis described by Thiery pertains to disruption of cell adhesion and increased cell motility (161), for which it is known CD155 can impact. CD155 contributes to loss of contact inhibition in tumours, which enhances migration and proliferation of invasive and/or metastatic cancers (152, 155, 162, 163). Additionally, CD155 colocalizes at the edge of tumours with actin and integrin, and increases tumour growth by shortening the G0/G1 phase (136, 138, 139, 152). *In vitro* CD155 blockade of glioblastoma tumours with several anti-CD155 monoclonal antibodies significantly decreased tumour migration in transwell assays (152). Similarly, two studies performing CD155 knockdown by small interfering RNA (siRNA) in colon and lung cancer cell lines significantly impaired

tumour proliferation, measured by transwell migration and gel invasion assays (155, 163). Overexpression of CD155 also seems to increase VEGF production and angiogenesis in the TME (153). Nishiwada *et al.* measured intra-tumoral vessel density of excised pancreatic cancer tissue for 134 patients and noted a significant increase in angiogenesis if the tumour had high CD155 expression (153).

These pro-tumorigenic modifications caused by CD155 result in a direct increase in tumour burden and metastases, which are significantly minimized by blocking tumour CD155 (162, 164, 165). In a murine model of CD155-overexpressing CT26 colorectal cancer cells, injection of an anti-CD155 antibody led to a threefold decrease in lung metastases (162). Similarly, Li *et al.* used various CD155-KO cell lines including B16F10, LWT1 and MC38, and loss of tumour CD155 led to a significant decrease in tumour growth and metastases (164). Interestingly, in a survival model of orthotopic 4T1 breast cancer, mice receiving 4T1-CD155 KO had a much higher survival at 50 days compared to 4T1-WT tumours (60% vs 5%, $p<0.001$) (164).

The effect of CD155 is not limited to increased tumour invasion and proliferation. Several key studies have highlighted the impact of tumour CD155 upregulation on the suppressive NK cell phenotype (10, 32, 166, 167). The presence of DNAM-1 is required for engagement of NK cells with CD155-expressing tumours and resulting anti-tumour cytotoxic activity (31, 32, 167–169). However, overexpression of CD155 on various cancer cells leads to the direct downregulation of DNAM-1, and upregulation of TIGIT/CD96, tipping the balance towards NK cell and T cell suppression (10, 32, 136, 166, 167). Carlsten *et al.* measured DNAM-1 levels on NK cells from ovarian cancer patients. NK cells isolated from circulating PBMCs had greater expression of DNAM-1 compared to NK cells from the peritoneal fluid, but DNAM-1 was significantly downregulated upon *ex vivo* co-culture with several CD155-

expressing ovarian cancer lines (10). Okumara *et al.* detected a significant decrease in *ex vivo* NK-mediated cytotoxicity of B16F10 tumours, measured by CD107a degranulation and IFN-γ production, following DNAM-1 blockade using DNAM-1$^{-/-}$ mice and anti-DNAM-1 antibody (clone TX42) (166). Similarly, Gilfillan *et al.* performed *ex vivo* cytotoxicity studies of NK cells isolated from DNAM-1$^{-/-}$ and WT mice and revealed that absence of DNAM-1 led to a significant decrease, more than fivefold, in cytotoxicity of CD155-expressing B16F10 tumours (32). These DNAM-1$^{-/-}$ mice also had significantly more lung metastases in their spontaneous B16F10 intravenous (IV) model and larger primary tumour volumes following subcutaneous (SC) injections (32). In their follow-up study, DNAM-1$^{-/-}$ mice had impaired cytokine clearance of B16F10 lung metastases. Administering IL-2, IL-12 and IL-21 intraperitoneally (IP) significantly decreased metastases only in the WT mice without improving tumour burden in DNAM-1$^{-/-}$ mice (167).

In terms of cancer outcomes, tumour CD155 levels strongly correlate with cancer stage (157, 170–172) and high tumour CD155 expression has been associated with a poor prognosis in various malignancies including sarcoma, leukemia, melanoma, breast, lung, pancreatic, and bladder cancers where high CD155 leads to decreased disease-free survival (DFS) (153, 157–159, 172, 173) and overall survival (OS) (171, 172). In two studies measuring CD155 after surgical resection for lung cancer and breast cancer patients, tumour IHC staining confirmed that high CD155 expression was strongly associated with lymph node metastases, increased cancer stage, decreased DFS (35% vs 95% at 5 years, p=0.0004) (157) and reduced OS (50% vs 80% at 5 years, p=0.035) (171). Zhang *et al.* recently analyzed CD155 expression for several cancer outcomes. Most strikingly, in 228 patients with invasive bladder cancer undergoing curative resection, high tumour CD155 expression, determined as more than 50% by IHC

staining, led to a significant decrease in OS from 75% to less than 35% at 5 years (p<0.001) (172).

Together, these studies have highlighted the strong pro-tumorigenic effects of CD155, including increased proliferation, invasion and angiogenesis. Additionally, CD155 induces strong tumour-mediated suppression of NK cells and T cells by downregulating DNAM-1 and tipping the balance towards a greater TIGIT/CD96-to-DNAM-1 ratio. More recently, tumour infiltrating myeloid cell (TIMC) CD155 expression was found to play an equally important role in immunosuppression.

1.4.3. CD155 expression on myeloid cells

While much less is known on the effect of myeloid CD155 expression on tumour growth and metastases, some key studies have highlighted that host CD155 may contribute to the pro-metastatic and suppressive changes. Abe *et al.* studied CD155 in a murine model of spontaneous colitis-associated neoplasia. Interestingly, after injecting carcinogenic agents dextran sodium sulfate (DSS) and dimethylhydrazine (DMH), $CD155^{-/-}$ mice had significantly less inflammatory changes and colon tumours compared to WT (165). While they hypothesized that increased CD155-induced epithelial proliferation in WT mice instigated the malignant process, they did not determine the underlying mechanism of host CD155 expression in tumour formation (165).

Li *et al.* were the first to show that CD155 is not only overexpressed on tumours but also on TIMCs (164). In multiplex IHC of excised human melanoma tumours, they discovered a high co-localization of CD155 with $CD11c^{+}CD14^{+}$ myeloid cells(164). Furthermore, they used T cell (anti-CD4, anti-CD8) and NK cell (anti-asGM1) depleting antibodies to determine that the tumour growth was CD8+ T cell dependent and lung metastases were NK cell dependent.

Importantly, compared to $CD155^{-/-}$ mice, presence of host CD155 expression in WT mice caused an increase in tumour growth and metastases, regardless of tumour CD155 expression (B16F10-WT or B16F10-CD155 KO cells), indicating an important role for myeloid CD155 expression in tumour immune evasion. Lastly, by administering anti-DNAM-1 antibody (clone 480.1) in $CD155^{-/-}$ mice, they convincingly showed that DNAM-1 expression is required for the anti-tumour effect as DNAM-1 blockade led to a significant increase in tumour volume (164).

Similarly, Wu *et al.* also performed multispectral IHC of resected human head and neck squamous cell carcinoma (HNSCC) tumours and determined that CD155 was strongly co-expressed with $CD11b^{+}$ tumour-infiltrating stromal cells (174). Interestingly, in their murine *ex vivo* co-culture suppression assays of CD8+ T cells with M-MDSCs or PMN-MDSCs, blocking TIGIT with anti-TIGIT antibody (clone 1G9) resulted in greater proliferation of CD8+ T cells, although they did not examine the impact of CD155 blockade (174). These findings created a provocative link between myeloid CD155 expression and NK cell suppression. However, there are no known studies examining CD155 expression directly on MDSC populations, nor the contribution of surgically-induced CD155 expression on the suppressive MDSC phenotype, which provides strong rationale for this research project. The proposed mechanism of Sx-MDSC CD155 suppression is summarized in figure 1 comparing the pathway at baseline (A) to the postoperative state (B).

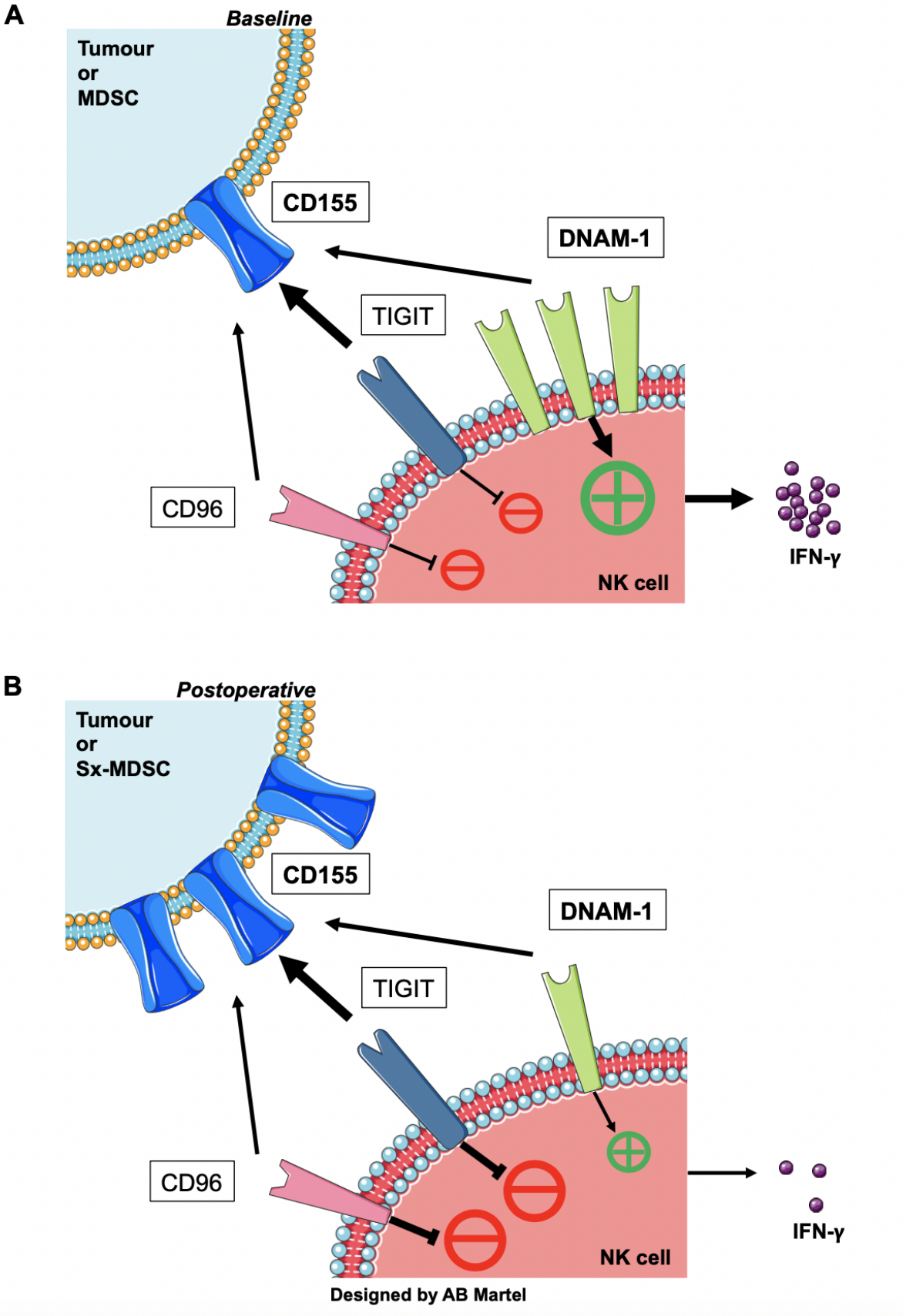
A
Baseline
Tumour
or
MDSC
CD155
DNAM-1
TIGIT
CD96
NK cell
IFN-γ
B
Postoperative
Tumour
or
Sx-MDSC
CD155
DNAM-1
TIGIT
CD96
NK cell
IFN-γ
Designed by AB Martel

Figure 2. Tipping the balance: Proposed Mechanism of Surgery-Induced MDSC (Sx-MDSC) CD155 Suppression Following Surgical Stress.
A) At baseline without surgery, CD155 is shown with its three NK cell ligands DNAM-1 (activating) and TIGIT, CD96 (inhibitory). The higher ratio of DNAM-1 to TIGIT/CD96 leads to an activating signal with increased IFN-γ production. **B)** Postoperatively, CD155 is upregulated on Sx-MDSCs, leading to the downregulation of NK cell DNAM-1 and tipping the balance towards an inhibitory signal with decreased IFN-γ. Image created by Andre B. Martel.

2. RATIONALE AND HYPOTHESIS

2.1. Rationale:

Although barely expressed in normal epithelial tissue, CD155 is overexpressed in various types of cancer (152, 154, 156) and has strong immunosuppressive and pro-metastatic effects in several cancer models (136, 164, 173). CD155 has been shown to increase tumour cell invasion and proliferation, thereby increasing tumour volume and worsening metastatic burden (152, 155, 162, 163). More recently, studies have discovered high co-localization of CD155 on TIMCs (164, 174), creating a provocative role for myeloid CD155 expression in tumour immune evasion. To date, CD155 has never been studied on specific MDSC populations. Furthermore, its expression has never been measured in the perioperative setting. It is well known that Sx-MDSCs expand significantly following surgical stress (127, 128, 131), directly inhibit NK cells in suppression assays (131) and worsen tumour growth and metastases (112, 129). Through the downregulation of DNAM-1, expansion of CD155 on Sx-MDSCs immediately following surgical stress could be responsible for the suppressive postoperative NK cell phenotype, which makes it a very appealing perioperative target for immunotherapy in cancer patients.

2.2. Hypothesis:

CD155 expression increases significantly on Sx-MDSCs following surgery and is responsible for postoperative NK cell suppression and cancer metastases.

2.3. Research Aims:

2.3.1. Measure the perioperative Sx-MDSC CD155 expression in cancer surgery patients and animal models of surgical stress.

2.3.2. Determine whether targeting CD155 *in vivo* is sufficient to restore NK cell function and reduce metastases in the murine model of surgical stress.

2.3.3. Investigate the role of Sx-MDSC CD155 expression on the suppressive NK cell phenotype in human cancer patients.

3. METHODOLOGY

3.1. Cell Lines

K562 (human leukemia, ATCC CCL-243™) and YAC-1 (murine lymphoma, ATCC TIB-160™) cells were obtained from the American Type Culture Collection (ATCC; Manassas, VA) and maintained in HyClone™ Roswell Park Memorial Institute (RPMI) medium (GE Healthcare; Mississauga, ON) supplemented with 10% Fetal Bovine Serum (FBS; Sigma-Aldrich, St. Louis, MO). NK92 MI (human NK cell, ATCC CRL-2408™) was also obtained from ATCC but maintained in HyClone™ RPMI (GE Healthcare) supplemented with 10% FBS (Sigma-Aldrich), 50,000 Units (U) of Penicillin-Streptomycin (Pen-Strep; Thermo Fisher Scientific, Waltham, MA), 10 mM HEPES (Sigma-Aldrich) and 55 μM β-mercaptoethanol (Sigma-Aldrich). B16F10-LacZ (murine melanoma expressing LacZ) were previously transfected by Christiano T. de Souza and maintained in HyClone™ Dulbecco's Modified Eagle's Media (DMEM; GE Healthcare) supplemented with 10% FBS (Sigma-Aldrich). B16F10-CD155 KO and B16F10-parental wild-type (WT) cells were provided in kind by Dr. Mark J. Smyth's research group (QIMR Medical Research Institute, Herston, Queensland,

Australia). The B16F10-CD155 KO cell line was previously knocked out using CRISPR-Cas9 with CD155 small oligonucleotide RNA (sgRNAs) subcloned into the PX330 vector and transfected into B16F10 cells, as previously published(164). Both the B16F10-CD155KO and B16F10-parental WT cells were maintained in HyClone^{TM} DMEM (GE Healthcare), 10% FBS (Sigma-Aldrich) and 50,000 U Pen-Strep (Thermo Fisher Scientific).

All above cell lines were cultured in a 37^0C incubator with 5% CO_2 and mycoplasma contamination was verified by e-Myco^{TM} VALiD Mycoplasma PCR Detection Kit (iNtRON Biotechnology, Sangdaewon-Dong, South Korea). Passage cell viability was confirmed by counting on the Vi-Cell XR Cell Viability Analyzer^{TM} (Beckman Coulter; Brea, CA, USA).

3.2. Animals

All female C57Bl/6 mice were purchased from Charles River Laboratories (Wilmington, VA) and housed under strict pathogen-free conditions at the University of Ottawa Animal Care and Veterinary Services (ACVS) facility (Ottawa, ON). Murine protocols complied with the Canadian Council on Animal Care guidelines and were approved by the University of Ottawa Animal Research Ethics Board prior to initiating experiments. Mice were between the ages of 6 to 10 weeks for all experiments.

3.3. Cancer Surgery Patients

Cancer patients were consented through the *Perioperative Human Blood and Tissue Collection Program* (PHBSP), which was previously approved by the Ottawa Health Science Network (OHSN) Research Ethics Board (REB) under protocol number 2011884. For recruitment, any patient at least 18 years of age with diagnosis of resectable primary malignancy was included. The following exclusion criteria were used: evidence of tumour metastasis,

immunosuppressive conditions such as Lupus, Rheumatoid Arthritis, or steroid use, as well as recent neoadjuvant chemotherapy and/or radiation therapy within the last 4 weeks. Blood was drawn by registered nurses (RNs) in the surgical day care unit (SDCU) at baseline before surgery (POD0) and on the surgical wards on POD1. A total of 40 mL of blood was collected into BD Vacutainer^{TM} sodium heparin collection tubes (Thermo Fisher Scientific) for each timepoint and processed in the laboratory within 2 hours. Blood was gently overlaid on Ficoll-Paque PLUS (Thomas Scientific; Swedesboro, NJ) and centrifuged at 400g for 30 minutes with slow acceleration and deceleration of 1/0. PBMCs were isolated from the mid-cloudy layer, washed in HyClone^{TM} Phosphate-Buffered Saline (PBS; GE Healthcare), counted on Vi-Cell XR^{TM} (Beckman Coulter) and resuspended to 1 x10e^{7} cells/mL (1 x10e^{6} cells/well) in Flow Buffer, comprised of PBS (GE Healthcare), 1 mL UltraPure^{TM} 0.5M EDTA (Thermo Fisher Scientific) and 2.5 g Bovine Serum Albumin (BSA; Bioshop Canada, Burlington, CA).

3.4. Murine Model of Surgical Stress

In our animal model of surgical stress (82, 91, 95), B16F10 melanoma cells (3 x10 e^{5} cells, minimum 90% viability) were injected via IV tail vein into C57Bl/6 WT mice (n=15 experiments), followed 10 minutes later by laparotomy, mobilization of bowel, left nephrectomy and stapled abdominal closure to induce surgical stress (Figure 3).

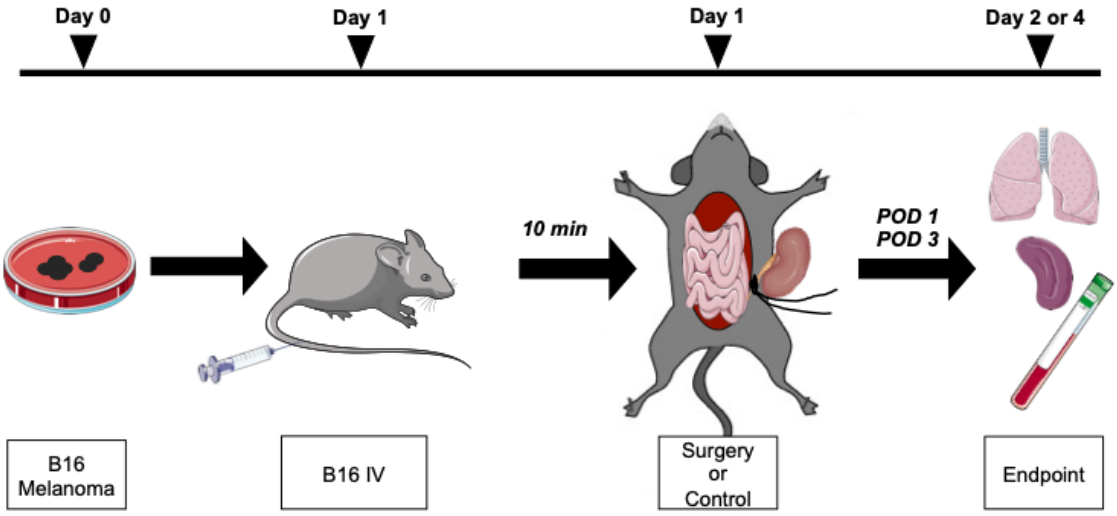
Day 0
Day 1
Day 1
Day 2 or 4
10 min
POD 1
POD 3
B16
Melanoma
B16 IV
Surgery
or
Control
Endpoint

Figure 3. Animal Model of Surgical Stress to Examine Perioperative CD155 Expression. Representative flow diagram of our animal model of surgical stress. After growing B16F10 melanoma *in vitro*, 3 x10e^5 cells are injected in mice via IV tail vein. Ten minutes later, mice undergo surgery (laparotomy, mobilizing of bowel, left nephrectomy and stapled closure). Endpoint is performed on POD1 or POD3 to process spleens, blood and/or lungs. *POD – Postoperative day.*

To minimize the effect of tumour CD155 expression on the postoperative immune response, B16F10 cell lines deficient in CD155 (B16F10-CD155 KO) were used for most experiments, unless specifically mentioned. B16F10 cells expressing LacZ (B16F10-LacZ) were used to visualize lung metastases for certain POD3 experiments, as previously done (82, 91, 95). On POD1 or POD3, the mice were sacrificed by lethal buprenorphine IP injection at 0.1 mg/kg body weight, followed by cervical dislocation. Blood was collected by cardiac puncture and stored in Microvette^{TM} CB 300 µl lithium heparin coated tubes (Sarstedt, Newton, NC, USA). Spleens were harvested via left upper quadrant abdominal incision and splenocytes were dissociated through Fisherbrand^{TM} Sterile 70 µm Cell Strainers (Thermo Fisher Scientific). Blood and spleen samples were processed using our standardized protocol, including Ammonia Chloride Potassium (ACK) lysis buffer to remove erythrocytes (once for splenocytes and twice for murine blood), washed with PBS and counted on Vi-Cell XR^{TM}. Cells were resuspended to 1 x10 e^7 cells/mL in Flow Buffer.

For lung processing on certain POD3 endpoints, our standard LacZ staining protocol was used. On the first day, lungs were washed twice in Wash Buffer (1M magnesium chloride, 1% deoxycholate, 2% nonidet-P40, 0.1M sodium phosphate buffer pH 7.3), and then stained overnight at 37^0C with X-Gal^{TM} solution, 25 mg/mL in Dimethylsulfoxide (X-Gal in DMSO; Bioshop Canada). The next day, lungs were washed twice with Wash Buffer and incubated for 24 hours at 4^0C. On the third day, lungs were transferred into 10% buffered formalin for permanent fixation. Images of each lung were obtained electronically using Axiovision software v4.8 (Zeiss; Oberkochen, Germany) on the Zeiss SteREO^{TM} Discovery Modular Microscope (Zeiss). From these electronic images, lung metastases were quantified visually.

3.5. Immune Cell Phenotyping

3.5.1. Human Samples

Human PBMCs were washed and stained with Fixable Viability Stain 510 (BD Biosciences; Franklin Lakes, NJ), followed by extracellular staining of MDSC surface receptors, including: CD33, CD14, CD15, HLA-DR, CD155 and an exclusion gate for lymphocytic lineage (Lin-) markers (CD3, CD56, CD19). Expression of CD155 was measured using PE-labelled mouse anti-human clone SKII.4 (Biolegend; San Diego, CA, USA) and compared to its isotype control PE-mouse IgG1 k clone MOPC-21 (Biolegend). For details on antibodies, see Appendix A: Antibody Table. Samples were fixed with paraformaldehyde solution 1% in PBS (PFA; Thermo Fisher Scientific) and analyzed within 24 hours on the BD LSR Fortessa™ (BD Biosciences) using the BD FACSDiva™ software version 8.0.3, at the University of Ottawa Flow Cytometry Core Facility (Ottawa, ON). Flow cytometric analysis of the human Sx-MDSC population was gated as $BV510^{-}/Lin^{-}/CD33^{+}/CD14^{+}/CD15^{lo}$ while the low-density (LD) neutrophils were gated $BV510^{-}/Lin^{-}/CD33^{+}/CD14^{-}/CD15^{hi}$.

3.5.2. Murine Samples

Murine cells were washed and stained with Fixable Viability Stain 510 (BD Biosciences), followed by BD Pharmingen™ Fc Block with Purified Rat Anti-Mouse CD16/32 (Mouse BD Fc Block™, BD Biosciences). These cells were then stained for extracellular murine MDSC surface markers (CD11b, GR1, CD155) and NK cell surface markers (CD122, DX5, DNAM-1 and NKG2D). CD155 expression was measured using APC-labelled rat anti-mouse clone TX56 (Biolegend) and compared to its isotype control APC-rat IgG2a k clone RTK2758 (Biolegend). In terms of NK markers, DNAM-1 was measured with BV421-rat anti-mouse

clone TX42.1 (Biolegend) and its isotype BV421-rat IgG2a k clone RTK2758 (Biolegend), while NKG2D with FITC-hamster anti-mouse clone C7 (Biolegend) and isotype FITC-armenian hamster IgG clone HTK888 (Biolegend). For details on antibodies, see Appendix A: Antibody Table. Samples were fixed with PFA and analyzed within 24 hours on the BD LSR Fortessa™ using the FACSDiva™ software version 8.0.3 (BD Biosciences) at the University of Ottawa Flow Cytometry Core Facility. Flow cytometric analysis of murine Sx-MDSCs, also known as M-MDSCs, were identified as $BV510^{-}/CD45^{+}/CD3^{-}/CD11b^{+}/GR1^{int}$ and granulocytes (which includes PMN-MDSCs and neutrophils) as $BV510^{-}/CD45^{+}/CD3^{-}/CD11b^{+}/GR1^{hi}$. NK cells were gated $BV510^{-}/CD45^{+}/ CD122^{+}/CD49b^{+}$.

3.6. *Ex Vivo* Murine NK Cytotoxicity Assay

On certain POD1 endpoints (n=3 experiments), processed splenocytes were pooled for each treatment group (minimum 4 mice per group). NK cells were isolated from pooled splenocytes using the EasySep™ Mouse NK Cell Isolation Kit (Stemcell; Vancouver, CA) as per the manufacturer's protocol for immunomagnetic negative selection. NK cells were washed twice in RPMI, counted by hemocytometer (HC) and resuspended to 1 $x10e^{6}$ cells/mL. NK cells were then plated in triplicates at the following diluted concentrations for effector-to-target (E:T) ratios 4:1 (20,000 cells/well), 2:1 (10,000 cells/well) and 1:1 (5,000 cells/well). At the same time, YAC-1 murine lymphoma target cells were washed in PBS, resuspended to 1 $x10e^{6}$ cells/mL and labelled with Cell Proliferation Dye eFluor™ 450 (CP450; eBioscience; San Diego, CA, USA) for 15 minutes at 37^{0}C. Labelling was stopped by washing in RPMI, counting by HC and resuspending to a concentration of 5 $x10e^{3}$ cells/mL (5,000 cells/well). CP450-YAC-1 cells were then plated with NK cells in triplicates, incubated for 4 hours at 37^{0}C, followed by addition of cell viability dye Invitrogen™ Propidium Iodide (PI; Thermo

Fisher Scientific). Samples were analyzed on the BD Celesta™ (BD Biosciences) at the University of Ottawa Flow Cytometry Core Facility. NK cytotoxicity was measured as the percentage of dead CP450-labelled YAC-1 target cells gated on $CP450^{+}/PI^{+}$.

3.7. *In Vivo* CD155 Blockade

The monoclonal anti-mouse CD155 clone 4.24.1 was previously shown to increase host NK cell DNAM-1 expression, as well as decrease tumour volume and lung metastases following IP injections(164). This antibody was administered in our murine model of surgical stress as described in 3.4 and outlined in Figure 4. Anti-mouse CD155 antibody (α-CD155) clone 4.24.1 (Leinco; St. Louis, MI, C2833 Low Endotoxin Functional Formulation) was injected IP at a dose of 500 ug on day 0. The next day, B16F10 CD155-KO melanoma cells were injected via IV tail vein (3 $x10e^{5}$ cells) followed 10 minutes later by laparotomy and nephrectomy. On POD1 or POD3, mice were sacrificed and splenocytes isolated by our standard protocol described in 3.4. Splenocytes were stained for flow cytometric analysis of extracellular NK cell surface markers, including DNAM-1 and NKG2D. Additionally, on POD1 NK cells were isolated for an *ex vivo* NK cytotoxicity assay as per our protocol described in 3.6. At one POD3 endpoint, B16F10-LacZ cells were used to visualize lung metastases. Lungs were stained and images were obtained using our protocol detailed in section 3.4.

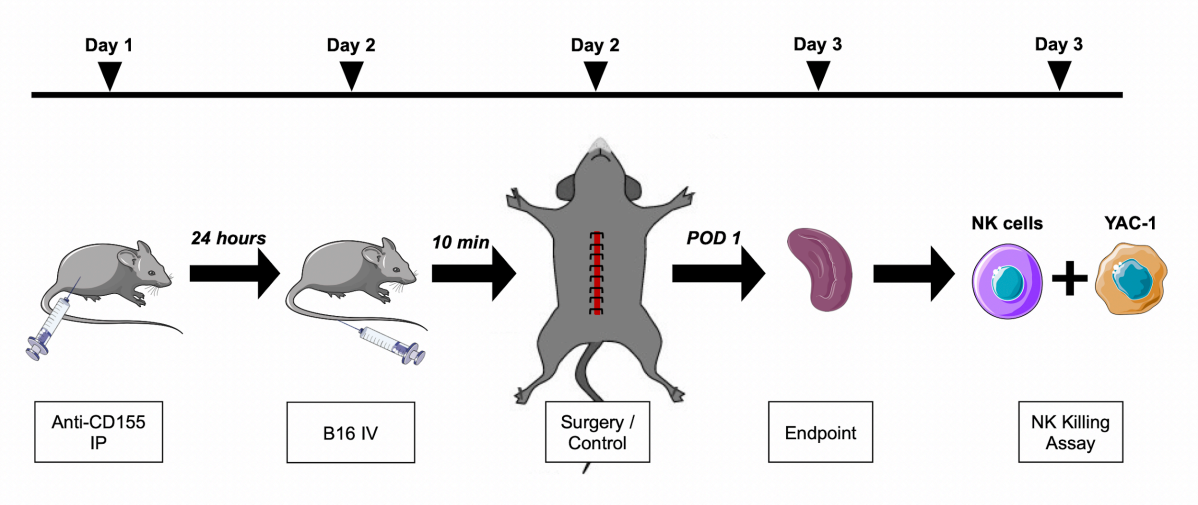
Day 1
Day 2
Day 2
Day 3
Day 3
24 hours
10 min
POD 1
NK cells
YAC-1
Anti-CD155 IP
B16 IV
Surgery / Control
Endpoint
NK Killing Assay

Figure 4. Modified Animal Model of Surgical Stress with *In Vivo* CD155 Blockade.
Representative flow diagram of the modified surgical stress model of *in vivo* CD155 blockade. The day before B16F10-CD155 KO tumour injections, mice receive α-CD155 IP (500 mg, clone 4.24.1). Surgery also consists of laparotomy and left nephrectomy. On POD1, NK cells are isolated from the splenocytes for *ex vivo* cytotoxicity assay with YAC-1 murine target cells. *POD – Postoperative day.*

3.8. *Ex Vivo* Human Suppression Assay

3.8.1. Cell preparation

Our laboratory and others have confirmed that the human NK92-MI cell line commonly used in NK cytotoxicity assays does not express DNAM-1 (ATCC, CRL-2408™, data not shown) and cannot be used as effector cell to examine the impact of *ex vivo* CD155 blockade on NK cell function. I therefore created and optimized a new protocol using healthy donor NK cells. In this new co-culture suppression model, NK cells were sorted on Miltenyi autoMACS Pro Separator™ (Miltenyi; Bergisch Gladbach, Germany) using StraightFrom™ Whole Blood CD56 Microbeads (Miltenyi) as per the manufacturer's standard protocol. Isolated NK cells were washed with RPMI, counted by HC and resuspended to 1.1 x10e^5 cells/mL in RPMI. PBMCs were isolated from POD1 cancer patient blood (n=3) using the standard Ficoll-Paque PLUS™ protocol described in 3.3. Sx-MDSCs were positively sorted on the autoMACS Pro Separator™ (Miltenyi) using CD33 MicroBeads™ (Miltenyi) as per the standard manufacturer protocol. Sx-MDSCs were then washed with RPMI, counted by HC, resuspended to 4 x10e^5 cells/mL and plated in triplicates. Minimum acceptable cell viability for the NK cells and Sx-MDSCs was set at 92%.

3.8.2. *Ex vivo CD155 blockade and plating*

Cell surface CD155 was blocked by incubating isolated Sx-MDSCs for 30 minutes with a purified monoclonal anti-human CD155 clone SKII.4 (Biolegend) or isotype control purified mouse IgG1 k (Biolegend). CD33$^+$ Sx-MDSCs were then co-incubated in triplicates for 20 hours with CD56$^+$ healthy NK cells at a ratio of 4:1 Sx-MDSCs (4 x10e^5 cells/well) to NK cells (1 x10e^5 cells/well). The next day, K562 leukemia target cells were washed in PBS,

resuspended to 1 x10e^6 cells/mL and labelled with CP450 (eBioscience) for 15 minutes at 37^{0}C. Labelling was stopped by washing in RPMI, counting by HC and resuspending to a concentration of 1 x10e^5 cells/mL. CP450-K562s were then plated at 5,000 cells/well for a final E:T ratio of 8:2:1 (MDSC:NK:K562), incubated for 4 hours at 37^{0}C, followed by plating of cell viability dye PI (Thermo Fisher Scientific). Samples were analyzed on the BD Celesta^{TM} (BD Biosciences) at the University of Ottawa Flow Cytometry Core Facility. NK cytotoxicity was measured as the percentage of dead CP450-K562s gated on CP450$^+$/PI$^+$. An outline of this novel suppression assay can be found in Figure 5.

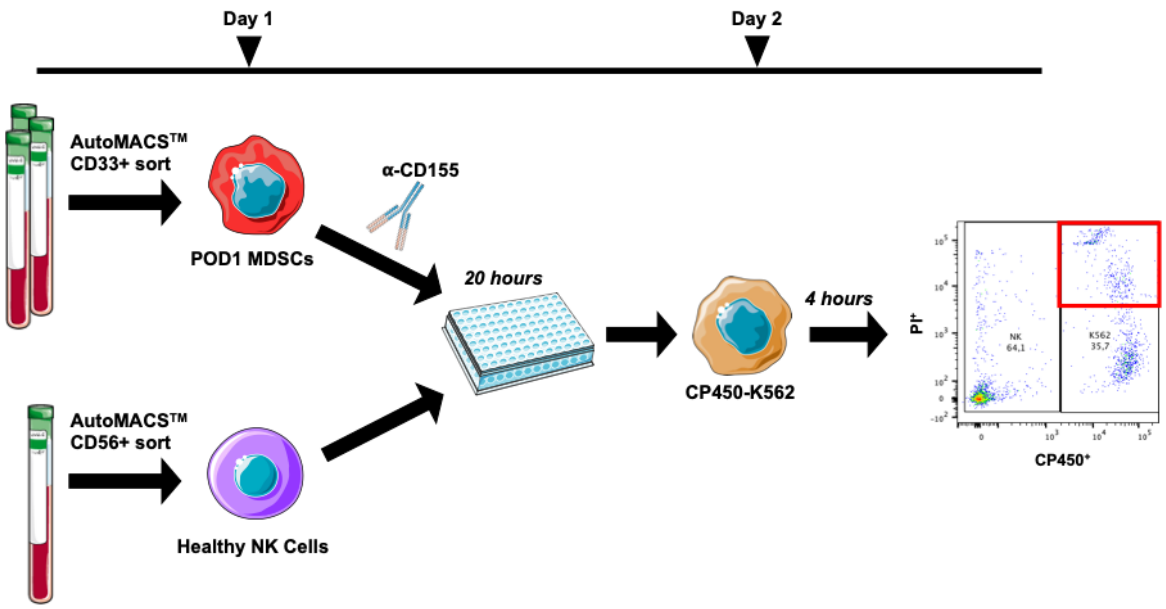
Day 1
Day 2
AutoMACS™
CD33+ sort
POD1 MDSCs
α-CD155
20 hours
4 hours
CP450-K562
PI+
NK
64,1
K562
35,7
CP450+
AutoMACS™
CD56+ sort
Healthy NK Cells

Figure 5. Representative Diagram of a Novel Human CD155 Suppression Assay.
Sx-MDSCs are isolated from POD1 cancer patient blood using $CD33^+$ Microbeads™ on the autoMACS Pro Separator™, incubated with purified human α-CD155 (clone SKII.4 or isotype control) and plated in triplicates. NK cells are isolated from healthy donor blood using StraightFrom™ whole blood CD56 Microbeads on the autoMACS Pro Separator™. Healthy NK cells are incubated ± Sx-MDSCs ± α-CD155 for 20 hours. On day 2, CP450-K562 target cells are plated for 4 hours for a final MDSC:NK:K562 ratio of 8:2:1. NK cytotoxicity is measured by flow cytometry as % dead K562s (gated $CP450^+/PI^+$).

3.9. Statistical Analysis and Software

FlowJo LLC software version 10.6.1 (FlowJo; Ashland, OR) was used for all flow cytometric gating and analyses (see 3.5 for gating details). Graphpad Prism software version 8.4, 464 (Graphpad; San Diego, CA, USA) was used for statistical analysis and to generate graphs. All data of biological and technical replicates for murine samples and cytotoxicity assays are represented in graphs as Mean ± Standard Deviation (SD). Because of inter-experimental variability in MFI and percentage for NKG2D and DNAM-1 (Figure 13), Mean of experimental replicates for POD1 and POD3 groups were normalized to the No Surgery group Mean and represented as fold change (FC) ± Standard Deviation (SD).

Due to the relatively small group sizes, all statistical analysis was done with non-parametric testing without assuming a normal distribution. Paired cancer patient samples comparing baseline to POD1 were analyzed by Wilcoxon matched rank test. For all unmatched human cancer patients and murine experiments, groups of two were analyzed by non-parametric Mann-Whitney test, while groups of 3 or more were compared by non-parametric Kruskal-Wallis testing. Statistical significance was determined as a p value < 0.05, and indicated in the figures as $*p < 0.05$, $**p < 0.005$, $***p < 0.0005$ and $****p < 0.0001$.

4. RESULTS

4.1. Perioperative profiling of CD155 in human cancer surgery patients

4.1.1. Clinical demographics of human cancer patients

For human studies, 20 cancer patients were recruited through PHBSP. Blood was processed at baseline the morning of surgery and on POD1. Details for human blood processing can be found in section 3.3. The cancer patients had a similar distribution between males (n=11) and females (n=9). Median age was 64, with 50% (10/20) of patients between 60-69 years of age. Most surgeries, 60% (12/20), were performed open by laparotomy compared to 40% (8/20) by minimally invasive surgery (MIS). For the types of cancers, there were 8 gastrointestinal (GI), 7 genitourinary (GU) and 5 lung cancers. Since we expected to observe the effect of MDSC CD155 expansion across all cancer subtypes, we did not restrict recruitment. Most patients recruited had early stage cancers as 90% (18/20) were either stage I (n=11) or stage II (n=7). There were only 2 stage III cancer patients and no stage IV patients since metastatic disease was part of the exclusion criteria in the study. However, these cancer patients were prospectively consented 1 to 3 days before surgery and final surgical pathology staging was used to determine cancer stage. Recruiting later stage cancers such as stage III was important to examine the CD155 mechanism in advanced cancers with possible micro-metastases around surgery. In terms of length of surgery, 85% (17/20) were greater than 2 hours with 35% (7/20) between 2-4 hours and 50% (10/20) greater than 4 hours. Of note, there were no significant differences in length of surgery between the open (mean 246 minutes) and MIS groups (mean 195 minutes, p=0.34). A summary of clinical demographics is outlined in Table 2.

Table 2. Clinical Demographics of CD155 Profiling in Cancer Patients.

Category	Subcategory	Cancer
Total (n)		20
Sex	Male (n)	11 (55%)
	Female (n)	9 (45%)
Patient Age (median years)		64; *45-83*
	< 60 years (n)	6
	60-69 years (n)	10
	> 70 years (n)	4
Type of Surgery	Open (n)	12 (60%)
	MIS (n)	8 (40%)
Type of Cancer	GI GU Lung	8 7 5
Cancer Stage	I II III IV	11 7 2 -
Length of Surgery	< 2 hours 2-4 hours > 4 hours	3 7 10

MIS – Minimally Invasive Surgery, GI – Gastrointestinal, GU – Genitourinary

4.1.2. Flow cytometry validation of perioperative human CD155 on Sx-MDSCs

The first step was to validate CD155 expression on human MDSCs by flow cytometry. A common flow cytometry gating strategy was used for all cancer patients (Figure 6A). After removing debris, doublets and dead cells, non-myeloid cells were excluded, including lymphocyte lineage (Lin) markers CD3, CD19, and CD56. Then, $CD33^+$ myeloid cells were further gated into Sx-MDSCs ($CD14^+/CD15^{lo}$) while the low-density (LD) neutrophils were gated $CD14^-/CD15^+$ (Figure 6A).

When comparing presentative histograms of a cancer patient for Sx-MDSC CD155 Mean Fluorescence Intensity (MFI) to its isotype, CD155 expression is much greater on POD1 (red) than at baseline before surgery (black, Figure 6B). Both POD1 and baseline samples were higher than the isotype control (green), which was the same at baseline or POD1 (Figure 6B). Additionally, POD1 LD neutrophils (blue) have significantly lower CD155 expression compared to POD1 Sx-MDSC (red, Figure 6C). In fact, LD-neutrophil CD155 MFI is almost equivalent to the isotype control (green, Figure 6C).

For the 20 cancer patients recruited, there is a statistically significant increase in Sx-MDSC CD155 expression on POD1 compared to baseline (BL; n=20, $p<0.0001$; red, Figure 6D) and this is much higher than the healthy donor (HD) controls (green, n=2, Figure 6D). However, CD155 is minimally expressed on other immune cell types and there is no increase with surgical stress, including $CD15^+$ LD-neutrophils (n=10, p=0.63; Figure 6E) and lymphocytes (NK cells, B cells and T cells; n=10, p=0.63; Figure 6E).

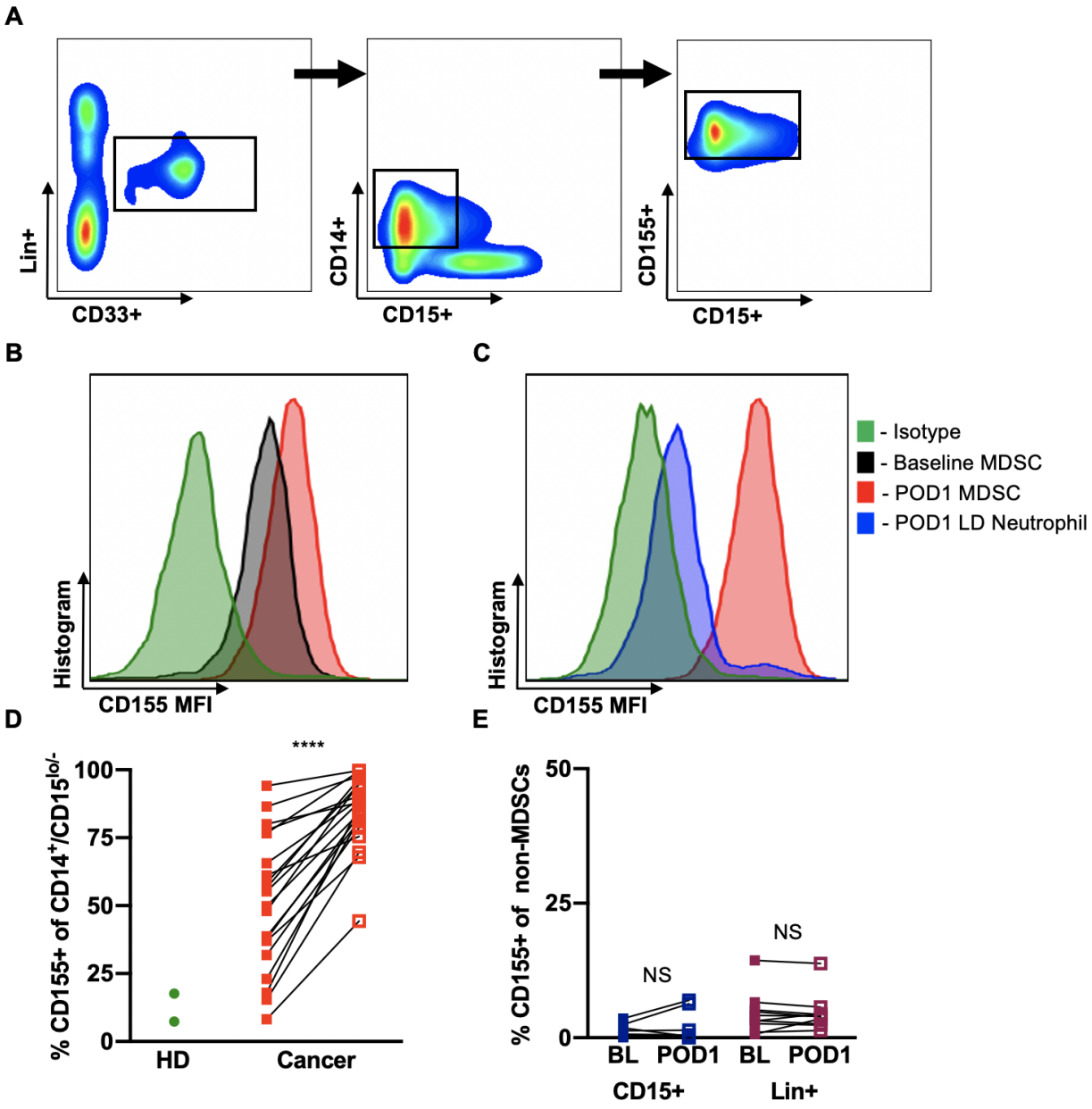
A
Lin+
CD33+
CD14+
CD15+
CD155+
CD15+
B
Histogram
CD155 MFI
C
Histogram
CD155 MFI
- Isotype
- Baseline MDSC
- POD1 MDSC
- POD1 LD Neutrophil
D
****
% CD155+ of CD14+/CD15lo/-
100
75
50
25
0
HD
Cancer
E
% CD155+ of non-MDSCs
50
25
0
NS
NS
BL
POD1
BL
POD1
CD15+
Lin+

Figure 6. Flow Phenotyping of Sx-MDSC CD155 in Human Cancer Patients.
A) Smooth plots representing the flow cytometry gating strategy for the human Sx-MDSC population, gated on $BV510^{-}/Lin^{-}/CD33^{+}/CD14^{+}/CD15^{lo}$ based on its isotype control. Lin gate excludes CD3, CD19, CD56. **B)** Representative histogram of CD155 MFI for one cancer patient at baseline (black) compared to POD1 (red). Isotype control also shown (green). **C)** Representative histogram of CD155 MFI for the same POD1 cancer patient. POD1 Sx-MDSC (red) compared to POD1 LD-neutrophils (blue). Isotype control shown (green). **D)** %CD155+ Sx-MDSCs on POD1 compared to baseline in cancer surgery patients (red, n=20). Healthy donor controls shown (HD, green, n=2). **E)** CD155 expression on POD1 compared to baseline for $CD15^{+}$ LD-neutrophils (blue, n=10) and Lin+ (NK/B/T cells; red, n=10). POD1 compared to baseline using paired non-parametric Wilcoxon matched rank test. NS= not significant, ****$p<0.0001$. *Lin – Lineage*, *LD – low density, HD – healthy donor*, *BL – baseline*

4.1.3. Subgroup analyses of Sx-MDSC CD155 in cancer patients

After confirming that the increase in postoperative CD155 expression is specific to the Sx-MDSC population, the next step was to perform CD155 subgroup analyses of these 20 cancer patients. Regardless of subgroup analysis, there was a profound upregulation of CD155 on POD1. When dividing based on age groups (<60, 60-69 and >70 years of age), although not statistically significant (p=0.27), CD155 appears to correlate with age where all low baseline CD155 (<25%) are patients younger than 60 years of age (Figure 7A). When comparing baseline CD155 between males and females, there does not appear to be a difference (Figure 7B, p=0.23).

In one set of subgroup analyses, we wanted to determine whether the degree of surgical stress could affect the increase in postoperative CD155 (Figure 7C-D). Although not statistically significant (p=0.1), the surgical approach may have an effect on CD155 levels by which open surgeries have a greater proportion of high (>50%) baseline CD155 (75%, 9/12) compared to MIS (12.5%, 1/8; Figure 7D).

Tumour biology itself may have an interesting correlation with baseline CD155. In terms of cancer type, there is a significant difference in baseline CD155 between GI, lung and GU cancers (p=0.02, Figure 7E). In fact, low baseline CD155 (30% or lower) were all GU while GI and lung cancers were above this threshold (Figure 7E). Additionally, CD155 correlated with cancer stage, where baseline CD155 was also significantly different between stage I, II and III cancers (p=0.02, Figure 7F). The low baseline levels of CD155 were all stage I cancers, whereas stage II and III all expressed greater than 50% at baseline. This appears to increase progressively with cancer stage, although only two stage III cancer patients were recruited (Figure 7F).

Together these results in human cancer patients suggest that human CD155 expression is specific to the M-MDSC population and baseline host CD155 may have important correlations with type of cancer and cancer stage. We next sought to examine whether this effect was recapitulated in our animal model of surgical stress.

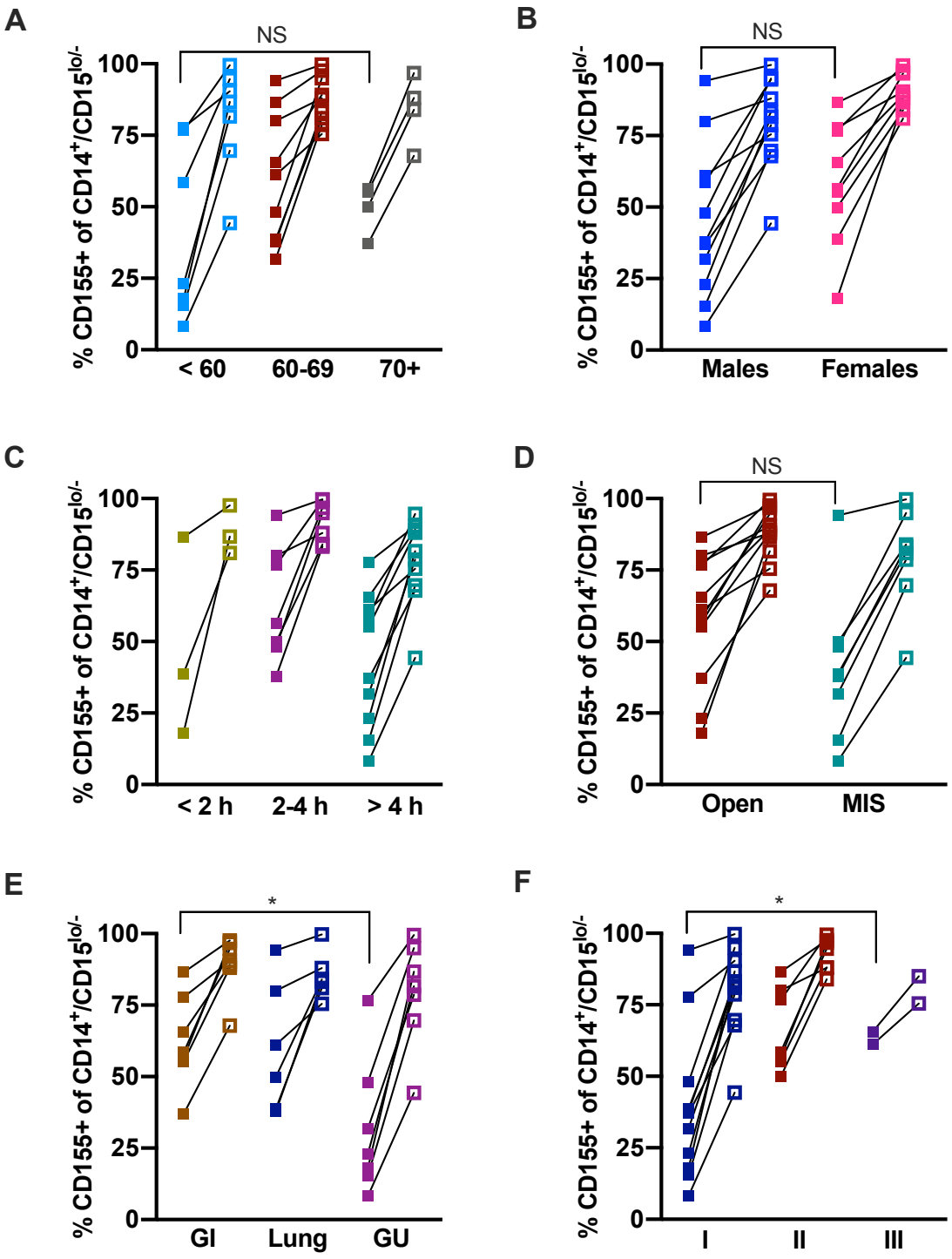
A
NS
% CD155+ of CD14+/CD15lo/-
100
75
50
25
0
< 60
60-69
70+
B
NS
% CD155+ of CD14+/CD15lo/-
Males
Females
C
% CD155+ of CD14+/CD15lo/-
< 2 h
2-4 h
> 4 h
D
NS
% CD155+ of CD14+/CD15lo/-
Open
MIS
E
*
% CD155+ of CD14+/CD15lo/-
GI
Lung
GU
F
*
% CD155+ of CD14+/CD15lo/-
I
II
III

Figure 7. Perioperative Sx-MDSC CD155 Profiling in Human Cancer Patients.
A) %CD155+ Sx-MDSC in patients < 60 years old (blue, n=7), 60-70 years old (red, n=9), >70 years old (grey, n=4). **B)** %CD155+ Sx-MDSC between males (blue, n=11) and females (pink, n=9). **C)** %CD155+ divided by length of surgery less than 2 hours (yellow, n=3), 2 to 4 hours (purple n=7) and more than 4 hours (teal, n=10). **D)** CD155+ between surgical approach, open (red, n=12) and MIS (teal, n=8). **E)** %CD155+ based on different types of cancer: GI (brown, n=8), lung (blue, n=5), GU (purple, n=7). **F)** %CD155+ between cancer stages, stage I (blue, n=11), stage II (red, n=7), stage III (purple, n=2). Non-matched baseline compared by non-parametric Mann-Whitney (2 groups) or Kruskal-Wallis (3 groups). NS= not significant, *$p<0.05$. *MIS – Minimally Invasive Surgery, GI – Gastrointestinal, GU – Genitourinary.*

4.2. MDSCs and granulocytes both expand postoperatively

Firstly, based on the theory of emergency myelopoiesis, one would expect to see a dramatic and immediate increase in immature myeloid cells (IMCs) following surgical stress. As explained in the introduction, human HD neutrophils were separated from PMN-MDSCs, also known as LD neutrophils, during Ficoll separation. In murine experiments however, PMN-MDSCs cannot be separated from neutrophils and these are both included in the granulocyte population. For that reason, and the fact that emergency myelopoiesis greatly expands immature monocytes, we decided to focus our investigations on the M-MDSC population specifically, termed Sx-MDSC following surgery.

In several murine experiments (n=15), I have seen a significantly increased frequency of myeloid cells postoperatively (Figure 8). Interestingly, these results highlight distinct differences in the accumulation of myeloid populations in the spleen with no significant increase in Sx-MDSCs until POD3 (n=63, $p<0.0001$; Figure 8A), whereas granulocytes increase on POD1 (n=45, $p<0.0001$) and remain elevated on POD3 (n=65, $p<0.0001$; Figure 8B). In the blood, Sx-MDSCs increase significantly on POD1 (n=15, $p<0.0001$) and remain elevated on POD3 (n=15, $p<0.0001$; Figure 8C) while granulocytes peak on POD1 (n=15, $p<0.0001$) but decrease by POD3 (n=15, $p=0.0003$; Figure 8D). These results were pooled with animal experiments previously completed in the laboratory by Leonard Angka, PhD candidate.

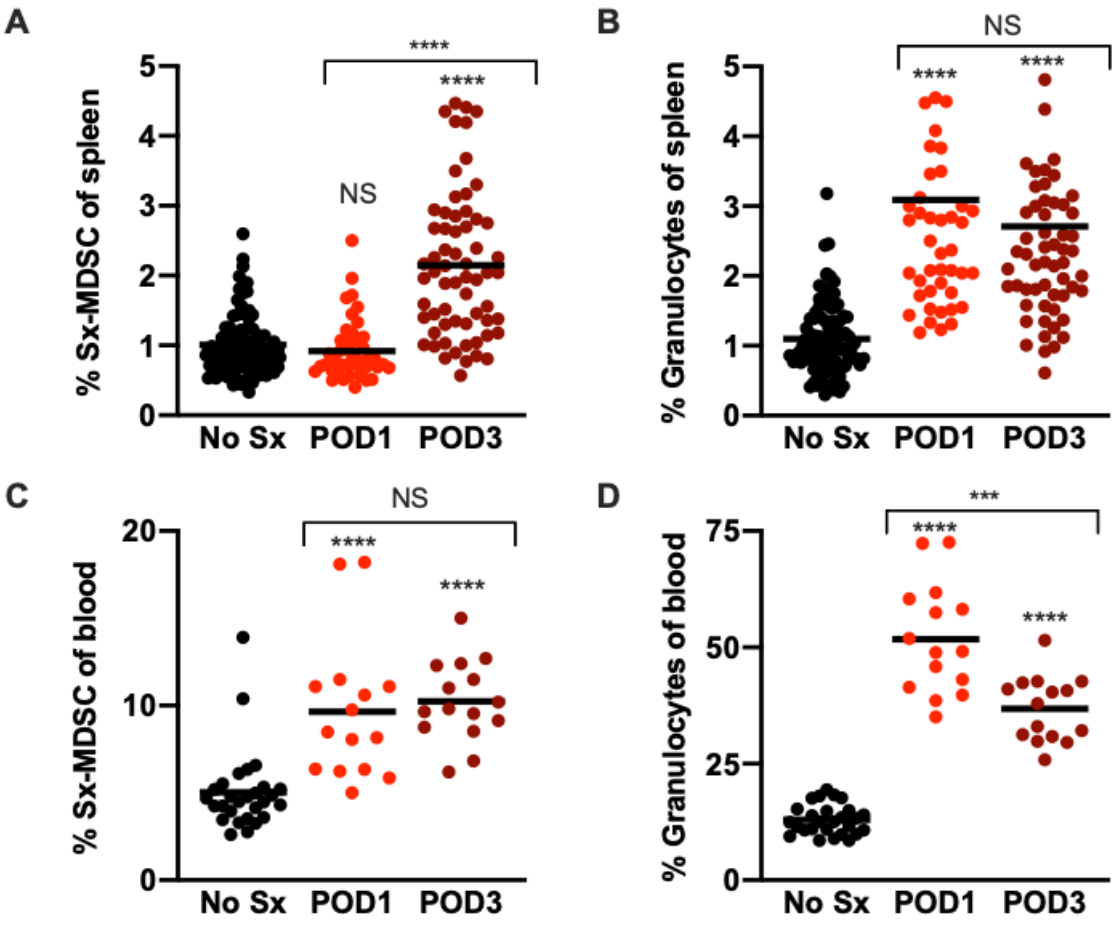
A
% Sx-MDSC of spleen
5
4
3
2
1
0
****
****
NS
No Sx
POD1
POD3
B
% Granulocytes of spleen
NS
****
****
C
% Sx-MDSC of blood
20
10
0
NS
****
****
D
% Granulocytes of blood
75
50
25
0
***
****
****

Figure 8. Surgery-Induced Myeloid-Derived Suppressor Cells (Sx-MDSCs) and Granulocytes Expand Following Surgical Stress.
A) Sx-MDSCs isolated from the spleen on POD1 (red, n=45) and POD3 (maroon, n=63) compared to no surgery (black, n=95). **B)** Granulocytes isolated from the spleen on POD1 (red, n=45) and POD3 (maroon, n=63) compared to no surgery (black, n=95). **C)** Sx-MDSCs isolated from blood on POD1 (red, n=15) and POD3 (maroon, n=15) compared to no surgery (black, n=30). **D)** Granulocytes isolated from blood on POD1 (red, n=15), and POD3 (maroon, n=15) compared to no surgery (black, n=30). All samples are shown as Mean of Scatter Dot Plots. Groups compared by non-parametric Mann-Whitney. NS= not significant, ****$p<0.0001$, ***$p<0.0005$. *No Sx – No Surgery, POD – Postoperative day.* NB – data is pooled with experiments completed by AB Martel and L Angka.

4.3. Flow cytometry validation of cell populations in our murine model of surgical stress

4.3.1. Confirming CD155 expression in murine melanoma cell lines

Prior to characterizing CD155 in our murine model of surgical stress, we initially wanted to confirm CD155 expression levels in the 3 murine B16F10 melanoma cell lines: B16F10-LacZ, B16F10-WT, and B16F10-CD155 KO. As detailed in methodology section 3.1, the latter 2 cell lines were provided by Dr. Smyth's research group (QIMR Medical Research Institute, Herston, Queensland, Australia). Flow cytometry gating of these melanoma cells was done by first excluding all debris and doublets based on FSC/SSC, excluding dead cells ($BV510^{+}$) and then measuring CD155 based on $CD45^{-}/CD3^{-}$ (Figure 9A). CD155 was gated based on its isotype control (Figure 9B). Both B16F10-LacZ and B16F10-WT cell lines expressed greater than 99% CD155 while the B16F10-CD155 KO did not express any (0.99%, Figure 9C). Importantly, in order to mitigate the effect tumour CD155 expression may have on the postoperative NK cell phenotype (DNAM-1 and NKG2D) and cytotoxicity, all following murine experiments were performed with the B16F10-CD155 KO cell line unless specifically stated.

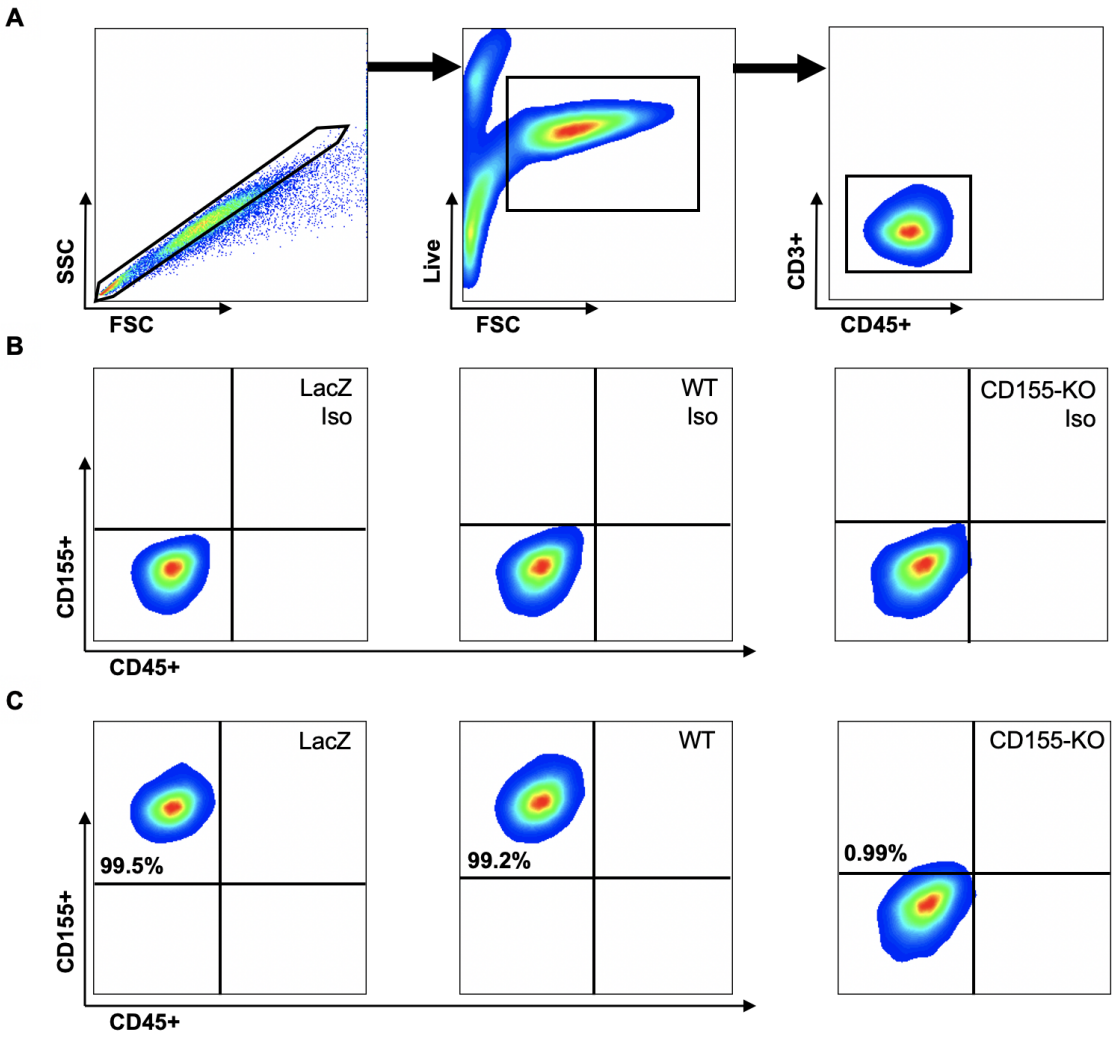
A
SSC
FSC
Live
FSC
CD3+
CD45+
B
LacZ
Iso
WT
Iso
CD155-KO
Iso
CD155+
CD45+
C
LacZ
99.5%
WT
99.2%
CD155-KO
0.99%
CD155+
CD45+

Figure 9. Validation of CD155 Expression in Murine B16F10 Melanoma Cells.
A) Smooth plots representing the flow cytometry gating strategy for murine melanoma tumour cell lines. After removing debris, doublets and dead cells, CD155 expression is measured after gating $CD45^{-}/CD3^{-}$. **B)** Smooth plots of the IgG2a isotype controls (clone RTK2758) for all 3 cell lines: B16F10-LacZ, B16F10-WT, and B16F10-CD155 KO. **C)** Smooth plots of tumour CD155 expression (clone TX56) for all 3 cell lines: B16F10-LacZ (99.5%), B16F10-WT (99.2%) and B16F10-CD155KO (0.99%). *SSC – Side scatter, FSC – Forward scatter, Iso – Isotype, WT – Wild type, KO – knockout*.

4.3.2. Phenotyping of immune cell populations

Our established animal model of surgical stress, detailed in section 3.4, is our standard model to examine the effect of cancer surgery on different immune cell populations. We used B16F10-CD155 KO melanoma injections prior to laparotomy and nephrectomy to minimize the effect of tumour CD155 on the immune response. On POD1, mice were endpointed and splenocytes processed for flow cytometry validation. Cell processing details can be found in section 3.5.

Figure 10 illustrates the key flow cytometry gating strategies used to identify the important murine immune cell populations: Sx-MDSCs, granulocytes and NK cells. After excluding debris and doublets based on FSC/SSC and dead cells ($BV510^{+}$), cells were further gated $CD45^{+}/CD3^{-}$. The $CD11b^{+}$ myeloid cells were separated based on granularity; granulocytes are $GR1^{hi}$ while Sx-MDSCs are $GR1^{int}$ (Figure 10A). The NK cells on the other hand were gated based on the double positive population of $CD122^{+}/DX5^{+}$ (Figure 10B). After validating and optimizing the general flow cytometry staining of these cells, specific perioperative surface markers of interest were analyzed, including CD155 on myeloid cells, as well as DNAM-1 and NKG2D on NK cells.

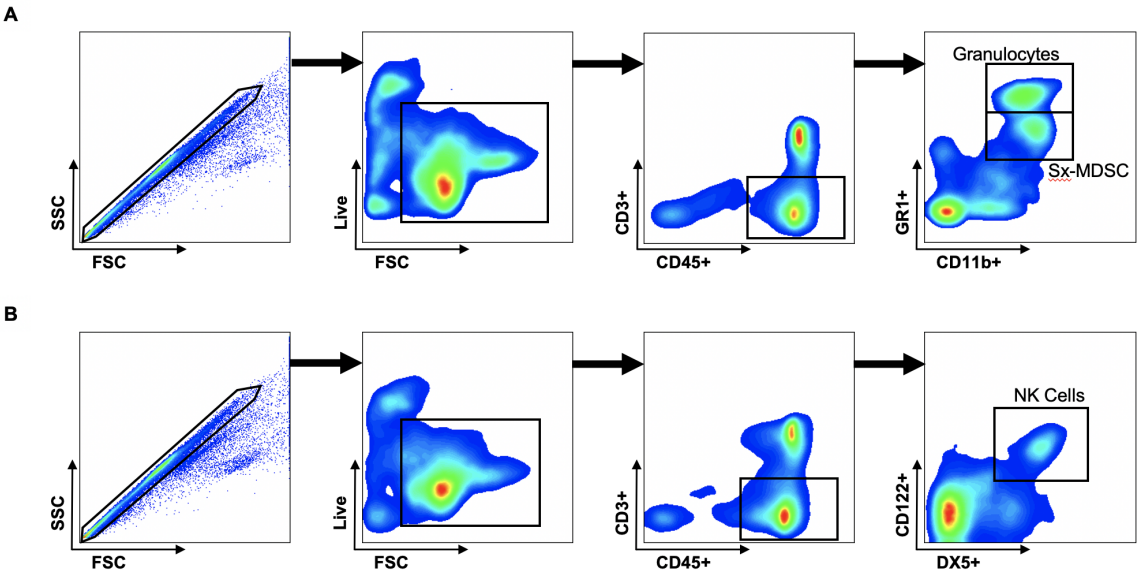
A
SSC
FSC
Live
FSC
CD3+
CD45+
Granulocytes
Sx-MDSC
GR1+
CD11b+
B
SSC
FSC
Live
FSC
CD3+
CD45+
NK Cells
CD122+
DX5+

Figure 10. Flow Cytometry Gating of Postoperative Murine Immune Cell Populations. **A)** Smooth plots representing the flow cytometry gating strategy for murine Granulocyte and Sx-MDSC populations. After removal of debris, doublets and $BV510^{+}$ dead cells, gating follows $CD45^{+}/CD3^{-}/CD11b^{+}$ and $GR1^{hi}$ for granulocytes whereas Sx-MDSC are $GR1^{int}$. **B)** Smooth plots illustrating the flow cytometry gating strategy for murine NK cells. Following removal of debris, doublets and dead cells, gating follows $CD45^{+}/CD3^{-}/CD122^{+}/DX5^{+}$. NK cells are identified as the double positive $CD122^{+}/DX5^{+}$ population.

4.4. Postoperative CD155 upregulation is specific to Sx-MDSCs in our murine model of surgical stress

The next step was to examine the effect surgical stress may have on CD155 expression for the $GR1^{hi}$ granulocytes and $GR1^{int}$ Sx-MDSCs. When comparing representative smooth plots of % CD155 expression, Sx-MDSCs have low levels of CD155 at baseline without surgical stress (7.14%) but this increases dramatically on POD1 (44.4%) and persists until POD3 (59.6%, Figure 11A). In contrast, granulocytes have minimal CD155 expression at baseline (1.89%), on POD1 (2.11%) and POD3 (1.86%, Figure 11B). These samples were all gated based on their specific isotype controls.

When analyzing samples from all murine experiments (n=7), examination of CD155 MFI (Figure 11C) and % CD155+ cells (Figure 11D) on these populations revealed a consistent and statistically significant upregulation of CD155 on postoperative Sx-MDSCs as early as POD1 ($n=25$, $p<0.0001$) and interestingly, the effect persists on POD3 ($n=11$, $p<0.0001$). However, minimal CD155 expression was observed on $GR1^{hi}$ granulocytes at all perioperative timepoints and there was no significant increase of granulocyte-CD155 expression on POD1 or POD3, regardless of MFI (POD1 $p=0.24$, POD3 $p=0.02$; Figure 11E) or percentage (POD1 $p=0.83$, POD3 $p=0.98$; Figure 11F). These findings in our animal model are in keeping with the human cancer patient results that postoperative CD155 expression is consistent and specific to Sx-MDSCs while granulocytes have minimal CD155 expression at any perioperative timepoint.

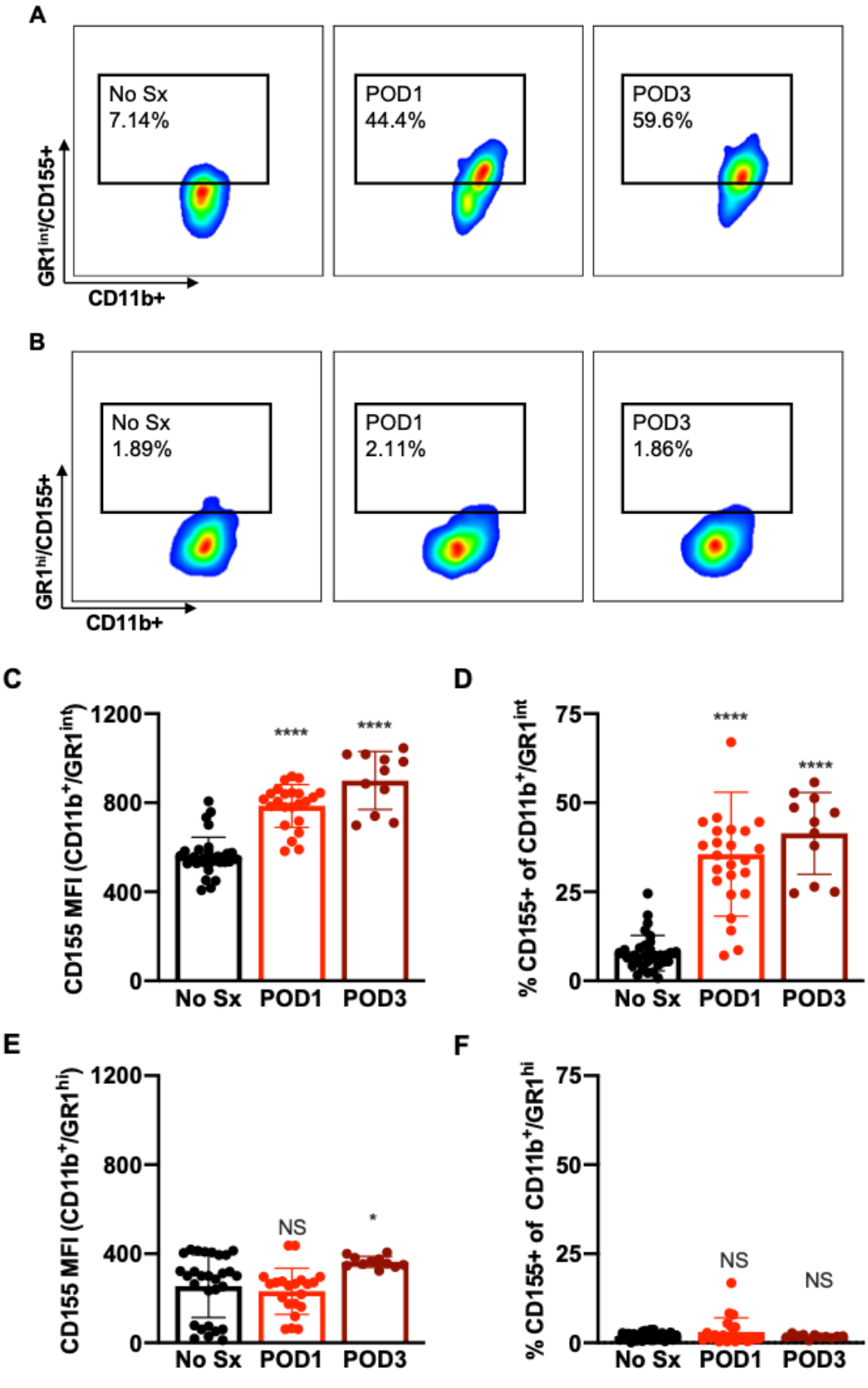
A
No Sx
7.14%
POD1
44.4%
POD3
59.6%
GR1int/CD155+
CD11b+
B
No Sx
1.89%
POD1
2.11%
POD3
1.86%
GR1hi/CD155+
CD11b+
C
CD155 MFI (CD11b+/GR1int)
1200
800
400
0
****
****
No Sx
POD1
POD3
D
% CD155+ of CD11b+/GR1int
75
50
25
0
****
****
No Sx
POD1
POD3
E
CD155 MFI (CD11b+/GR1hi)
1200
800
400
0
NS
*
No Sx
POD1
POD3
F
% CD155+ of CD11b+/GR1hi
75
50
25
0
NS
NS
No Sx
POD1
POD3

Figure 11. Postoperative CD155 is Specific to Surgery-Induced MDSCs (Sx-MDSCs)
A) Representative smooth plots of CD155 expression on $CD11b^{+}/GR1^{int}$ MDSCs at various perioperative timepoints: no surgery (7.14%), POD1 (44.4%) and POD3 (59.6%). **B)** Representative smooth plots of CD155 expression on $CD11b^{+}/GR1^{hi}$ granulocytes at various time points: no surgery (1.89%), POD1 (2.11%) and POD3 (1.86%). **C)** CD155 MFI of MDSCs on POD1 (red, n=25) and POD3 (maroon, n=11) compared to no surgery (black, n=33). **D)** %CD155+ MDSCs on POD1 (red, n=25) and POD3 (maroon, n=11). **E)** CD155 MFI of granulocytes on POD1 (red, n=21) and POD3 (maroon, n=11) compared to no surgery (black, n=33). **F)** %CD155+ granulocytes on POD1 (red, n=21) and POD3 (maroon, n=11). All samples shown are Mean ± SD. POD1 and POD3 groups compared to no surgery by non-parametric Mann-Whitney. NS= not significant, ****$p<0.0001$, *$p<0.05$.

4.5. Perioperative characterization of murine activating NK cell receptors

As a result of the increase in Sx-MDSC CD155 expression following surgical stress, one would expect a direct downregulation in its only known activating receptor DNAM-1 as previously seen in several cancer models (10, 32, 136, 164, 166, 167). While surgical stress does not lead to a significant decrease in DNAM-1 MFI on POD1 ($n=21$, $p=0.63$) or POD3 ($n=13$, $p=0.94$; Figure 12A), the percentage of DNAM-1+ NK cells is significantly decreased on POD1 ($n=12$, $p<0.0001$) and POD3 ($n=9$, $p=0.003$; Figure 13B). Because of inter-experimental variability, the NK cell data was normalized to the No Surgery group (Figure 13).

As an additional marker of NK cell dysfunction, we examined the stress-induced activating receptor NKG2D. Although its MFI is relatively normal on POD1 ($n=21$, $p=0.47$), the %NGK2D+ is significantly decreased on POD1 ($n=12$, $p<0.0001$; Figure 12C). Furthermore, NKG2D has a profound decrease on POD3 for both MFI ($n=13$, $p<0.0001$; Figure 12C) and % ($n=9$, $p=0.003$; Figure 12D), suggesting an exhausted NK cell phenotype by POD3.

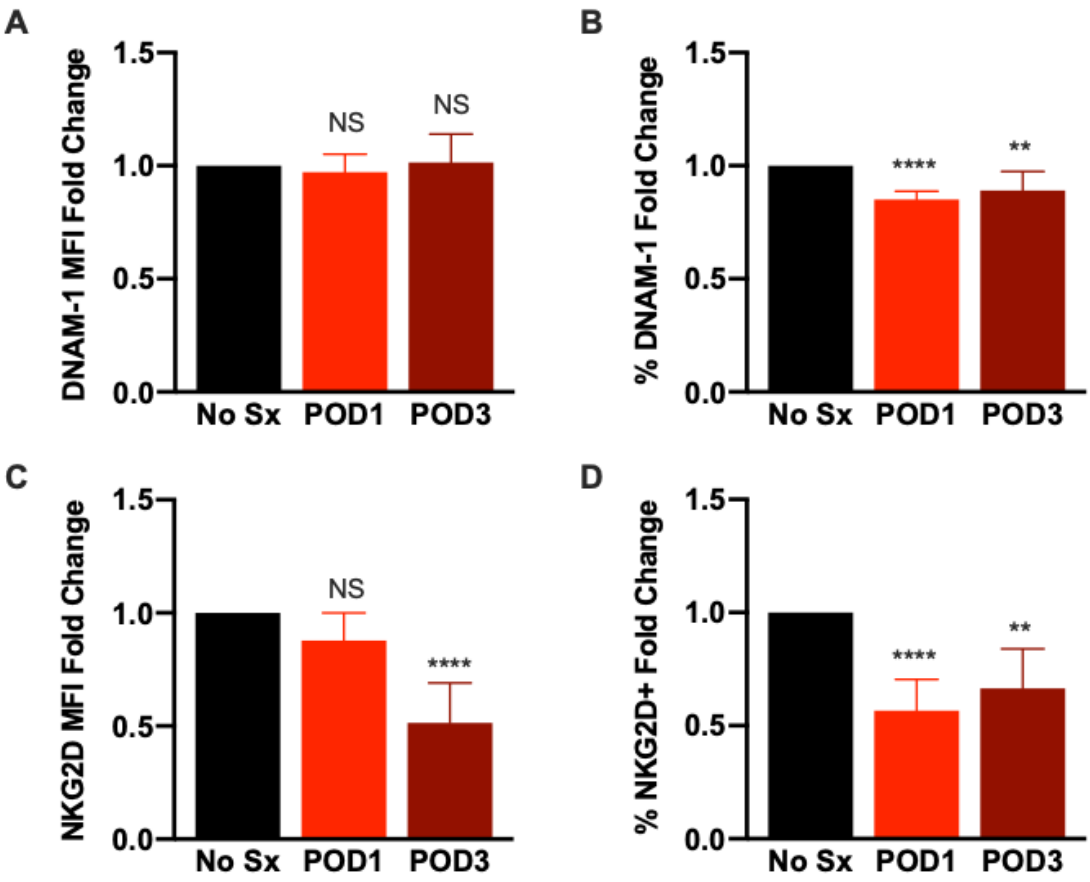
A
DNAM-1 MFI Fold Change
1.5
1.0
0.5
0.0
NS
NS
No Sx
POD1
POD3
B
% DNAM-1 Fold Change
1.5
1.0
0.5
0.0
****
**
No Sx
POD1
POD3
C
NKG2D MFI Fold Change
1.5
1.0
0.5
0.0
NS
****
No Sx
POD1
POD3
D
% NKG2D+ Fold Change
1.5
1.0
0.5
0.0
****
**
No Sx
POD1
POD3

Figure 12. Activating NK Cell Receptor Changes Following Surgical Stress.
A) DNAM-1 MFI fold change for $CD122^{+}/DX5^{+}$ NK cells on POD1 (red, n=21) and POD3 (maroon, n=13) normalized to no surgery (black, n=33). **B)** %DNAM-1+ fold change for NK cells on POD1 (red, n=12) and POD3 (maroon, n=9) normalized to no surgery (black, n=33). **C)** NKG2D MFI fold change for NK cells on POD1 (red, n=21) and POD3 (maroon, n=13) normalized to no surgery (black, n=21). **D)** %NKG2D+ fold change for NK cells on POD1 (red, n=12) and POD3 (maroon, n=9) compared to no surgery (black, n=21). All samples shown are Mean ± SD. POD1 and POD3 groups compared to no surgery by non-parametric Mann-Whitney. NS= not significant, ****p<0.0001, **p<0.005.

4.6. Targeting CD155 *in vivo* is sufficient to restore NK cell function and reduce metastases in our murine model of surgical stress

4.6.1. Titrating anti-CD155 blocking antibody in vivo

Flow phenotyping of the NK cell population suggests that following surgical stress, NK cells develop a dysfunctional phenotype as evidenced by a decrease in DNAM-1 and NKG2D. Based on our rationale that CD155 blockade should result in improved NK cell function through upregulation of DNAM-1, the next step consisted in optimizing the dose of *in vivo* anti-CD155 antibody. Li *et al.* previously used 250 ug of the mouse α-CD155 clone 4.24.1 to examine the effect on DNAM-1 expression in naïve mice (164).

We therefore titrated the same antibody clone at the following doses in our animal model of surgical stress: 0, 250, 500 and 750 µg. Although not statistically significant because of low group numbers (n=3), administering 500 µg of α-CD155 led to the greatest increase in DNAM-1 expression at baseline and on POD1 (Figure 13A). Additionally, mice receiving 500 µg of α-CD155 had higher levels of NKG2D at baseline and this was even more pronounced on POD1 (Figure 13B). When examining Sx-MDSCs for a corresponding decrease in CD155 expression, all 3 doses of α-CD155 (250, 500 and 750 µg) led to a similar amount of CD155 downregulation compared to the negative control for percentage (Figure 13C) and MFI (Figure 13D).

Following dose titration, 500 µg was determined as the optimal dose, as measured by the greatest increase in DNAM-1 expression while minimizing the postoperative downregulation of NKG2D. We then proceeded to further investigate the effects of *in vivo* blockade on the postoperative NK cell phenotype, including NK cytotoxicity.

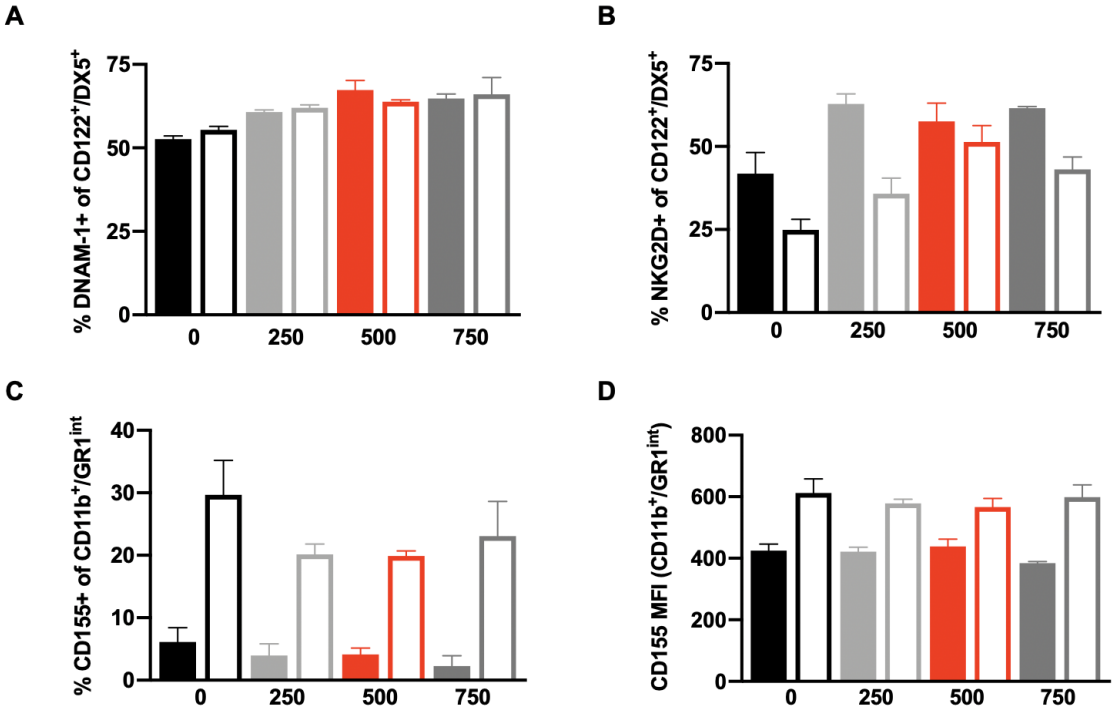
A
% DNAM-1+ of CD122+/DX5+
75
50
25
0
0
250
500
750
B
% NKG2D+ of CD122+/DX5+
75
50
25
0
0
250
500
750
C
% CD155+ of CD11b+/GR1int
40
30
20
10
0
0
250
500
750
D
CD155 MFI (CD11b+/GR1int)
800
600
400
200
0
0
250
500
750

Figure 13. *In Vivo* Titration of α-CD155 in our Animal Model of Surgical Stress.
A) % DNAM-1+ of $CD122^{+}/DX5^{+}$ NK cells for the following α-CD155 IP doses (clone 4.24.1): 0 mg, 250 mg, 500 mg and 750 mg. Full boxes represent no surgery (n=3 per dose), empty boxes POD1 (n=3 per dose). **B)** %NKG2D+ of NK cells with the same α-CD155 conditions. **C)** %CD155+ of $CD11b^{+}/GR1^{int}$ MDSCs with the same α-CD155 doses. No surgery (full boxes, n=3 per dose) compared to POD1 (empty boxes, n=3 per dose). **D)** CD155 expression of $CD11b^{+}/GR1^{hi}$ granulocytes with the same conditions. All samples shown are Mean ± SD.

4.6.2. In Vivo CD155 blockade improves NK cell phenotype and cytotoxicity

In all *in vivo* blockade experiments (n=3) with the optimal α-CD155 dose of 500 μg, expression of DNAM-1 was significantly increased in the groups receiving the antibody. At baseline, there was a significant increase (n=13, p=0.04) and the effect was greatest on POD1 (n=5, p=0.008; Figure 14A). Importantly, without α-CD155 there was a significant downregulation of DNAM-1 on POD1 (n=5, p=0.0002), but administering α-CD155 prevented the decrease in DNAM-1 after surgery (n=5, p=0.55; Figure 14A).

When compared to baseline, NKG2D expression decreased on POD1 without α-CD155 (n=8, p<0.0001) and with α-CD155 (n=8, p=0.01). While NKG2D expression did not change following CD155 blockade at baseline (n=13, p=0.24), NKG2D significantly increased on POD1 in the mice receiving α-CD155 (n=8, p=0.0002; Figure 14B). Together these results highlight an important role for Sx-MDSC CD155 expression on the postoperative NK cell phenotype.

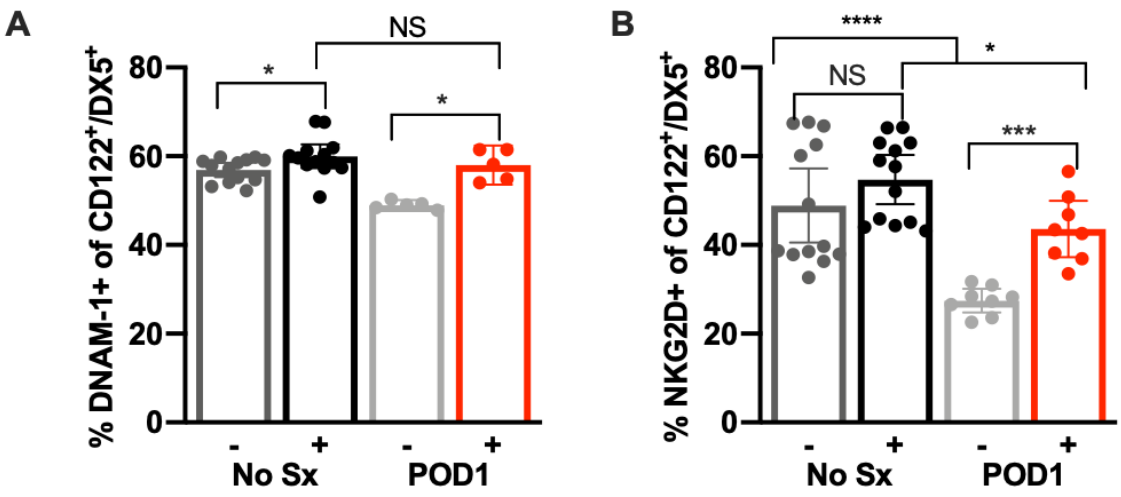
A
% DNAM-1+ of CD122+/DX5+
80
60
40
20
0
*
NS
*
-
+
-
+
No Sx
POD1
B
% NKG2D+ of CD122+/DX5+
80
60
40
20
0
****
*
NS
***
-
+
-
+
No Sx
POD1

Figure 14. *In vivo* CD155 Blockade Improves the Postoperative NK Cell Phenotype. **A**) % DNAM1+ NK cells ($CD122^+/DX5^+$). In no surgery groups, + α-CD155 (black, n=13) compared to – α-CD155 (dark grey, n=13). On POD1, + α-CD155 (red, n=5) compared to – α-CD155 (light grey, n=5). **B)** %NKG2D+ NK cells. In no surgery croups, + α-CD155 (black, n=13) compared to – α-CD155 (dark grey, n=13). On POD1, + α-CD155 (red, n=5) compared to – α-CD155 (light grey, n=5). All samples shown are Mean ± SD. Groups compared by non-parametric Mann-Whitney test. NS= not significant, ****$p<0.0001$, ***$p<0.0005$, *$p<0.05$.

Additionally, during *ex vivo* NK cytotoxicity assays, NK cells were isolated from pooled splenocytes using the EasySep™ Mouse NK Cell Isolation Kit (Stemcell, section 3.6 for details). This cytotoxicity assay was completed once, with increasing Effector-to-Target (E:T) ratios of 1:1, 2:1, and 4:1. Compared to the mice without antibody treatment, mice receiving α-CD155 injections at a dose of 500 µg IP prior to surgical stress showed enhanced killing of YAC-1 target cells. Of note, there was no isotype control used in the negative control for this experiment. At baseline (No Surgery groups), NK cytotoxicity of α-CD155 treated mice was slightly higher (black) than the control mice (dark grey, Figure 15A). Interestingly, this effect was even more pronounced following surgical stress at which time CD155 blockade led to greater cytotoxicity (red) than the control mice (light grey, Figure 15B-C). In fact, the greatest difference can be seen on POD1 at an E:T ratio of 4:1, with a mean NK killing of 52% with α-CD155 compared to 37.8% without antibody (Figure 15B-C). Since this was a single experiment of technical replicates (n=3), statistical significance was not determined due to low numbers.

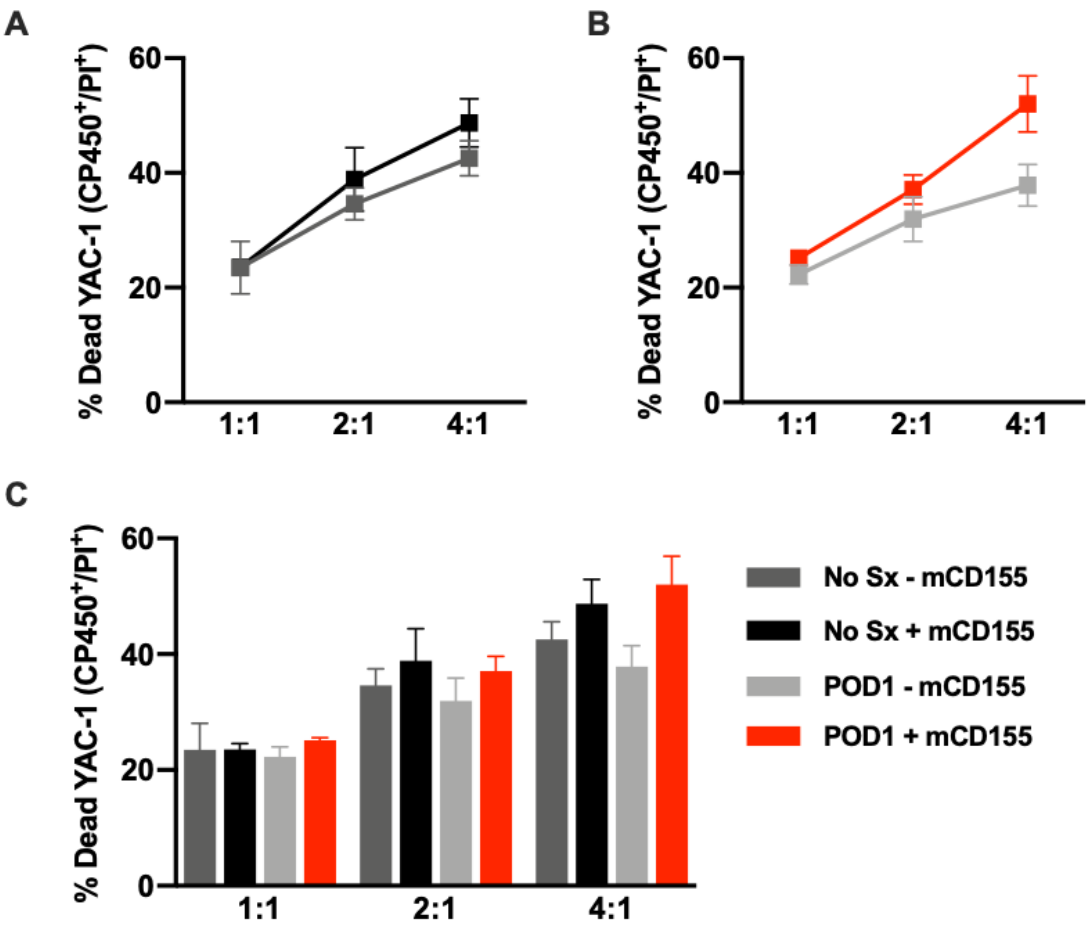
A
B
C
% Dead YAC-1 (CP450+/PI+)
60
40
20
0
1:1
2:1
4:1
No Sx - mCD155
No Sx + mCD155
POD1 - mCD155
POD1 + mCD155

Figure 15. NK Cytotoxicity Following *In Vivo* CD155 Blockade.
A) Baseline NK cytotoxicity assay of % dead YAC-1 ($CP450^{+}/PI^{+}$) with effector to target ratio 1:1, 2:1, 4:1. + α-CD155 (black) compared to – α-CD155 (dark grey). **B)** POD1 NK cytotoxicity assay of % dead YAC-1 cells with effector to target ratio 1:1, 2:1, 4:1. + α-CD155 (red) compared to – α-CD155 (light grey). **C)** Overview of combined baseline and POD1 NK cytotoxicity assay in bar graph format. All samples shown are Mean of triplicates ± SD.

4.6.3. In Vivo CD155 blockade decreases postoperative lung metastases

The same *in vivo* CD155 blockade model, consisting of α-CD155 500 μg injected IP preoperatively, was used to examine lung metastases (mets) on POD3. Of note, the B16F10-LacZ cell line was used in order to visualize the melanoma lung deposits. Lung mets were quantified following our standard lung staining protocol. Without CD155 blockade, surgical stress led to a significantly increased number of lung mets postoperatively (p=0.03; Figure 16A).

Interestingly, compared to mice without antibody blockade at baseline (mean 72.8, dark grey), mice receiving α-CD155 injections had significantly less mets (mean of 21, black, p=0.03; Figure 16A). On POD3, CD155 blockade also led to a significant decrease in lung mets (mean 120, red vs mean 190, light grey; p=0.03; Figure 16A). When comparing representative images, a POD3 lung without CD155 blockade (Figure 16B) has a much higher number of B16F10 melanoma lesions compared to a POD3 lung with α-CD155 treatment (Figure 16C).

These important findings confirm that *in vivo* CD155 blockade ultimately leads to an improved postoperative NK cell phenotype as measured by DNAM-1 and NKG2D, as well as increased NK cytotoxicity and less lung metastases. In order to determine a translational potential to these findings, the last results focus on *ex vivo* blockade of human CD155 in cancer patients.

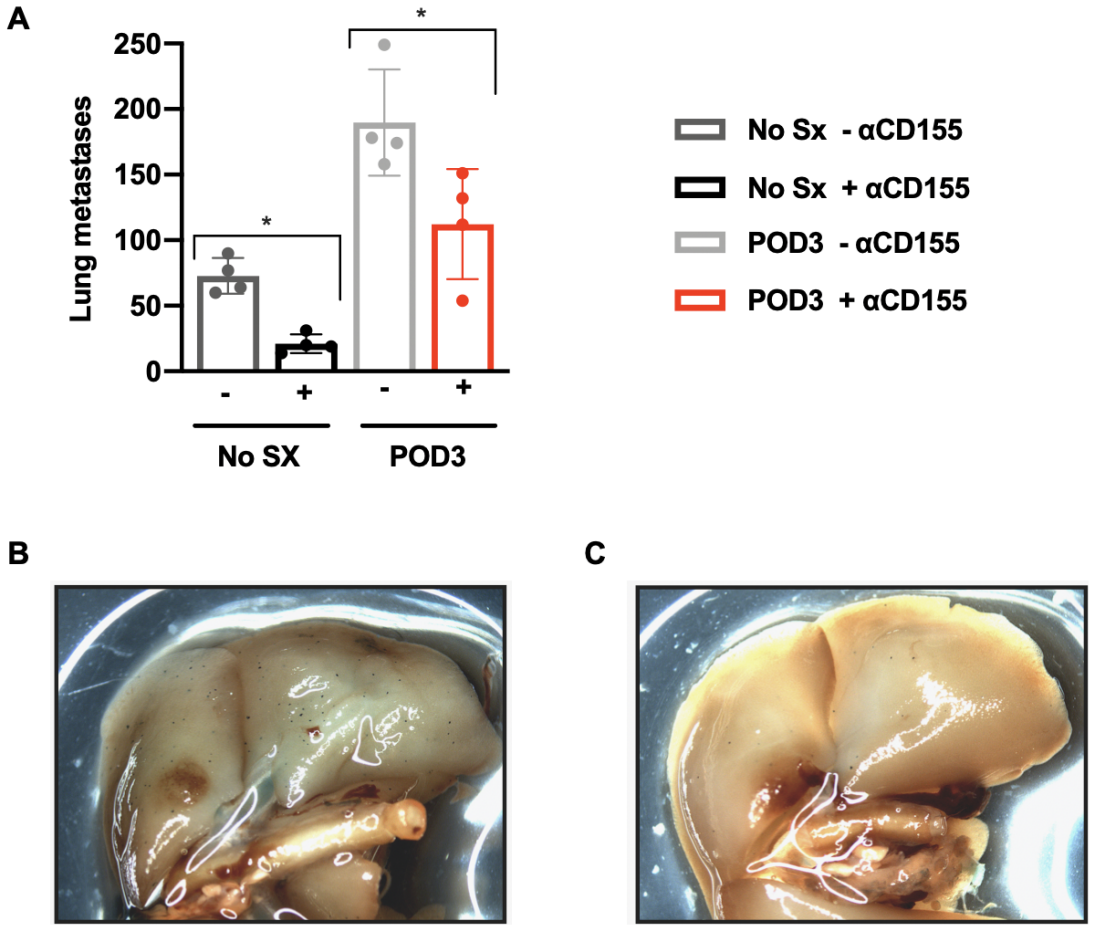
A
250
200
150
100
50
0
Lung metastases
*
*
-
+
-
+
No SX
POD3
No Sx - αCD155
No Sx + αCD155
POD3 - αCD155
POD3 + αCD155
B
C

Figure 16. *In Vivo* CD155 Blockade Leads to Reduced B16F10 Lung Metastases.
A) Quantification of B16F10-LacZ lung metastases based on standard X-Gal staining protocol. In the no surgery groups, + α-CD155 (black) compared to – α-CD155 (dark grey). On POD3, + α-CD155 (red) compared to – α-CD155 (light grey). Samples shown are mean (n=4) ± SD. **p*<0.05. **B)** Representative image of a POD3 right lung without CD155 blockade. B16F10 lung mets are identified as small black lesions. **C)** Representative image of a POD3 right lung following CD155 blockade.

4.7. *Ex vivo* blockade of human CD155 improves NK cell cytotoxicity

4.7.1. Optimization of a novel human suppression assay

The purpose of this *ex vivo* suppression assay was to examine the impact of CD155 expressed by Sx-MDSCs on NK cell cytotoxicity in human cancer patients. The first step was to ensure the protocol was successful with the NK92-MI cell line as positive control, which is our standard effector cell for killing assays. As shown in Figure 17A, adding POD1 Sx-MDSCs decreased NK cytotoxicity by nearly 50% (blue, MDSC:NK:K562) compared to NK92 cells and K562 cells alone (red, NK:K562). Since previous work from our laboratory has shown that NK92-MI cells do not express DNAM-1 (data not shown), freshly isolated NK cells from healthy donors were used (details in section 3.8 and Figure 5).

In terms of MDSC surface CD155 blockade, manufacturer recommendations for antibody dosing (human anti-CD155 clone SKII.4) were a maximum of 2 µg/mL (Biolegend). For early dose titration experiments we therefore compared the following conditions of α-CD155: 0, 0.25, 0.5 and 2 µg/mL (Figure 17B). The dose of 0.5 µg/mL was associated with the greatest improvement in NK cytotoxicity, measured by % dead $CP450^{+}/PI^{+}$ K562s, with Sx-MDSC present (blue, Figure 17B). In fact, adding 0.5 µg/mL of α-CD155 nearly doubled killing compared to the negative control without antibody (Figure 17B). In order to stimulate NK cells and attempt to better detect a difference with antibody blockade, low-dose IL-2 (40 U/mL) was added as a control. While significantly enhancing cytotoxicity, adding IL-2 abrogated the effects of Sx-MDSC suppression, regardless whether α-CD155 was added (Figure 17C). Therefore, after optimizing the protocol, all suppression assays were completed with α-CD155 at a dose of 0.5 µg/mL in the absence of IL-2 stimulation.

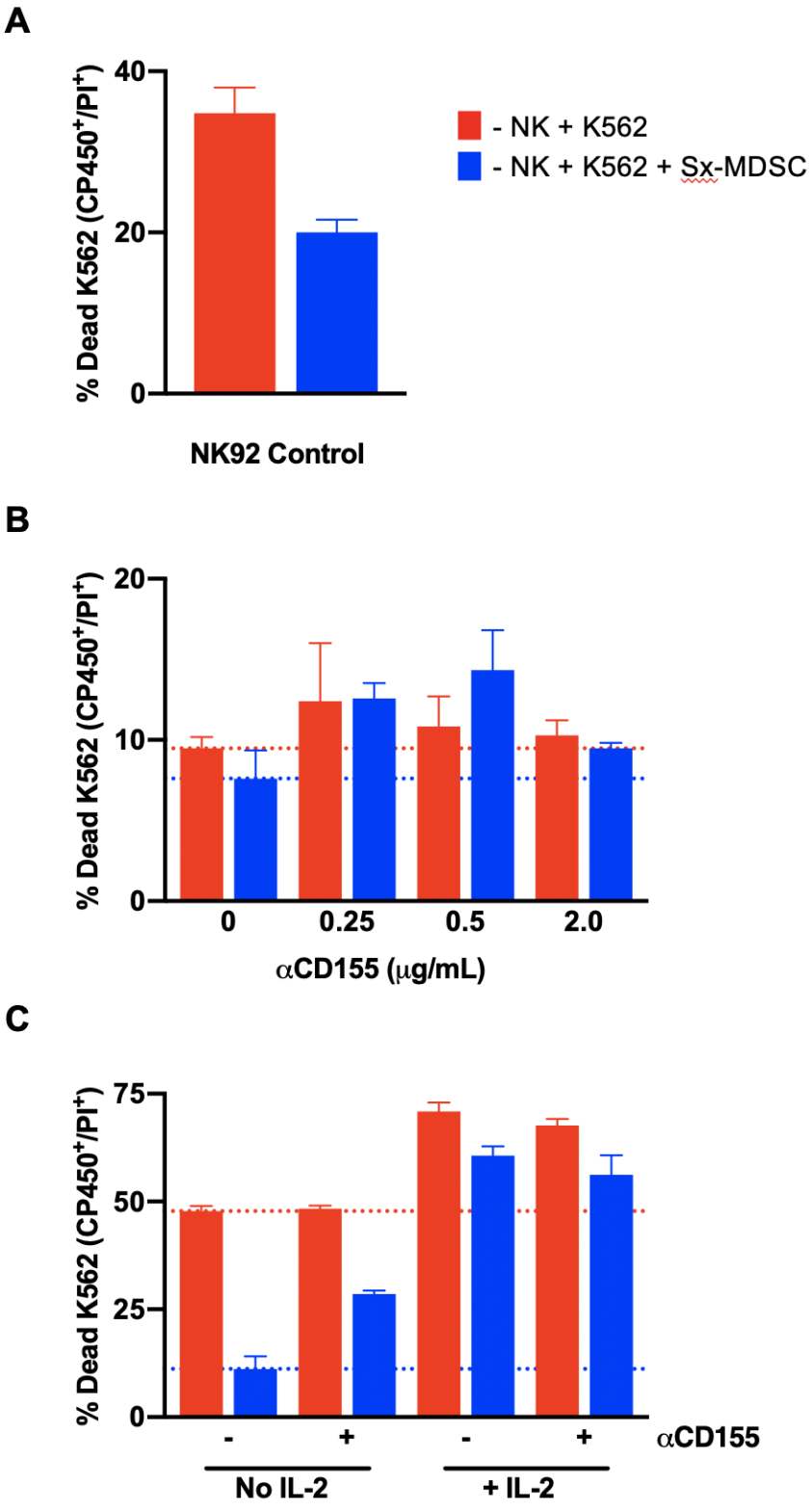
A
% Dead K562 (CP450+/PI+)
40
20
0
- NK + K562
- NK + K562 + Sx-MDSC
NK92 Control
B
% Dead K562 (CP450+/PI+)
20
10
0
0
0.25
0.5
2.0
αCD155 (μg/mL)
C
% Dead K562 (CP450+/PI+)
75
50
25
0
-
+
-
+
αCD155
No IL-2
+ IL-2

Figure 17. Optimization of a Novel *Ex Vivo* CD155 Human Suppression Assay.
A) Suppression assay for the NK92-MI positive control. NK cytotoxicity measured as % dead K562 ($CP450^{+}/PI^{+}$) without Sx-MDSC (red, NK:K562) or with Sx-MDSC (blue, MDSC:NK:K562). **B)** Dose titration of α-CD155 at various concentrations: 0, 0.25, 0.5 and 2 (μg/mL). % killing without Sx-MDSC (red) or with Sx-MDSC (blue). **C)** Low-dose IL-2 optimization. Suppression assay with or without α-CD155 (0.5 μg/mL) compared in presence or absence of low dose IL-2 stimulation (40 U/mL). All samples shown are Mean of triplicates ± SD.

The next step to characterize CD155 blockade in this *ex vivo* suppression assay was to determine whether α-CD155 remains stably bound to surface CD155 for the duration of the 20-hour assay. The rationale was that if blocking α-CD155 is still surface-bound 24 hours later, this would result in a decrease of CD155 detection by flow cytometry. In order to do so, flow phenotyping was performed on freshly isolated Sx-MDSCs with α-CD155 after a short 30-minute incubation, and compared to Sx-MDSCs after a 24-hour incubation.

As illustrated in Figure 18A-B, both fresh and 24-hour samples had similar CD155 MFI profiles for each of the following α-CD155 concentrations: 0 (blue, isotype control), low-dose 0.5 μg/mL (red), and high-dose 5 μg/mL (black). Additionally, low and high-dose blockade both caused a near-identical downregulation of CD155 MFI, reinforcing 0.5 μg/mL as the optimal dose for the suppression assay. This corresponded to a similar profile of %CD155+ Sx-MDSCs when comparing fresh (Figure 18C) to 24-hour samples (Figure 18D). Both had approximately 70% expression without α-CD155 blockade (blue), which decreased to less than 5% with low-dose (0.5 μg/mL, red) and high-dose (5 μg/mL, black).

After optimizing this novel *ex vivo* suppression assay for the following conditions; low-dose α-CD155 (0.5 μg/mL), no IL-2 and 8:2:1 effector-to-target (E:T) ratio (MDSC:NK:K562), we next sought to evaluate the effect of CD155 blockade on Sx-MDSCs isolated from POD1 cancer surgery patients.

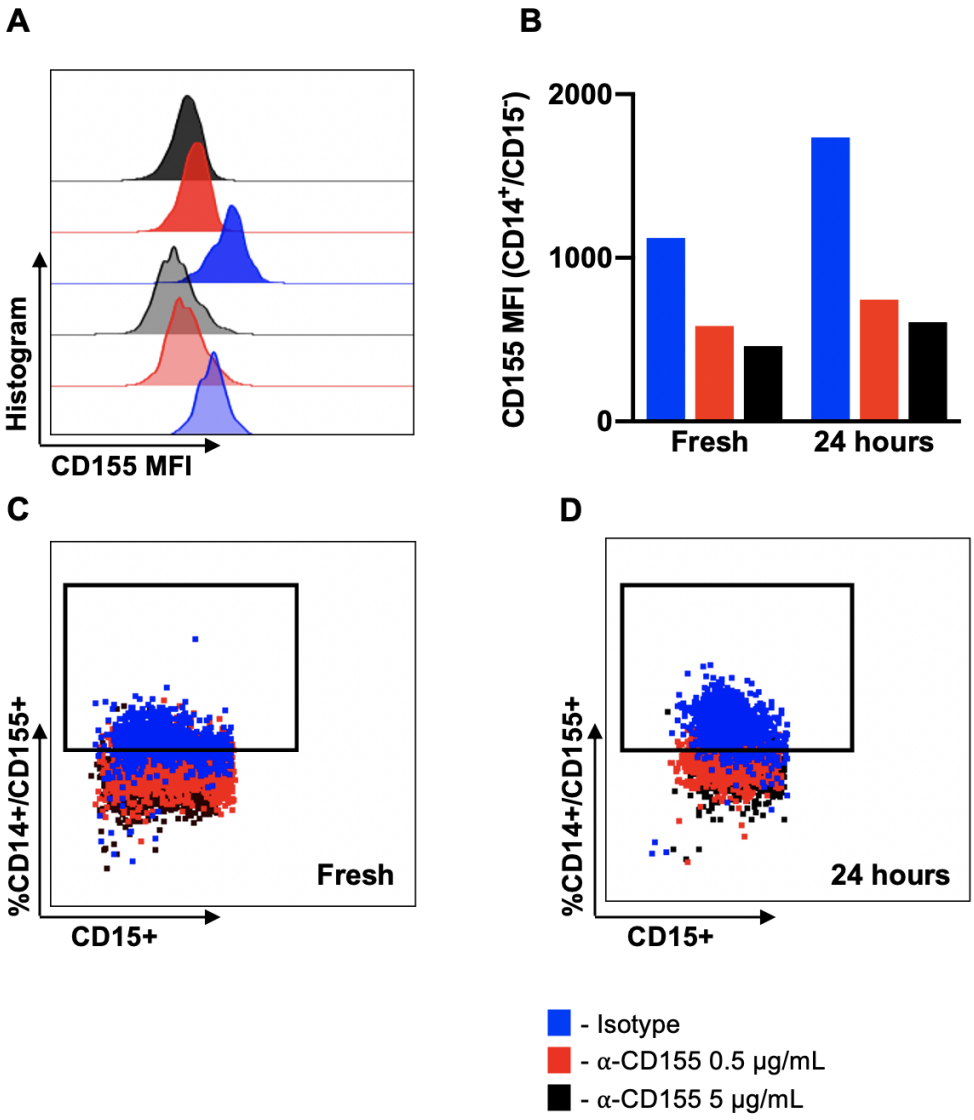
A
Histogram
CD155 MFI
B
CD155 MFI (CD14+/CD15-)
2000
1000
0
Fresh
24 hours
C
%CD14+/CD155+
CD15+
Fresh
D
%CD14+/CD155+
CD15+
24 hours
- Isotype
- α-CD155 0.5 µg/mL
- α-CD155 5 µg/mL

Figure 18. α-CD155 is Stably Bound to Surface CD155 on Human Sx-MDSCs.
A) CD155 MFI histograms of human Sx-MDSC ($CD33^{+}/CD14^{+}/CD15^{lo}$) at various α-CD155 blocking antibody concentrations: 0 µg/mL (blue, isotype), 0.5 µg/mL (red) and 5 µg/mL (black). CD155 MFI of samples analyzed fresh (shaded colours) compared to after a 24-hour incubation (solid colours). **B)** Bar graph representing CD155 MFI at the same α-CD155 blocking conditions, comparing fresh to 24 hours. **C)** %CD155+ Sx-MDSC of fresh samples for the following α-CD155 concentrations: 0 µg/mL (blue, 76.2%), 0.5 µg/mL (red, 20.1%) and 5 µg/mL (black, 6.45%). **D)** %CD155+ Sx-MDSC of 24hour samples for the same α-CD155 concentrations: 0 µg/mL (blue, 65.1%), 0.5 µg/mL (red, 0.33%) and 5 µg/mL (black, 0.086%).

4.7.2. Clinical demographics for ex vivo CD155 blockade

This *ex vivo* suppression assay was performed with POD1 Sx-MDSCs isolated from 3 different cancer patients. Mean age was 65 (55-72) and cancer types included one retroperitoneal sarcoma, which is a rare type of stromal tumour, and two lung cancers. Clinical demographics are summarized in Table 3. Importantly, in order to obtain a consistent suppressive effect from the POD1 Sx-MDSCs, only cancer patients with planned high surgical stress were recruited. This can be seen in Table 3, with all patients having surgery length greater than 4 hours (mean 413 minutes). In fact, any patient with planned low surgical stress, determined as minimally invasive robotic surgery (i.e. prostate cancer) or short surgeries less than 2 hours, were excluded.

In terms of cell quality, POD1 Sx-MDSC viability was high for all patients, well above the minimum pre-set viability of 92% (median 94.5%, Table 3). The measurement of cell viability was performed by hemocytometer (HC) and confirmed by flow cytometry, gating $CP450^{-}/PI^{-}$ as the live proportion of Sx-MDSCs (gating can be found in Appendix E). Similarly, the viability for isolated healthy NK cells was always above 95%, as measured manually by HC (data not shown).

Table 3. Clinical demographics of cancer patients for *ex vivo* CD155 Suppression Assay.

Category	Subcategory	Cancer
Total (n)		3
Sex	Male (n)	1 (33%)
	Female (n)	2 (67%)
Patient Age (mean years)		65; *55-72*
	< 60 years (n)	1
	60-69 years (n)	1
	> 70 years (n)	1
Type of Surgery	Open (n)	1 (33%)
	MIS (n)	2 (67%)
Type of Cancer	Lung GI	2 1
Cancer Stage	I II III IV	2 (67%) 1 (33%) - -
Length of Surgery	< 2 hours 2-4 hours > 4 hours	- - 3
Sx-MDSC Viability (%)	P1 P2 P3	94.5% 95.2% 93.8%

MIS – Minimally Invasive Surgery, GI – Gastrointestinal, P1 – Patient 1, P2 – Patient 2, P3 – Patient 3

4.7.3. Ex Vivo CD155 blockade decreases Sx-MDSC suppression

Ex vivo blockade of surface CD155 on POD1 Sx-MDSC using the purified human anti-CD155 antibody (clone SKII.4) led to increased NK cytotoxicity in all 3 cancer patients (Figure 19A-C) compared to the isotype alone (IgG1 k isotype control, clone MOPC-21). As defined by the area above the blue dotted line, adding the α-CD155 resulted in a nearly 40 to 50% increase in NK cytotoxicity with Sx-MDSCs present (blue, Figure 19-A-C). Although the third patient (Figure 19C) did not have as significant MDSC suppression at baseline prior to CD155 blockade (blue compared to red), the improvement with α-CD155 is still profound.

When plotting the mean NK cytotoxicity of triplicates for all 3 cancer patients, presence of low-dose α-CD155 0.5 μg/mL leads to a statistically significant increase in killing of K562 target cells ($p=0.008$, Figure 19D). Combined, these 3 assays have a mean % NK cytotoxicity that is more than twofold greater with α-CD155 present (36.5%) compared to without α-CD155 (17.9%). In other words, *ex vivo* CD155 blockade with α-CD155 led to a significantly decreased suppression by the Sx-MDSCs.

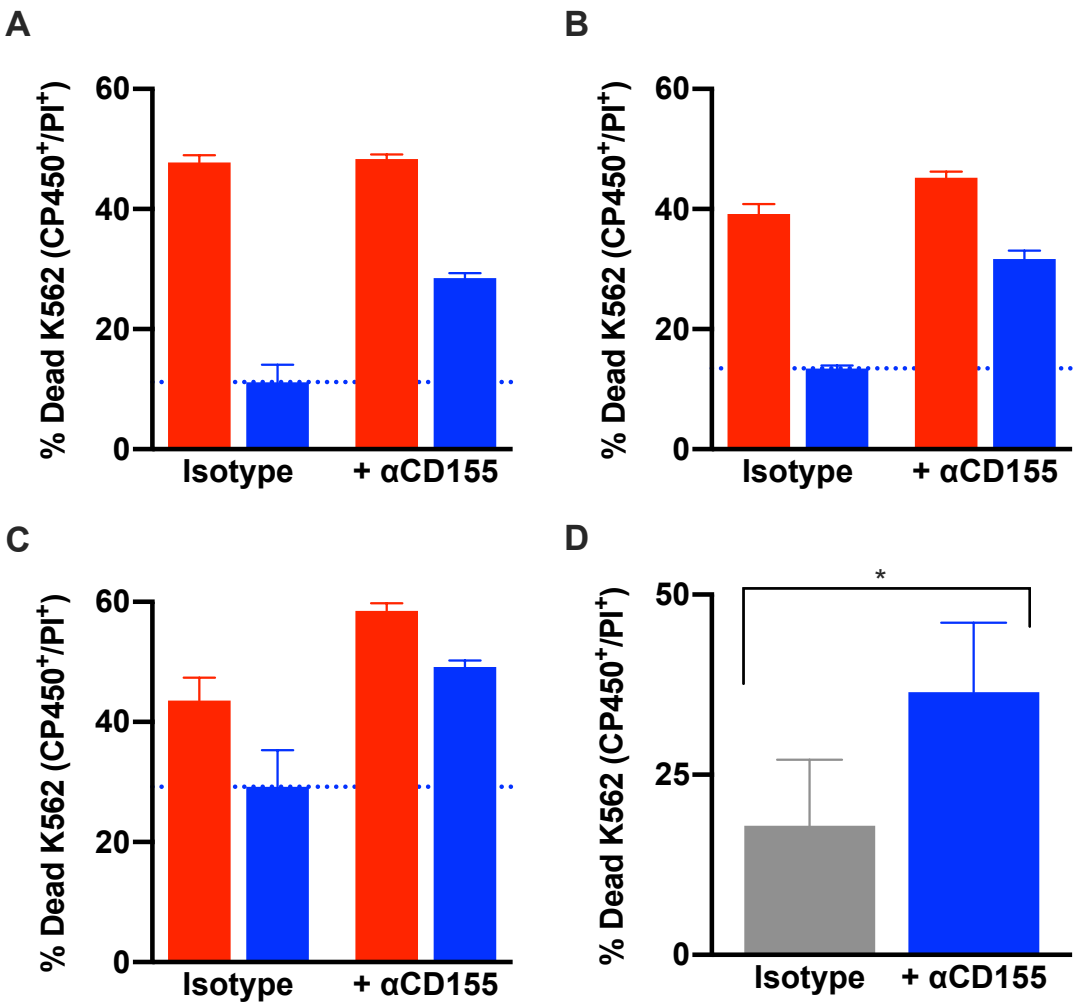
A
B
C
D
% Dead K562 (CP450+/PI+)
60
40
20
0
50
25
Isotype
+ αCD155
*

Figure 19. *Ex vivo* CD155 Blockade Decreases the Suppressive Effect of Sx-MDSCs. **A-C)** Suppression assays with POD1 Sx-MDSCs of 3 cancer patients (A – lung cancer lobectomy, B – retroperitoneal sarcoma resection, C – lung cancer lobectomy). % killing of K562s with Sx-MDSCs (blue, MDSC:NK:K562) or without Sx-MDSCs (red, NK:562). The suppression control with isotype alone (IgG1 k isotype control, clone MOPC-21) is represented as the blue dotted line. Increase in killing with α-CD155 (0.5 μg/mL) is the proportion above this blue line. **D)** Mean % killing with Sx-MDSCs of all triplicates (n=9), comparing isotype (grey) to α-CD155 (blue). All samples shown are Mean of triplicates ± SD. **p*<0.05.

5. DISCUSSION

5.1. Surgical stress

5.1.1. Surgical stress and NK cell suppression

Without a doubt, surgery is a critical component for the curative treatment of cancer patients (48–50). However many groups, including our laboratory, have convincingly shown that NK cell function is significantly impaired following surgical stress, regardless of surgical approach, length of surgery or cancer type (14, 55, 88, 90, 131). In keeping with these studies, my results highlight the detrimental impact surgical stress can have on NK cell suppression. The postoperative NK cell phenotype is significantly dysfunctional, marked by a profound downregulation in activating receptors NKG2D and DNAM-1, as well as impaired *ex vivo* cytotoxicity of YAC-1 target cells (Figures 12, 15). Importantly, in murine models this suppression of NK cytotoxicity correlates with increased postoperative tumour metastases and poor survival (83, 91, 92, 95). As highlighted in Figure 16, I have also seen a significant increase in lung metastases following surgical stress. While I did not perform experiments to determine a direct correlation between NK function and metastases, we previously completed adoptive NK cell transfers of surgically stressed mice into naïve mice to confirm that NK cells are an essential population responsible for clearance of metastases following surgery (91, 95). Importantly, NK cell dysfunction is strongly related to expansion of myeloid cells following surgical stress.

5.1.2. Expansion of granulocytes and monocytes after surgery

Several previous studies have shown that surgical stress leads to an immediate release of growth factors such as EGF, PDGF and VEGF, pro-inflammatory cytokines IL-1, IL-6, TNF-

α, and IFN-γ, as well as DAMPs (51, 61–63). Together these factors cause a recruitment of granulocytes and monocytes to the site of injury for the first phase of wound healing (61, 63, 68). Additionally, surgical stress is thought to cause a significant release of IMCs from the bone marrow (BM) in order to respond to these signals. The Sx-MDSCs are a key subset of IMCs that accumulate significantly in the circulation after surgery (127–129, 131). We have previously measured MDSCs in various murine compartments including the bone marrow (BM) and spleen perioperatively. On POD1, MDSCs decrease significantly in the BM while increasing in the spleen, supporting the theory that emergency myelopoiesis causes a massive and immediate release of IMCs after surgery (131).

While my results also confirm that MDSCs and granulocytes expand after surgery (Figure 6), measuring these populations at multiple timepoints (POD1 and POD3) in both the spleen and blood helped gain a better understanding of their postoperative expansion. Granulocytes are significantly upregulated on POD1 but decrease in the blood by POD3 (Figure 6), suggesting they are already present in circulation and have an immediate, although short response. This is in keeping with the fact that the majority of granulocytes on POD1 are neutrophils and these cells are the first to be recruited to the site of injury, but peak early by 24 hours (51, 67, 175). Interestingly, the Sx-MDSC upregulation is not immediately noted in the spleen until POD3. Although not a direct confirmation, these results support that Sx-MDSCs are released from the BM only following surgical trauma through emergency myelopoiesis, which is strongly mediated by postoperative inflammatory cytokines such as IL-6 and G-CSF (72, 125).

While my postoperative timepoints were only until POD3, it would have been very interesting to compare the granulocyte and Sx-MDSC expansion at later intervals such as POD5 and POD7. The granulocyte levels appear to correlate with the short yet intense pro-inflammatory response or Ebb phase, while the Sx-MDSCs would likely have been upregulated until at least

POD7 for the duration of the anti-inflammatory phase (see Ebb and Flow phases of surgical stress, Figure 1).

5.1.3. Flow cytometry validation of postoperative immune populations

MDSCs are a very heterogeneous population of immature cells with varying levels of granularity, which makes their characterization difficult. As outlined in the introduction (section 1.3.1), key studies have helped develop a common phenotyping strategy based on their surface markers. For murine MDSC populations, M-MDSCs were identified as $CD11b^{+}/GR1^{int}/Ly6G^{-}/Ly6C^{+}$ while PMN-MDSCs were $CD11b^{+}/GR1^{hi}/Ly6G^{+}/Ly6C^{Lo}$ (99, 101, 102). It is important to note that the granulocyte population in mice consists of a combination of granulocytes, such as neutrophils, as well as PMN-MDSCs but there are no known strategies to separate these two populations by flow cytometry. During initial flow cytometry validation experiments, gating the populations based on Ly6G/Ly6C molecules did not yield as clear a separation as their relative GR1 expression only. As shown in figure 10A, $CD11b^{+}/GR1^{int}$ M-MDSCs are a clearly defined and separate population from the $CD11b^{+}/GR1^{hi}$ granulocytes.

However, humans do not express the GR1 marker, which makes the flow cytometry characterization of MDSCs even more difficult for human samples (103, 108). Bronte *et al.* published guidelines on MDSC characterization standards in 2016 and advised that CD33 can confidently be used as the sole myeloid marker for human MDSCs (102). Therefore, I identified human MDSCs following Bronte's recommendations: absence of Lin markers (CD3, CD19 and CD56) and presence of myeloid lineage marker CD33. M-MDSCs can be separated by the presence of monocyte marker CD14 and absence of CD15 ($Lin^{-}/CD33^{+}/CD14^{+}/CD15^{lo}$), while the opposite is true for PMN-MDSCs ($Lin^{-}/CD33^{+}/CD14^{-}$

/CD15^{+}) (102). Again, HD neutrophils were removed in the high-density layer during Ficoll centrifugation. Therefore, the CD33^{+}/CD14^{-}/CD15^{+} gate included the PMN-MDSCs or low-density (LD) neutrophils. For the purpose of consistency, the term surgery-induced MDSCs (Sx-MDSCs) was used throughout to describe M-MDSCs that expand following surgical stress.

5.2. Perioperative profiling of CD155

5.2.1. CD155 in human cancer patients

The first step in the cancer patient experiments was to optimize the processing method. Several clinical studies rely on cryopreserving samples to enhance efficiency of processing and analysis, especially for multicenter trials (176–178). However, cryopreserving MDSC subsets causes decreased viability and frequencies, leading to an underrepresentation of the samples (178). I have seen similar results during early experiments for my MDSC staining panel comparing fresh to frozen samples (data not shown). Therefore, processing and isolating PBMCs for all cancer patients were done fresh to ensure accurate results. In terms of CD155 detection, this study is the first to measure perioperative changes of CD155 on myeloid populations. I therefore titrated 2 different CD155 antibody clones (SKII.4 and PV404.19), both commonly used for CD155 flow phenotyping. SKII.4 was chosen as it provided the clearest separation between isotype control and sample once titrated, particularly on POD1 (Appendix B).

As previously mentioned, the human high density (HD) neutrophils were removed during the Ficoll PBMC isolation. The detailed gating strategy for human MDSCs is outlined in Figure 6A and Appendix C. Using CD14 and CD15, I was able to separate CD14^{+}/CD15^{-} M-MDSCs

from $CD14^{-}/CD15^{+}$ PMN-MDSCs, or LD neutrophils. As shown in Figure 6, CD155 expression is markedly upregulated on Sx-MDSCs on POD1 compared to baseline. Also, baseline cancer CD155 is much higher than the healthy donors, although only 2 were tested and these were not age-matched. Importantly, this CD155 expansion appears very specific to the Sx-MDSC population since $CD15^{+}$ LD neutrophils and Lin^{-} lymphocytes have minimal CD155 expression before or after surgery (Figure 6E). In fact, $CD15^{+}$ LD neutrophil CD155 expression is much closer to the isotype control (blue compared to green, Figure 6C). This is a key result that highlights for the very first time the perioperative therapeutic potential of CD155 blockade, which would be specific to targeting Sx-MDSCs with minimal effects on other immune cell populations.

During the CD155 baseline subgroup analyses, I discovered a few interesting correlations. It is known from previous work that tumour CD155 levels correlate with cancer stage and poor prognosis in cancer patients (153, 157, 170–173), but there are no known studies examining correlations of myeloid CD155 expression. Firstly, there appears to be a trend with age, where all low baseline CD155 levels below 25% are in patients less than 60 years of age (Figure 7A). Immunosenescence, or age-related impairment in immune responses, is well known to decrease innate responsiveness and vaccination efficacy in the elderly (179–182). Although there are no such studies yet, it would be interesting in the future to examine the contribution of age-related MDSC CD155 expression in immunosenescence.

In terms of surgical approach, the proportion of high baseline CD155 (>50%) was much greater in the open group (9/12) compared to the MIS group (1/8, Figure 7D). This could be partly due to the fact that larger or locally advanced tumours often require planned open (laparotomy) surgeries, as highlighted by the fact that all stage 3 cancers were of open approach. Additionally, although not statistically significant, the mean of 246 minutes for open surgeries

compared to 195 minutes for MIS suggests more difficult and longer cancer resections in the open group. Cancer type and stage are another interesting CD155 correlation, where all the low baseline CD155 cancers were either less invasive, such as GU prostate cancers, or early stage I (Figure 7E-F). Together these findings suggest that higher levels of tumour burden, marked by cancer invasiveness and cancer stage, may have a greater impact on host MDSC recruitment and CD155 upregulation. In fact, this study is the first to discover such associations between MDSC CD155 expression and cancer parameters.

To better understand the contribution of surgical stress in postoperative immune suppression, I also measured perioperative MDSC CD155 expression in a subset of 5 non-cancer patients. As shown in Appendix D, even in non-cancer surgeries there is an increase in Sx-MDSC CD155 on POD1 compared to baseline. Although not statistically significant likely due to low numbers (n=5), the upregulation still seems profound (p=0.06, Appendix D). This key result reinforces the theory that surgical stress causes an immediate and profound release of Sx-MDSCs from the BM, regardless of indication, cancer or surgical approach. Interestingly, baseline CD155 levels in the non-cancer patients are also quite varied, up to nearly 60%. These results are not unexpected, as MDSCs can still greatly expand in benign conditions such as infection, inflammation and auto-immune disorders (103, 104, 122). Particularly in the perioperative setting, such non-cancer conditions could still be influenced by MDSC CD155 expansion and resulting immune suppression.

5.2.2. CD155 in the murine model of surgical stress

We have previously validated our experimental B16F10 and spontaneous 4T1 models of surgical stress, during which mice undergo laparotomy, mobilization of bowel and left nephrectomy (83, 91, 95, 131). My results show that the levels of stress and trauma during

these surgeries are sufficient to induce profound NK cell suppression, marked by a decrease in NK cell activating receptors NKG2D and DNAM-1, as well as NK cytotoxicity (Figures 12, 15). During murine *ex vivo* cytotoxicity assays, we usually detect a 20 to 25% decrease in NK-mediated killing following surgery (131), but the decrease was not as profound in my experiment (Figure 15C, dark grey to light grey). Our surgery protocol is very consistent, but it is possible that lack of tumour CD155 expression (B16F10-CD155 KO) induced a smaller suppressive effect on postoperative NK cells. In the future, it would be worthwhile to compare NK-mediated killing following B16F10-CD155 KO and B16F10-WT injections.

While I was able to clearly characterize murine immune cell populations (section 5.1.3.), I had to also validate CD155 detection in our murine model. Because tumour CD155 overexpression is known to induce several pro-tumorigenic changes such as invasiveness, metastases, angiogenesis and NK cell suppression, the first key step was to validate melanoma cell lines. In order to study the effect of host myeloid CD155 expression specifically, it was critical to use a CD155-KO line (kindly provided by Dr. Smyth's research group). Validation of these cell lines confirmed that B16F10-CD155 KO does not express any CD155 (Figure 9).

Similar to the human results, postoperative CD155 is significantly upregulated on $CD11b^{+}/GR1^{int}$ Sx-MDSC on POD1 and POD3 compared to baseline (Figure 11). It is also interesting that CD155 is still significantly upregulated on POD3. While I did not specifically address in this study, CD155 expression on Sx-MDSC may be an important component of the delayed anti-inflammatory, or Flow, phase following surgery (Ebb and Flow of surgery, Figure 1). Furthermore, $CD11b^{+}/GR1^{hi}$ granulocytes have minimal CD155 expression at any perioperative timepoint (Figure 11). Although I did attempt murine Ficoll separation to isolate PMN-MDSCs perioperatively, the yield was too low for any functional assessment (data not shown). To our knowledge, there are no gating strategies to separate murine PMN-MDSCs

from other granulocytes. However, the $GR1^{hi}$ granulocytes contain mostly neutrophils, particularly in the postoperative state, which are a key mediator of the inflammatory response. Having the ability to block Sx-MDSC via CD155 while protecting the neutrophil expansion for wound healing once again highlights the perioperative therapy potential of CD155 blockade.

5.3. Perioperative changes in activating NK cell receptors

Activating NK cell receptors DNAM-1 and NKG2D play important roles in anti-tumour immune surveillance as their ligands are often overexpressed on tumour cells (5, 26, 27, 30, 146). Importantly, at least one of the two receptors DNAM-1 or NKG2D is required to maintain effective NK-mediated cytotoxicity of tumour cells (31, 32). My murine results characterized a profound dysfunction in NK cells following surgical stress. Postoperative NK cells have decreased expression in both activating receptors DNAM-1 and NKG2D (Figure 12). The DNAM-1 downregulation is probably directly caused by CD155 overexpression on Sx-MDSCs, as this inhibitory mechanism was demonstrated in previous cancer studies (10, 32, 136, 166, 167).

The decrease in NKG2D expression from CD155 upregulation, however, is not as clear and has not been previously described. The fact that NKG2D MFI is not profoundly impaired until POD3 (Figure 12) suggests it is due to an exhausted phenotype following exposure to its stress-induced murine ligand RAE-1ε. Thompson *et al*. studied the effect of RAE-1ε exposure to NKG2D *in vivo*. Interestingly, RAE-1ε binding to NKG2D caused internalization of NKG2D, leading to NK cell hypo-responsiveness and impaired activity measured by degranulation and IFN-γ production (183). It is quite possible that this mechanism of hypo-responsiveness occurs following surgery, when the profound stress causes RAE-1ε upregulation on endothelial cells.

Hypoxic stress can cause tumour shedding of NKG2D ligands, which antagonizes and downregulates NKG2D on NK cells (30, 40, 42). Importantly, RAE-1ε can be significantly upregulated on endothelial cells following stress signals, particularly in tumour-associated vasculature (183). It is possible that the significant stress caused by surgery induces shedding of RAE-1ε and secondary internalization and downregulation of NKG2D.

Another likely contributor to the decrease in postoperative NKG2D is from the significant release of TGF-β following surgical stress. It is known that tumour-secreted TGF-β causes NKG2D downregulation in cancer models (44, 45) and surgery results in an immediate and substantial increase in this suppressive cytokine (48, 63, 81). In fact, the postoperative effect of TGF-β on the NK cell phenotype was thoroughly investigated by a laboratory colleague Marisa Market (data not shown, manuscript pending).

5.4. CD155 blockade to improve postoperative NK cell function

5.4.1. In vivo blockade in the animal model of surgical stress

Although much less was known about myeloid cell CD155 expression, the work by Li *et al.* provided a strong rationale to investigate perioperative CD155 blockade. In their experiments, loss of host CD155 led to decreased tumour volume and lung metastases for various tumour cell lines *in vivo* (164). When they blocked CD155 in naïve mice with anti-CD155 (clone 4.24.1, 250 μg), they noticed a significant upregulation in DNAM-1 on NK cells (164). However, they did not examine cancer endpoints such as tumour volume or metastases following anti-CD155 injections. This provided strong evidence for our *in vivo* blockade experiments. Assuming slightly higher doses of antibody would be required in the perioperative setting to block all surface CD155 on Sx-MDSCs, I titrated doses of 250 μg up

to 750 μg, with 500 μg discovered as the optimal dose (Figure 13). The fact that *in vivo* CD155 blockade significantly increased both DNAM-1 and NKG2D expression on NK cells confirms the role Sx-MDSC CD155 expansion plays on the suppressive NK cell phenotype. Additionally, CD155 blockade prevented the postoperative decrease in DNAM-1 that was usually seen on POD1 (Figure 14). Interestingly, CD155 blockade did not increase NKG2D under normal conditions, only after surgical stress on POD1 (baseline, Figure 14B). This suggests that the CD155 antibody, directly or indirectly, prevented binding of NKG2D with its stress-induced NKG2D ligand RAE-1ε.

Importantly, the increase in activating NK cell receptors following CD155 blockade correlated with enhanced cytotoxicity of YAC-1 target cells and this effect was most pronounced after surgery (Figure 15, red compared to light grey). These killing assays may have underestimated the effect of CD155 blockade on cytotoxicity, because of the YAC-1 target cell line that was used. Gilfillan *et al.* determined that YAC-1 cells overexpress CD155 as well asl NKG2D ligands. Therefore, even after CD155 blockade in this killing assay, NKG2D ligands can still be used as a compensatory mechanism for NK-mediated killing on these YAC-1 cells (32). Additionally, the NK-mediated killing of YAC-1 cells may have been confounded by the downregulation of postoperative NKG2D on NK cells. In retrospect, comparing NK killing with non-NKG2D ligand expressing cell lines like B16F10, and specifically B16F10-CD155 KO, would have been important controls to determine the exact contribution of CD155 overexpression on the suppressive NK cell phenotype, and this should be pursued in future experiments.

The last key modification following CD155 blockade relates to lung metastases. Mice receiving anti-CD155 had significantly less lung mets at baseline and on POD3 (Figure 16). It is important to note that these experiments were completed with B16F10-LacZ in order to

visualize the melanoma lung deposits after X-gal staining. However, since this cell line has a high expression of CD155 (Figure 9), it is impossible to know how much of the effect seen on lung mets was caused by Sx-MDSCs versus the tumour itself. At the time of the COVID-19 closures, experiments had begun to transfect Lenti-LacZ into the B16F10-CD155 KO cell line to minimize the effect of tumour CD155 and better understand the impact of Sx-MDSC CD155 expression on postoperative lung mets. While previous studies have determined that tumour CD155 blockade leads to improved NK cell function and decreased tumour growth (162, 164, 165), this project is the first of its kind to convincingly link Sx-MDSC CD155 blockade to an improved NK cell phenotype and cytotoxicity, as well as lung metastases.

5.4.2. A novel ex vivo CD155 suppression assay

The experiments above helped characterize the postoperative expansion of CD155 on Sx-MDSCs and blocking this expansion caused an improvement in NK cell phenotype and cytotoxicity. In order to determine a translational potential to these findings, I sought to create a novel *ex vivo* human suppression assay of CD155 blockade. In several human cancer studies, tumour CD155 levels were associated with cancer stage and prognosis (153, 157, 158, 170–172). To our knowledge, there are no known studies examining the effects of *ex vivo* blockade of human CD155 and in our postoperative model, this expression is very specific to Sx-MDSCs (Figure 7). Since this was never characterized before, several parameters had to be optimized. First and foremost, the NK92-MI cell line commonly used in human killing and suppression assays does not express DNAM-1 (data not shown). I therefore adapted our whole blood NK isolation protocol to use healthy donor NK cells, which provides a greater functional relevance to the *in vivo* DNAM-1/CD155 interactions. Based on our previous work, MDSC suppression assays usually yield an average of 40 to 50% suppression for POD1 Sx-MDSCs (manuscript

in preparation by Leonard Angka and Tai *el al.* 2018) (131). I was able to recapitulate this effect during my first experiments using the NK92-MI cells as a positive control (Figure 18A). In terms of CD155 blockade, I titrated the anti-CD155 antibody at several doses, from 0.25 up to 5 μg/mL (data not shown) and the lower dose range was clearly more effective at blocking the suppressive effect. I therefore compared 0.25 to 2 μg/mL and 0.5 μg/ml was determined as the optimal dose for improving NK-mediated killing with Sx-MDSCs present (Figure 18). The most plausible explanation for this effect is through antibody-dependent cellular cytotoxicity (ADCC). The K562 target cells are known to overexpress CD155 (10, 184) and at higher doses of antibody, excess anti-CD155 likely binds surface CD155 on K562s, triggering ADCC from the healthy NK cells. To prevent this nonspecific ADCC killing, we had started a CRISPR-Cas9 knock-out experiment to create a stable K562-CD155 KO cell line but this was postponed due to the COVID-19 closures. Nonetheless, this effect was minimally seen at the lower antibody dose of 0.5 μg/mL as the killing of NK:K562 only (red bars) was very similar with or without anti-CD155 present (Figures 18-19).

Variability in healthy donor NK cell killing remains the greatest issue in this functional suppression assay, which can never be fully controlled based on inter-patient variation of NK cell activity. However, the anti-CD155 still significantly improved NK-mediated killing of target cells by 40 to 50%, regardless of the healthy donor patient (Figure 19). In order to measure a consistent and quantifiable suppression by the POD1 Sx-MDSCs, only patients undergoing high surgical stress procedures were included. All other patients, such as robotic prostatectomy or minimally invasive gynecologic surgeries, were excluded. As highlighted in table 3, the patients included all had long surgeries greater than 4 hours in keeping with high stress procedures. The suppression assays for all three cancer patients showed a significant improvement in NK-mediated killing when blocking surface CD155 expression on the Sx-

MDSCs (Figure 19A-C). When pooling the results, mean cytotoxicity is more than twofold greater with anti-CD155 present (Figure 19D). This novel suppression assay confirmed for the first time that blocking postoperative Sx-MDSC CD155 in human cancer patients results in a significant and reproducible improvement in NK-mediated cytotoxicity. Previous work from our laboratory has shown that baseline MDSCs do not induce suppression in such assays and the effect is limited to POD1 Sx-MDSCs. In order to further characterize the specificity of CD155 blockade in this assay, future work should compare the suppressive effect of Sx-MDSCs with preoperative baseline MDSCs, as well as other immune populations such as LD-neutrophils.

5.5. The translational potential of CD155 blockade

As highlighted in a commentary by Bronte, the clinical translational potential of CD155 relies on the ability to develop CD155 blocking therapies, such as small molecules and antibodies (26). My results have convincingly shown that monoclonal anti-CD155 antibody is a very promising blockade therapy. Its benefit has been shown *in vivo* in our murine model of surgical stress and *ex vivo* during human suppression assays, revealing that CD155 blockade greatly minimizes the suppressive effect of Sx-MDSCs. Interestingly, Bronte commented on utilizing both CD155 axes to fully maximize the therapeutic potential, by blocking the CD155-TIGIT/CD96 pathway but preserving DNAM-1 expression to engage tumour cells through the CD155 receptor (26). While TIGIT/CD96 was outside of the scope of my research project, dual blockade would be an interesting approach and should be investigated in future work.

Additionally, CD155 blockade as a therapy should have high tissue specificity for Sx-MDSCs, since there is minimal to no CD155 in normal human tissue (152) and other immune populations such as granulocytes and lymphocytes (Figures 7, 11). Administering the anti-

CD155 antibody in mice seemed well tolerated and did not cause any adverse events (AEs). The next direction of this research would be to perform a small phase I safety clinical trial with a subset of cancer patients to determine antibody safety and tolerance.

5.6. Conclusion

In summary, surgery is a central component for the curative treatment of most solid malignancies and induces an immediate release of pro-inflammatory cytokines to recruit granulocytes and monocytes to the site of injury. In parallel, there is a profound and immediate release of IMCs from the bone marrow. A subset of these IMCs, the Sx-MDSCs, expand significantly after surgery and have a strong suppressive effect on NK cells.

To our knowledge, this research work is the first of its kind to clearly characterize perioperative CD155 expression on Sx-MDSCs in animal models and human cancer patients. Through our animal model of surgical stress and *ex vivo* analysis of postoperative cancer patients, we have discovered a significant yet specific upregulation of CD155 on Sx-MDSCs with minimal expression on other immune cell populations. *In vivo* CD155 blocking experiments showed a convincing improvement in the postoperative NK cell phenotype, measured by activating NK cell receptors DNAM-1 and NKG2D, as well as enhanced cytotoxicity which coincides with decreased lung metastases. Additionally, these findings have a promising translational therapeutic potential. In the novel *ex vivo* human suppression assay we showed that CD155 blockade significantly decreases the suppressive effect of Sx-MDSCs and improves NK-mediated cytotoxicity.

While previous studies elucidated the role of CD155 in tumour progression and measured CD155 on myeloid cells isolated from the TME, this research project established for the first time a critical role of Sx-MDSC CD155 expansion in postoperative immunosuppression.

Future work should further characterize the specificity of *ex vivo* CD155 blockade by comparing Sx-MDSCs with preoperative MDSCs and other populations such as neutrophils. Also, assessing safety of CD155 blockade in a small phase I clinical trial of cancer patients could be entertained to bridge the gap towards a perioperative clinical trial in the future. Ultimately, targeting CD155 blockade in the critical perioperative window of opportunity appears to be a very promising novel therapy, which has the potential to greatly improve outcomes for cancer patients undergoing curative surgical resection.

6. REFERENCES

1. Kiessling, R., E. Klein, and H. Wigzell. 1975. “Natural” killer cells in the mouse. I. Cytotoxic cells with specificity for mouse Moloney leukemia cells. Specificity and distribution according to genotype. *Eur. J. Immunol.* 5: 112–117.

2. Hamerman, J. A., K. Ogasawara, and L. L. Lanier. 2005. NK cells in innate immunity. *Curr. Opin. Immunol.* 17: 29–35.

3. Cerwenka, A., and L. L. Lanier. 2001. Natural killer cells, viruses and cancer. *Nat. Rev. Immunol.* 1: 41–49.

4. Lanier, L. L. 2005. NK cell recognition. *Annu. Rev. Immunol.* 23: 225–274.

5. Pegram, H. J., D. M. Andrews, M. J. Smyth, P. K. Darcy, and M. H. Kershaw. 2011. Activating and inhibitory receptors of natural killer cells. *Immunol. Cell Biol.* 89: 216–224.

6. Yang, Q., S. R. Goding, M. E. Hokland, and P. H. Basse. 2006. Antitumor activity of NK cells. *Immunol. Res.* 36: 13–25.

7. Lodoen, M. B., and L. L. Lanier. 2006. Natural killer cells as an initial defense against pathogens. *Curr. Opin. Immunol.* 18: 391–398.

8. Cooper, M. A., T. A. Fehniger, S. C. Turner, K. S. Chen, B. A. Ghaheri, T. Ghayur, W. E. Carson, and M. A. Caligiuri. 2001. Human natural killer cells: a unique innate immunoregulatory role for the CD56(bright) subset. *Blood* 97: 3146–3151.

9. Robertson, M. J., and J. Ritz. 1990. Biology and clinical relevance of human natural killer cells. *Blood* 76: 2421–2438.

10. Carlsten, M., H. Norell, Y. T. Bryceson, I. Poschke, K. Schedvins, H.-G. Ljunggren, R. Kiessling, and K.-J. Malmberg. 2009. Primary human tumor cells expressing CD155 impair tumor targeting by down-regulating DNAM-1 on NK cells. *J. Immunol.* 183: 4921–4930.

11. Michel, T., A. Poli, A. Cuapio, B. Briquemont, G. Iserentant, M. Ollert, and J. Zimmer. 2016. Human CD56bright NK Cells: An Update. *J. Immunol.* 196: 2923–2931.

12. Lanier, L. L., A. M. Le, C. I. Civin, M. R. Loken, and J. H. Phillips. 1986. The relationship of CD16 (Leu-11) and Leu-19 (NKH-1) antigen expression on human peripheral blood NK cells and cytotoxic T lymphocytes. *J. Immunol.* 136: 4480–4486.

13. Nagler, A., L. L. Lanier, S. Cwirla, and J. H. Phillips. 1989. Comparative studies of human FcRIII-positive and negative natural killer cells. *J. Immunol.* 143: 3183–3191.

14. Angka, L., A. B. Martel, M. Kilgour, A. Jeong, M. Sadiq, C. T. de Souza, L. Baker, M.

A. Kennedy, N. Kekre, and R. C. Auer. 2018. Natural Killer Cell IFNγ Secretion is Profoundly Suppressed Following Colorectal Cancer Surgery. *Ann. Surg. Oncol.* 25: 3747–3754.

15. Zamai, L., C. Ponti, P. Mirandola, G. Gobbi, S. Papa, L. Galeotti, L. Cocco, and M. Vitale. 2007. NK cells and cancer. *J. Immunol.* 178: 4011–4016.

16. Smyth, M. J., Y. Hayakawa, K. Takeda, and H. Yagita. 2002. New aspects of natural-killer-cell surveillance and therapy of cancer. *Nat. Rev. Cancer* 2: 850–861.

17. Bauer, S., V. Groh, J. Wu, A. Steinle, J. H. Phillips, L. L. Lanier, and T. Spies. 1999. Activation of NK cells and T cells by NKG2D, a receptor for stress-inducible MICA. *Science* 285: 727–729.

18. Ljunggren, H. G., and K. Kärre. 1990. In search of the "missing self": MHC molecules and NK cell recognition. *Immunol. Today* 11: 237–244.

19. Paust, S., B. Senman, and U. H. von Andrian. 2010. Adaptive immune responses mediated by natural killer cells. *Immunol. Rev.* 235: 286–296.

20. Pahl, J., and A. Cerwenka. 2017. Tricking the balance: NK cells in anti-cancer immunity. *Immunobiology* 222: 11–20.

21. O'Leary, J. G., M. Goodarzi, D. L. Drayton, and U. H. von Andrian. 2006. T cell- and B cell-independent adaptive immunity mediated by natural killer cells. *Nat. Immunol.* 7: 507–516.

22. Kärre, K., H. G. Ljunggren, G. Piontek, and R. Kiessling. 1986. Selective rejection of H-2-deficient lymphoma variants suggests alternative immune defence strategy. *Nature* 319: 675–678.

23. Bottino, C., R. Castriconi, D. Pende, P. Rivera, M. Nanni, B. Carnemolla, C. Cantoni, J. Grassi, S. Marcenaro, N. Reymond, M. Vitale, L. Moretta, M. Lopez, and A. Moretta. 2003. Identification of PVR (CD155) and Nectin-2 (CD112) as cell surface ligands for the human DNAM-1 (CD226) activating molecule. *J. Exp. Med.* 198: 557–567.

24. Takai, Y., J. Miyoshi, W. Ikeda, and H. Ogita. 2008. Nectins and nectin-like molecules: roles in contact inhibition of cell movement and proliferation. *Nat. Rev. Mol. Cell Biol.* 9: 603–615.

25. Morisaki, T., H. Onishi, and M. Katano. 2012. Cancer immunotherapy using NKG2D and DNAM-1 systems. *Anticancer Res.* 32: 2241–2247.

26. Bronte, V. 2018. The expanding constellation of immune checkpoints: a DNAMic control by CD155. *J. Clin. Invest.* 128: 2199–2201.

27. Shibuya, A., D. Campbell, C. Hannum, H. Yssel, K. Franz-Bacon, T. McClanahan, T.

Kitamura, J. Nicholl, G. R. Sutherland, L. L. Lanier, and J. H. Phillips. 1996. DNAM-1, a novel adhesion molecule involved in the cytolytic function of T lymphocytes. *Immunity* 4: 573–581.

28. Chan, C. J., L. Martinet, S. Gilfillan, F. Souza-Fonseca-Guimaraes, M. T. Chow, L. Town, D. S. Ritchie, M. Colonna, D. M. Andrews, and M. J. Smyth. 2014. The receptors CD96 and CD226 oppose each other in the regulation of natural killer cell functions. *Nat. Immunol.* 15: 431–438.

29. Guerra, N., Y. X. Tan, N. T. Joncker, A. Choy, F. Gallardo, N. Xiong, S. Knoblaugh, D. Cado, N. M. Greenberg, and D. H. Raulet. 2008. NKG2D-deficient mice are defective in tumor surveillance in models of spontaneous malignancy. *Immunity* 28: 571–580.

30. Dhar, P., and J. D. Wu. 2018. NKG2D and its ligands in cancer. *Curr. Opin. Immunol.* 51: 55–61.

31. El-Sherbiny, Y. M., J. L. Meade, T. D. Holmes, D. McGonagle, S. L. Mackie, A. W. Morgan, G. Cook, S. Feyler, S. J. Richards, F. E. Davies, G. J. Morgan, and G. P. Cook. 2007. The requirement for DNAM-1, NKG2D, and NKp46 in the natural killer cell-mediated killing of myeloma cells. *Cancer Res.* 67: 8444–8449.

32. Gilfillan, S., C. J. Chan, M. Cella, N. M. Haynes, A. S. Rapaport, K. S. Boles, D. M. Andrews, M. J. Smyth, and M. Colonna. 2008. DNAM-1 promotes activation of cytotoxic lymphocytes by nonprofessional antigen-presenting cells and tumors. *J. Exp. Med.* 205: 2965–2973.

33. Duan, S., W. Guo, Z. Xu, Y. He, C. Liang, Y. Mo, Y. Wang, F. Xiong, C. Guo, Y. Li, X. Li, G. Li, Z. Zeng, W. Xiong, and F. Wang. 2019. Natural killer group 2D receptor and its ligands in cancer immune escape. *Mol. Cancer* 18: 29.

34. Jiang, X., J. Wang, X. Deng, F. Xiong, J. Ge, B. Xiang, X. Wu, J. Ma, M. Zhou, X. Li, Y. Li, G. Li, W. Xiong, C. Guo, and Z. Zeng. 2019. Role of the tumor microenvironment in PD-L1/PD-1-mediated tumor immune escape. *Mol. Cancer* 18: 10.

35. Koch, J., A. Steinle, C. Watzl, and O. Mandelboim. 2013. Activating natural cytotoxicity receptors of natural killer cells in cancer and infection. *Trends Immunol.* 34: 182–191.

36. Parks, S. K., Y. Cormerais, and J. Pouysségur. 2017. Hypoxia and cellular metabolism in tumour pathophysiology. *J. Physiol.* 595: 2439–2450.

37. Manoochehri Khoshinani, H., S. Afshar, and R. Najafi. 2016. Hypoxia: A Double-Edged Sword in Cancer Therapy. *Cancer Invest.* 34: 536–545.

38. Jing, X., F. Yang, C. Shao, K. Wei, M. Xie, H. Shen, and Y. Shu. 2019. Role of hypoxia in cancer therapy by regulating the tumor microenvironment. *Mol. Cancer* 18: 157.

39. Mantovani, A., P. Allavena, A. Sica, and F. Balkwill. 2008. Cancer-related inflammation.

Nature 454: 436–444.

40. Baginska, J., E. Viry, J. Paggetti, S. Medves, G. Berchem, E. Moussay, and B. Janji. 2013. The critical role of the tumor microenvironment in shaping natural killer cell-mediated anti-tumor immunity. *Front. Immunol.* 4: 490.

41. Balsamo, M., C. Manzini, G. Pietra, F. Raggi, F. Blengio, M. C. Mingari, L. Varesio, L. Moretta, M. C. Bosco, and M. Vitale. 2013. Hypoxia downregulates the expression of activating receptors involved in NK-cell-mediated target cell killing without affecting ADCC. *Eur. J. Immunol.* 43: 2756–2764.

42. Baragaño Raneros, A., B. Suarez-Álvarez, and C. López-Larrea. 2014. Secretory pathways generating immunosuppressive NKG2D ligands: New targets for therapeutic intervention. *Oncoimmunology* 3: e28497.

43. Iguchi-Manaka, A., H. Kai, Y. Yamashita, K. Shibata, S. Tahara-Hanaoka, S.-I. Honda, T. Yasui, H. Kikutani, K. Shibuya, and A. Shibuya. 2008. Accelerated tumor growth in mice deficient in DNAM-1 receptor. *J. Exp. Med.* 205: 2959–2964.

44. Lee, J.-C., K.-M. Lee, D.-W. Kim, and D. S. Heo. 2004. Elevated TGF-beta1 secretion and down-modulation of NKG2D underlies impaired NK cytotoxicity in cancer patients. *J. Immunol.* 172: 7335–7340.

45. Lin, C.-T., M.-T. Yu, C. Li, Y.-C. Ho, C.-H. Shen, D.-W. Liu, D.-C. Chang, and S.-F. Wu. 2010. Dysfunction of natural killer cells in patients with transitional cell carcinoma. *Cancer Lett.* 291: 39–45.

46. Mamessier, E., A. Sylvain, M.-L. Thibult, G. Houvenaeghel, J. Jacquemier, R. Castellano, A. Gonçalves, P. André, F. Romagné, G. Thibault, P. Viens, D. Birnbaum, F. Bertucci, A. Moretta, and D. Olive. 2011. Human breast cancer cells enhance self tolerance by promoting evasion from NK cell antitumor immunity. *J. Clin. Invest.* 121: 3609–3622.

47. Fortner, J. G. 1993. Inadvertent spread of cancer at surgery. *J. Surg. Oncol.* 53: 191–196.

48. Goldfarb, Y., L. Sorski, M. Benish, B. Levi, R. Melamed, and S. Ben-Eliyahu. 2011. Improving postoperative immune status and resistance to cancer metastasis: a combined perioperative approach of immunostimulation and prevention of excessive surgical stress responses. *Ann. Surg.* 253: 798–810.

49. Espí, A., J. Arenas, E. García-Granero, E. Martí, and S. Lledó. 1996. Relationship of curative surgery on natural killer cell activity in colorectal cancer. *Dis. Colon Rectum* 39: 429–434.

50. De Rosa, M., U. Pace, D. Rega, V. Costabile, F. Duraturo, P. Izzo, and P. Delrio. 2015. Genetics, diagnosis and management of colorectal cancer (Review). *Oncol. Rep.* 34: 1087–1096.

51. Sabiston, D. C. 2004. *Sabiston Textbook of Surgery: The Biological Basis of Modern Surgical Practice*,. Elsevier Saunders.

52. Demicheli, R., M. W. Retsky, W. J. M. Hrushesky, M. Baum, and I. D. Gukas. 2008. The effects of surgery on tumor growth: a century of investigations. *Annals of Oncology* 19: 1821–1828.

53. Coffey, J. C., J. H. Wang, M. J. F. Smith, D. Bouchier-Hayes, T. G. Cotter, and H. P. Redmond. 2003. Excisional surgery for cancer cure: therapy at a cost. *Lancet Oncol.* 4: 760–768.

54. Horowitz, M., E. Neeman, E. Sharon, and S. Ben-Eliyahu. 2015. Exploiting the critical perioperative period to improve long-term cancer outcomes. *Nat. Rev. Clin. Oncol.* 12: 213–226.

55. Pollock, R. E., E. Lotzová, and S. D. Stanford. 1992. Surgical stress impairs natural killer cell programming of tumor for lysis in patients with sarcomas and other solid tumors. *Cancer* 70: 2192–2202.

56. Tyzzer, E. E. 1913. Factors in the Production and Growth of tumor Metastases. *J. Med. Res.* 28: 309–332.1.

57. Marie, P., and J. Clunet. 1910. Fréquence des métastases viscérales chez les souris cancéreuses aprés ablation chirurgicale de leur tumeur. *Bull. Assoc. Fr. Etud. Cancer* 3: 19–23.

58. Baum, M. 1996. Does surgery disseminate or accelerate cancer? *Lancet* 347: 260.

59. Ogawa, K., M. Hirai, T. Katsube, M. Murayama, K. Hamaguchi, T. Shimakawa, Y. Naritake, T. Hosokawa, and T. Kajiwara. 2000. Suppression of cellular immunity by surgical stress. *Surgery* 127: 329–336.

60. Bakos, O., C. Lawson, S. Rouleau, and L.-H. Tai. 2018. Combining surgery and immunotherapy: turning an immunosuppressive effect into a therapeutic opportunity. *J Immunother Cancer* 6: 86.

61. Ceelen, W., P. Pattyn, and M. Mareel. 2014. Surgery, wound healing, and metastasis: recent insights and clinical implications. *Crit. Rev. Oncol. Hematol.* 89: 16–26.

62. Pera, M., H. Nelson, S. V. Rajkumar, T. M. Young-Fadok, and L. J. Burgart. 2003. Influence of postoperative acute-phase response on angiogenesis and tumor growth: open vs. laparoscopic-assisted surgery in mice. *J. Gastrointest. Surg.* 7: 783–790.

63. Alazawi, W., N. Pirmadjid, R. Lahiri, and S. Bhattacharya. 2016. Inflammatory and Immune Responses to Surgery and Their Clinical Impact. *Annals of Surgery* 264: 73–80.

64. Angka, L., S. T. Khan, M. K. Kilgour, R. Xu, M. A. Kennedy, and R. C. Auer. 2017. Dysfunctional Natural Killer Cells in the Aftermath of Cancer Surgery. *Int. J. Mol. Sci.* 18.

65. Carmeliet, P., and R. K. Jain. 2000. Angiogenesis in cancer and other diseases. *Nature* 407: 249–257.

66. Belizon, A., E. Balik, D. L. Feingold, M. Bessler, T. D. Arnell, K. A. Forde, P. K. Horst, S. Jain, V. Cekic, I. Kirman, and R. L. Whelan. 2006. Major abdominal surgery increases plasma levels of vascular endothelial growth factor: open more so than minimally invasive methods. *Ann. Surg.* 244: 792–798.

67. Brøchner, A. C., and P. Toft. 2009. Pathophysiology of the systemic inflammatory response after major accidental trauma. *Scand. J. Trauma Resusc. Emerg. Med.* 17: 43.

68. Bartal, I., R. Melamed, K. Greenfeld, S. Atzil, A. Glasner, V. Domankevich, R. Naor, B. Beilin, I. Z. Yardeni, and S. Ben-Eliyahu. 2010. Immune perturbations in patients along the perioperative period: alterations in cell surface markers and leukocyte subtypes before and after surgery. *Brain Behav. Immun.* 24: 376–386.

69. Salo, M. 1992. Effects of anaesthesia and surgery on the immune response. *Acta Anaesthesiol. Scand.* 36: 201–220.

70. Ng, C. S. H., and K. K. W. Lau. 2015. Surgical trauma and immune functional changes following major lung resection. *Indian J. Surg.* 77: 49–54.

71. Velásquez, J. F., M. F. Ramírez, D. I. Ai, V. Lewis, and J. P. Cata. 2015. Impaired Immune Function in Patients Undergoing Surgery for Bone Cancer. *Anticancer Res.* 35: 5461–5466.

72. Narita, S., N. Tsuchiya, T. Kumazawa, S. Maita, K. Numakura, T. Obara, H. Tsuruta, M. Saito, T. Inoue, Y. Horikawa, S. Satoh, and T. Habuchi. 2013. Comparison of surgical stress in patients undergoing open versus laparoscopic radical prostatectomy by measuring perioperative serum cytokine levels. *J. Laparoendosc. Adv. Surg. Tech. A* 23: 33–37.

73. Ng, C. S. H., T. W. Lee, S. Wan, I. Y. P. Wan, A. D. L. Sihoe, A. A. Arifi, and A. P. C. Yim. 2005. Thoracotomy is associated with significantly more profound suppression in lymphocytes and natural killer cells than video-assisted thoracic surgery following major lung resections for cancer. *J. Invest. Surg.* 18: 81–88.

74. Veenhof, A. A. F. A., M. S. Vlug, M. H. G. M. van der Pas, C. Sietses, D. L. van der Peet, E. S. M. de Lange-de Klerk, H. J. Bonjer, W. A. Bemelman, and M. A. Cuesta. 2012. Surgical stress response and postoperative immune function after laparoscopy or open surgery with fast track or standard perioperative care: a randomized trial. *Ann. Surg.* 255: 216–221.

75. Finnerty, C. C., N. T. Mabvuure, A. Ali, R. A. Kozar, and D. N. Herndon. 2013. The surgically induced stress response. *JPEN J. Parenter. Enteral Nutr.* 37: 21S–9S.

76. Da Costa, M. L., H. P. Redmond, N. Finnegan, M. Flynn, and D. Bouchier-Hayes. 1998. Laparotomy and laparoscopy differentially accelerate experimental flank tumour growth. *Br. J. Surg.* 85: 1439–1442.

77. Tsuchiya, Y., S. Sawada, I. Yoshioka, Y. Ohashi, M. Matsuo, Y. Harimaya, K. Tsukada, and I. Saiki. 2003. Increased surgical stress promotes tumor metastasis. *Surgery* 133: 547–555.

78. Mutter, D., A. Hajri, V. Tassetti, C. Solis-Caxaj, M. Aprahamian, and J. Marescaux. 1999. Increased tumor growth and spread after laparoscopy vs laparotomy: influence of tumor manipulation in a rat model. *Surg. Endosc.* 13: 365–370.

79. Lee, J.-W., M. M. K. Shahzad, Y. G. Lin, G. Armaiz-Pena, L. S. Mangala, H.-D. Han, H.-S. Kim, E. J. Nam, N. B. Jennings, J. Halder, A. M. Nick, R. L. Stone, C. Lu, S. K. Lutgendorf, S. W. Cole, A. E. Lokshin, and A. K. Sood. 2009. Surgical stress promotes tumor growth in ovarian carcinoma. *Clin. Cancer Res.* 15: 2695–2702.

80. Munford, R. S., and J. Pugin. 2001. Normal responses to injury prevent systemic inflammation and can be immunosuppressive. *Am. J. Respir. Crit. Care Med.* 163: 316–321.

81. Decker, D., R. Tolba, W. Springer, H. Lauschke, A. Hirner, and A. von Ruecker. 2005. Abdominal surgical interventions: local and systemic consequences for the immune system--a prospective study on elective gastrointestinal surgery. *J. Surg. Res.* 126: 12–18.

82. Ananth, A. A., L.-H. Tai, C. Lansdell, A. A. Alkayyal, K. E. Baxter, L. Angka, J. Zhang, C. Tanese de Souza, K. B. Stephenson, K. Parato, J. L. Bramson, J. C. Bell, B. D. Lichty, and R. C. Auer. 2016. Surgical Stress Abrogates Pre-Existing Protective T Cell Mediated Anti-Tumor Immunity Leading to Postoperative Cancer Recurrence. *PLoS One* 11: e0155947.

83. Tai, L.-H., J. Zhang, K. J. Scott, C. T. de Souza, A. A. Alkayyal, A. A. Ananth, S. Sahi, R. A. Adair, A. B. Mahmoud, S. Sad, J. C. Bell, A. P. Makrigiannis, A. A. Melcher, and R. C. Auer. 2013. Perioperative influenza vaccination reduces postoperative metastatic disease by reversing surgery-induced dysfunction in natural killer cells. *Clin. Cancer Res.* 19: 5104–5115.

84. Ishikawa, M., M. Nishioka, N. Hanaki, T. Miyauchi, Y. Kashiwagi, H. Ioki, A. Kagawa, and Y. Nakamura. 2009. Perioperative immune responses in cancer patients undergoing digestive surgeries. *World J. Surg. Oncol.* 7: 7.

85. Berger, A. 2000. Th1 and Th2 responses: what are they? *BMJ* 321: 424.

86. van der Bij, G. J., S. J. Oosterling, R. H. J. Beelen, S. Meijer, J. C. Coffey, and M. van

Egmond. 2009. The perioperative period is an underutilized window of therapeutic opportunity in patients with colorectal cancer. *Ann. Surg.* 249: 727–734.

87. Menezes, A. S., A. Barnes, A. S. Scheer, G. Martel, H. Moloo, R. P. Boushey, E. Sabri, and R. C. Auer. 2013. Clinical research in surgical oncology: an analysis of ClinicalTrials.gov. *Ann. Surg. Oncol.* 20: 3725–3731.

88. Ramirez, M. F., D. Ai, M. Bauer, J.-N. Vauthey, V. Gottumukkala, S. Kee, D. Shon, M. Truty, H. M. Kuerer, A. Kurz, M. Hernandez, and J. P. Cata. 2015. Innate immune function after breast, lung, and colorectal cancer surgery. *J. Surg. Res.* 194: 185–193.

89. Benish, M., I. Bartal, Y. Goldfarb, B. Levi, R. Avraham, A. Raz, and S. Ben-Eliyahu. 2008. Perioperative use of beta-blockers and COX-2 inhibitors may improve immune competence and reduce the risk of tumor metastasis. *Ann. Surg. Oncol.* 15: 2042–2052.

90. Pollock, R. E., E. Lotzová, and S. D. Stanford. 1991. Mechanism of surgical stress impairment of human perioperative natural killer cell cytotoxicity. *Arch. Surg.* 126: 338–342.

91. Tai, L.-H., C. T. de Souza, S. Bélanger, L. Ly, A. A. Alkayyal, J. Zhang, J. L. Rintoul, A. A. Ananth, T. Lam, C. J. Breitbach, T. J. Falls, D. H. Kirn, J. C. Bell, A. P. Makrigiannis, and R. A. Auer. 2013. Preventing postoperative metastatic disease by inhibiting surgery-induced dysfunction in natural killer cells. *Cancer Res.* 73: 97–107.

92. Ben-Eliyahu, S., G. G. Page, R. Yirmiya, and G. Shakhar. 1999. Evidence that stress and surgical interventions promote tumor development by suppressing natural killer cell activity. *Int. J. Cancer* 80: 880–888.

93. Watt, S. K., H. C. Hasselbalch, V. Skov, L. Kjær, M. Thomassen, T. A. Kruse, M. Burton, and I. Gögenur. 2018. Whole Blood Gene Expression Profiling in patients undergoing colon cancer surgery identifies differential expression of genes involved in immune surveillance, inflammation and carcinogenesis. *Surg. Oncol.* 27: 208–215.

94. Leung, K. L., K. S. Tsang, M. H. L. Ng, K. J. Leung, P. B. S. Lai, J. F. Y. Lee, and W. Y. Lau. 2003. Lymphocyte subsets and natural killer cell cytotoxicity after laparoscopically assisted resection of rectosigmoid carcinoma. *Surg. Endosc.* 17: 1305–1310.

95. Seth, R., L.-H. Tai, T. Falls, C. T. de Souza, J. C. Bell, M. Carrier, H. Atkins, R. Boushey, and R. A. Auer. 2013. Surgical stress promotes the development of cancer metastases by a coagulation-dependent mechanism involving natural killer cells in a murine model. *Ann. Surg.* 258: 158–168.

96. Brøchner, A. C., S. Mikkelsen, I. Hegelund, M. Hokland, O. Mogensen, and P. Toft. 2016. The immune response is affected for at least three weeks after extensive surgery for ovarian cancer. *Dan. Med. J.* 63.

97. Young, M. R., M. Newby, and H. T. Wepsic. 1987. Hematopoiesis and suppressor bone

marrow cells in mice bearing large metastatic Lewis lung carcinoma tumors. *Cancer Res.* 47: 100–105.

98. Buessow, S. C., R. D. Paul, and D. M. Lopez. 1984. Influence of mammary tumor progression on phenotype and function of spleen and in situ lymphocytes in mice. *J. Natl. Cancer Inst.* 73: 249–255.

99. Gabrilovich, D. I., and S. Nagaraj. 2009. Myeloid-derived suppressor cells as regulators of the immune system. *Nat. Rev. Immunol.* 9: 162–174.

100. Kusmartsev, S., Y. Nefedova, D. Yoder, and D. I. Gabrilovich. 2004. Antigen-specific inhibition of CD8+ T cell response by immature myeloid cells in cancer is mediated by reactive oxygen species. *J. Immunol.* 172: 989–999.

101. Youn, J.-I., S. Nagaraj, M. Collazo, and D. I. Gabrilovich. 2008. Subsets of myeloid-derived suppressor cells in tumor-bearing mice. *J. Immunol.* 181: 5791–5802.

102. Bronte, V., S. Brandau, S.-H. Chen, M. P. Colombo, A. B. Frey, T. F. Greten, S. Mandruzzato, P. J. Murray, A. Ochoa, S. Ostrand-Rosenberg, P. C. Rodriguez, A. Sica, V. Umansky, R. H. Vonderheide, and D. I. Gabrilovich. 2016. Recommendations for myeloid-derived suppressor cell nomenclature and characterization standards. *Nat. Commun.* 7: 12150.

103. Goh, C., S. Narayanan, and Y. S. Hahn. 2013. Myeloid-derived suppressor cells: the dark knight or the joker in viral infections? *Immunol. Rev.* 255: 210–221.

104. Janols, H., C. Bergenfelz, R. Allaoui, A.-M. Larsson, L. Rydén, S. Björnsson, S. Janciauskiene, M. Wullt, A. Bredberg, and K. Leandersson. 2014. A high frequency of MDSCs in sepsis patients, with the granulocytic subtype dominating in gram-positive cases. *J. Leukoc. Biol.* 96: 685–693.

105. Marvel, D., and D. I. Gabrilovich. 2015. Myeloid-derived suppressor cells in the tumor microenvironment: expect the unexpected. *J. Clin. Invest.* 125: 3356–3364.

106. Almand, B., J. I. Clark, E. Nikitina, J. van Beynen, N. R. English, S. C. Knight, D. P. Carbone, and D. I. Gabrilovich. 2001. Increased production of immature myeloid cells in cancer patients: a mechanism of immunosuppression in cancer. *J. Immunol.* 166: 678–689.

107. Ostrand-Rosenberg, S., and P. Sinha. 2009. Myeloid-derived suppressor cells: linking inflammation and cancer. *J. Immunol.* 182: 4499–4506.

108. Solito, S., I. Marigo, L. Pinton, V. Damuzzo, S. Mandruzzato, and V. Bronte. 2014. Myeloid-derived suppressor cell heterogeneity in human cancers. *Ann. N. Y. Acad. Sci.* 1319: 47–65.

109. Terabe, M., S. Matsui, J.-M. Park, M. Mamura, N. Noben-Trauth, D. D. Donaldson,

W. Chen, S. M. Wahl, S. Ledbetter, B. Pratt, J. J. Letterio, W. E. Paul, and J. A. Berzofsky. 2003. Transforming growth factor-beta production and myeloid cells are an effector mechanism through which CD1d-restricted T cells block cytotoxic T lymphocyte-mediated tumor immunosurveillance: abrogation prevents tumor recurrence. *J. Exp. Med.* 198: 1741–1752.

110. Fichtner-Feigl, S., M. Terabe, A. Kitani, C. A. Young, I. Fuss, E. K. Geissler, H.-J. Schlitt, J. A. Berzofsky, and W. Strober. 2008. Restoration of tumor immunosurveillance via targeting of interleukin-13 receptor-alpha 2. *Cancer Res.* 68: 3467–3475.

111. Kusmartsev, S., and D. I. Gabrilovich. 2003. Inhibition of myeloid cell differentiation in cancer: the role of reactive oxygen species. *J. Leukoc. Biol.* 74: 186–196.

112. Wang, J., L. Yang, L. Yu, Y.-Y. Wang, R. Chen, J. Qian, Z.-P. Hong, and X.-S. Su. 2017. Surgery-induced monocytic myeloid-derived suppressor cells expand regulatory T cells in lung cancer. *Oncotarget* 8: 17050–17058.

113. Diaz-Montero, C. M., M. L. Salem, M. I. Nishimura, E. Garrett-Mayer, D. J. Cole, and A. J. Montero. 2009. Increased circulating myeloid-derived suppressor cells correlate with clinical cancer stage, metastatic tumor burden, and doxorubicin-cyclophosphamide chemotherapy. *Cancer Immunol. Immunother.* 58: 49–59.

114. Cole, S., A. Montero, E. Garret-Mayer, G. Onicescu, T. Vandenberg, S. Hutchens, and C. Diaz-Montero. 2009. Elevated Circulating Myeloid Derived Suppressor Cells (MDSC) Are Associated with Inferior Overall Survival (OS) and Correlate with Circulating Tumor Cells (CTC) in Patients with Metastatic Breast Cancer. *Poster Session Abstracts*.

115. Wang, L., E. W. Y. Chang, S. C. Wong, S.-M. Ong, D. Q. Y. Chong, and K. L. Ling. 2013. Increased myeloid-derived suppressor cells in gastric cancer correlate with cancer stage and plasma S100A8/A9 proinflammatory proteins. *J. Immunol.* 190: 794–804.

116. Song, X., Y. Krelin, T. Dvorkin, O. Bjorkdahl, S. Segal, C. A. Dinarello, E. Voronov, and R. N. Apte. 2005. CD11b+/Gr-1+ immature myeloid cells mediate suppression of T cells in mice bearing tumors of IL-1beta-secreting cells. *J. Immunol.* 175: 8200–8208.

117. Sevko, A., and V. Umansky. 2013. Myeloid-derived suppressor cells interact with tumors in terms of myelopoiesis, tumorigenesis and immunosuppression: thick as thieves. *J. Cancer* 4: 3–11.

118. Sinha, P., V. K. Clements, A. M. Fulton, and S. Ostrand-Rosenberg. 2007. Prostaglandin E2 promotes tumor progression by inducing myeloid-derived suppressor cells. *Cancer Res.* 67: 4507–4513.

119. Murdoch, C., M. Muthana, S. B. Coffelt, and C. E. Lewis. 2008. The role of myeloid cells in the promotion of tumour angiogenesis. *Nat. Rev. Cancer* 8: 618–631.

120. Yang, L., J. Huang, X. Ren, A. E. Gorska, A. Chytil, M. Aakre, D. P. Carbone, L. M. Matrisian, A. Richmond, P. C. Lin, and H. L. Moses. 2008. Abrogation of TGF beta signaling in mammary carcinomas recruits Gr-1+CD11b+ myeloid cells that promote metastasis. *Cancer Cell* 13: 23–35.

121. Yang, L., L. M. DeBusk, K. Fukuda, B. Fingleton, B. Green-Jarvis, Y. Shyr, L. M. Matrisian, D. P. Carbone, and P. C. Lin. 2004. Expansion of myeloid immune suppressor Gr+CD11b+ cells in tumor-bearing host directly promotes tumor angiogenesis. *Cancer Cell* 6: 409–421.

122. Goh, C. C., K. M. Roggerson, H.-C. Lee, L. Golden-Mason, H. R. Rosen, and Y. S. Hahn. 2016. Hepatitis C Virus-Induced Myeloid-Derived Suppressor Cells Suppress NK Cell IFN-γ Production by Altering Cellular Metabolism via Arginase-1. *J. Immunol.* 196: 2283–2292.

123. Dancey, J. T., K. A. Deubelbeiss, L. A. Harker, and C. A. Finch. 1976. Neutrophil kinetics in man. *J. Clin. Invest.* 58: 705–715.

124. Manz, M. G., and S. Boettcher. 2014. Emergency granulopoiesis. *Nature Reviews Immunology* 14: 302–314.

125. Chiba, Y., I. Mizoguchi, H. Hasegawa, M. Ohashi, N. Orii, T. Nagai, M. Sugahara, Y. Miyamoto, M. Xu, T. Owaki, and T. Yoshimoto. 2018. Regulation of myelopoiesis by proinflammatory cytokines in infectious diseases. *Cell. Mol. Life Sci.* 75: 1363–1376.

126. Schultze, J. L., E. Mass, and A. Schlitzer. 2019. Emerging Principles in Myelopoiesis at Homeostasis and during Infection and Inflammation. *Immunity* 50: 288–301.

127. Jones, R. O., M. Brittan, N. H. Anderson, A. Conway Morris, J. T. Murchison, W. S. Walker, and A. J. Simpson. 2014. Serial characterisation of monocyte and neutrophil function after lung resection. *BMJ Open Respir Res* 1: e000045.

128. Yuan, L., B. Xu, H. Fan, P. Yuan, P. Zhao, and Z. Suo. 2015. Pre- and post-operative evaluation: percentages of circulating myeloid-derived suppressor cells in rectal cancer patients. *Neoplasma* 62: 239–249.

129. Wang, J., X. Su, L. Yang, F. Qiao, Y. Fang, L. Yu, Q. Yang, Y. Wang, Y. Yin, R. Chen, and Z. Hong. 2016. The influence of myeloid-derived suppressor cells on angiogenesis and tumor growth after cancer surgery. *Int. J. Cancer* 138: 2688–2699.

130. Uchida, A., R. Kolb, and M. Micksche. 1982. Generation of suppressor cells for natural killer activity in cancer patients after surgery. *J. Natl. Cancer Inst.* 68: 735–741.

131. Tai, L.-H., A. A. Alkayyal, A. L. Leslie, S. Sahi, S. Bennett, C. Tanese de Souza, K. Baxter, L. Angka, R. Xu, M. A. Kennedy, and R. C. Auer. 2018. Phosphodiesterase-5 inhibition reduces postoperative metastatic disease by targeting surgery-induced myeloid derived suppressor cell-dependent inhibition of Natural Killer cell cytotoxicity.

Oncoimmunology 7: e1431082.

132. Kuhlmann, L., E. Cummins, I. Samudio, and T. Kislinger. 2018. Cell-surface proteomics for the identification of novel therapeutic targets in cancer. *Expert Rev. Proteomics* 15: 259–275.

133. Zunke, F., and S. Rose-John. 2017. The shedding protease ADAM17: Physiology and pathophysiology. *Biochim. Biophys. Acta Mol. Cell Res.* 1864: 2059–2070.

134. Martinet, L., and M. J. Smyth. 2015. Balancing natural killer cell activation through paired receptors. *Nat. Rev. Immunol.* 15: 243–254.

135. Mendelsohn, C. L., E. Wimmer, and V. R. Racaniello. 1989. Cellular receptor for poliovirus: molecular cloning, nucleotide sequence, and expression of a new member of the immunoglobulin superfamily. *Cell* 56: 855–865.

136. Gao, J., Q. Zheng, N. Xin, W. Wang, and C. Zhao. 2017. CD155, an onco-immunologic molecule in human tumors. *Cancer Sci.* 108: 1934–1938.

137. Hirota, T., K. Irie, R. Okamoto, W. Ikeda, and Y. Takai. 2005. Transcriptional activation of the mouse Necl-5/Tage4/PVR/CD155 gene by fibroblast growth factor or oncogenic Ras through the Raf-MEK-ERK-AP-1 pathway. *Oncogene* 24: 2229–2235.

138. Kakunaga, S., W. Ikeda, T. Shingai, T. Fujito, A. Yamada, Y. Minami, T. Imai, and Y. Takai. 2004. Enhancement of serum- and platelet-derived growth factor-induced cell proliferation by Necl-5/Tage4/poliovirus receptor/CD155 through the Ras-Raf-MEK-ERK signaling. *J. Biol. Chem.* 279: 36419–36425.

139. Ikeda, W., S. Kakunaga, K. Takekuni, T. Shingai, K. Satoh, K. Morimoto, M. Takeuchi, T. Imai, and Y. Takai. 2004. Nectin-like molecule-5/Tage4 enhances cell migration in an integrin-dependent, Nectin-3-independent manner. *J. Biol. Chem.* 279: 18015–18025.

140. Abercrombie, M., and J. E. Heaysman. 1954. Observations on the social behaviour of cells in tissue culture. II. Monolayering of fibroblasts. *Exp. Cell Res.* 6: 293–306.

141. Abercrombie, M. 1970. Contact inhibition in tissue culture. *In Vitro* 6: 128–142.

142. Zegers, M. M. P., M.-A. Forget, J. Chernoff, K. E. Mostov, M. B. A. ter Beest, and S. H. Hansen. 2003. Pak1 and PIX regulate contact inhibition during epithelial wound healing. *EMBO J.* 22: 4155–4165.

143. Fujito, T., W. Ikeda, S. Kakunaga, Y. Minami, M. Kajita, Y. Sakamoto, M. Monden, and Y. Takai. 2005. Inhibition of cell movement and proliferation by cell-cell contact-induced interaction of Necl-5 with nectin-3. *J. Cell Biol.* 171: 165–173.

144. de Andrade, L. F., M. J. Smyth, and L. Martinet. 2014. DNAM-1 control of natural

killer cells functions through nectin and nectin-like proteins. *Immunol. Cell Biol.* 92: 237–244.

145. Tahara-Hanaoka, S., K. Shibuya, Y. Onoda, H. Zhang, S. Yamazaki, A. Miyamoto, S.-I. Honda, L. L. Lanier, and A. Shibuya. 2004. Functional characterization of DNAM-1 (CD226) interaction with its ligands PVR (CD155) and nectin-2 (PRR-2/CD112). *Int. Immunol.* 16: 533–538.

146. Chan, C. J., M. J. Smyth, and L. Martinet. 2014. Molecular mechanisms of natural killer cell activation in response to cellular stress. *Cell Death Differ.* 21: 5–14.

147. Stanietsky, N., T. L. Rovis, A. Glasner, E. Seidel, P. Tsukerman, R. Yamin, J. Enk, S. Jonjic, and O. Mandelboim. 2013. Mouse TIGIT inhibits NK-cell cytotoxicity upon interaction with PVR. *Eur. J. Immunol.* 43: 2138–2150.

148. Stanietsky, N., H. Simic, J. Arapovic, A. Toporik, O. Levy, A. Novik, Z. Levine, M. Beiman, L. Dassa, H. Achdout, N. Stern-Ginossar, P. Tsukerman, S. Jonjic, and O. Mandelboim. 2009. The interaction of TIGIT with PVR and PVRL2 inhibits human NK cell cytotoxicity. *Proc. Natl. Acad. Sci. U. S. A.* 106: 17858–17863.

149. Dougall, W. C., S. Kurtulus, M. J. Smyth, and A. C. Anderson. 2017. TIGIT and CD96: new checkpoint receptor targets for cancer immunotherapy. *Immunol. Rev.* 276: 112–120.

150. Molfetta, R., B. Zitti, M. Lecce, N. D. Milito, H. Stabile, C. Fionda, M. Cippitelli, A. Gismondi, A. Santoni, and R. Paolini. 2020. CD155: A Multi-Functional Molecule in Tumor Progression. *Int. J. Mol. Sci.* 21.

151. Seth, S., Q. Qiu, S. Danisch, M. K. Maier, A. Braun, I. Ravens, N. Czeloth, R. Hyde, O. Dittrich-Breiholz, R. Förster, and G. Bernhardt. 2011. Intranodal interaction with dendritic cells dynamically regulates surface expression of the co-stimulatory receptor CD226 protein on murine T cells. *J. Biol. Chem.* 286: 39153–39163.

152. Sloan, K. E., B. K. Eustace, J. K. Stewart, C. Zehetmeier, C. Torella, M. Simeone, J. E. Roy, C. Unger, D. N. Louis, L. L. Ilag, and D. G. Jay. 2004. CD155/PVR plays a key role in cell motility during tumor cell invasion and migration. *BMC Cancer* 4: 73.

153. Nishiwada, S., M. Sho, S. Yasuda, K. Shimada, I. Yamato, T. Akahori, S. Kinoshita, M. Nagai, N. Konishi, and Y. Nakajima. 2015. Clinical significance of CD155 expression in human pancreatic cancer. *Anticancer Res.* 35: 2287–2297.

154. Gromeier, M., and S. K. Nair. 2018. Recombinant Poliovirus for Cancer Immunotherapy. *Annu. Rev. Med.* 69: 289–299.

155. Zheng, Q., B. Wang, J. Gao, N. Xin, W. Wang, X. Song, Y. Shao, and C. Zhao. 2018. CD155 knockdown promotes apoptosis via AKT/Bcl-2/Bax in colon cancer cells. *J. Cell. Mol. Med.* 22: 131–140.

156. Gromeier, M., S. Lachmann, M. R. Rosenfeld, P. H. Gutin, and E. Wimmer. 2000. Intergeneric poliovirus recombinants for the treatment of malignant glioma. *Proc. Natl. Acad. Sci. U. S. A.* 97: 6803–6808.

157. Nakai, R., Y. Maniwa, Y. Tanaka, W. Nishio, M. Yoshimura, Y. Okita, C. Ohbayashi, N. Satoh, H. Ogita, Y. Takai, and Y. Hayashi. 2010. Overexpression of Necl-5 correlates with unfavorable prognosis in patients with lung adenocarcinoma. *Cancer Sci.* 101: 1326–1330.

158. Atsumi, S., A. Matsumine, H. Toyoda, R. Niimi, T. Iino, and A. Sudo. 2013. Prognostic significance of CD155 mRNA expression in soft tissue sarcomas. *Oncol. Lett.* 5: 1771–1776.

159. Bevelacqua, V., Y. Bevelacqua, S. Candido, E. Skarmoutsou, A. Amoroso, C. Guarneri, A. Strazzanti, P. Gangemi, M. C. Mazzarino, F. D'Amico, J. A. McCubrey, M. Libra, and G. Malaponte. 2012. Nectin like-5 overexpression correlates with the malignant phenotype in cutaneous melanoma. *Oncotarget* 3: 882–892.

160. Masson, D., A. Jarry, B. Baury, P. Blanchardie, C. Laboisse, P. Lustenberger, and M. G. Denis. 2001. Overexpression of the CD155 gene in human colorectal carcinoma. *Gut* 49: 236–240.

161. Thiery, J. P. 2002. Epithelial-mesenchymal transitions in tumour progression. *Nat. Rev. Cancer* 2: 442–454.

162. Morimoto, K., K. Satoh-Yamaguchi, A. Hamaguchi, Y. Inoue, M. Takeuchi, M. Okada, W. Ikeda, Y. Takai, and T. Imai. 2008. Interaction of cancer cells with platelets mediated by Necl-5/poliovirus receptor enhances cancer cell metastasis to the lungs. *Oncogene* 27: 264–273.

163. Tane, S., Y. Maniwa, D. Hokka, S. Tauchi, W. Nishio, Y. Okita, and M. Yoshimura. 2013. The role of Necl-5 in the invasive activity of lung adenocarcinoma. *Exp. Mol. Pathol.* 94: 330–335.

164. Li, X.-Y., I. Das, A. Lepletier, V. Addala, T. Bald, K. Stannard, D. Barkauskas, J. Liu, A. R. Aguilera, K. Takeda, M. Braun, K. Nakamura, S. Jacquelin, S. W. Lane, M. W. Teng, W. C. Dougall, and M. J. Smyth. 2018. CD155 loss enhances tumor suppression via combined host and tumor-intrinsic mechanisms. *J. Clin. Invest.* 128: 2613–2625.

165. Abe, A., H. Fukui, S. Fujii, T. Kono, K. Mukawa, N. Yoshitake, A. Sekikawa, K. Ichikawa, S. Tomita, H. Yamagishi, Y. Imai, M. Shinoda, H. Ishizaki, M. Tanaka-Okamoto, K. Kubota, J. Miyoshi, Y. Takai, and T. Fujimori. 2009. Role of Necl-5 in the pathophysiology of colorectal lesions induced by dimethylhydrazine and/or dextran sodium sulphate. *J. Pathol.* 217: 42–53.

166. Okumura, G., A. Iguchi-Manaka, R. Murata, Y. Yamashita-Kanemaru, A. Shibuya, and K. Shibuya. 2020. Tumor-derived soluble CD155 inhibits DNAM-1-mediated antitumor activity of natural killer cells. *J. Exp. Med.* 217.

167. Chan, C. J., D. M. Andrews, N. M. McLaughlin, H. Yagita, S. Gilfillan, M. Colonna, and M. J. Smyth. 2010. DNAM-1/CD155 interactions promote cytokine and NK cell-mediated suppression of poorly immunogenic melanoma metastases. *J. Immunol.* 184: 902–911.

168. Castriconi, R., A. Dondero, M. V. Corrias, E. Lanino, D. Pende, L. Moretta, C. Bottino, and A. Moretta. 2004. Natural killer cell-mediated killing of freshly isolated neuroblastoma cells: critical role of DNAX accessory molecule-1-poliovirus receptor interaction. *Cancer Res.* 64: 9180–9184.

169. Tahara-Hanaoka, S., K. Shibuya, H. Kai, A. Miyamoto, Y. Morikawa, N. Ohkochi, S.-I. Honda, and A. Shibuya. 2006. Tumor rejection by the poliovirus receptor family ligands of the DNAM-1 (CD226) receptor. *Blood* 107: 1491–1496.

170. Iguchi-Manaka, A., G. Okumura, H. Kojima, Y. Cho, R. Hirochika, H. Bando, T. Sato, H. Yoshikawa, H. Hara, A. Shibuya, and K. Shibuya. 2016. Increased Soluble CD155 in the Serum of Cancer Patients. *PLoS One* 11: e0152982.

171. Yong, H., R. Cheng, X. Li, G. Gao, X. Jiang, H. Cheng, X. Zhou, and W. Zhao. 2019. CD155 expression and its prognostic value in postoperative patients with breast cancer. *Biomed. Pharmacother.* 115: 108884.

172. Zhang, J., Y. Zhu, Q. Wang, Y. Kong, H. Sheng, J. Guo, J. Xu, and B. Dai. 2020. Poliovirus receptor CD155 is up-regulated in muscle-invasive bladder cancer and predicts poor prognosis. *Urol. Oncol.* 38: 41.e11–41.e18.

173. Stamm, H., F. Klingler, E.-M. Grossjohann, J. Muschhammer, E. Vettorazzi, M. Heuser, U. Mock, F. Thol, G. Vohwinkel, E. Latuske, C. Bokemeyer, R. Kischel, C. Dos Santos, S. Stienen, M. Friedrich, M. Lutteropp, D. Nagorsen, J. Wellbrock, and W. Fiedler. 2018. Immune checkpoints PVR and PVRL2 are prognostic markers in AML and their blockade represents a new therapeutic option. *Oncogene* 37: 5269–5280.

174. Wu, L., L. Mao, J.-F. Liu, L. Chen, G.-T. Yu, L.-L. Yang, H. Wu, L.-L. Bu, A. B. Kulkarni, W.-F. Zhang, and Z.-J. Sun. 2019. Blockade of TIGIT/CD155 Signaling Reverses T-cell Exhaustion and Enhances Antitumor Capability in Head and Neck Squamous Cell Carcinoma. *Cancer Immunol Res* 7: 1700–1713.

175. Toft, P., E. Tønnesen, H. S. Helbo-Hansen, S. T. Lillevang, J. W. Rasmussen, and N. J. Christensen. 1994. Redistribution of granulocytes in patients after major surgical stress. *APMIS* 102: 43–48.

176. Sambor, A., A. Garcia, M. Berrong, J. Pickeral, S. Brown, W. Rountree, A. Sanchez, J. Pollara, N. Frahm, S. Keinonen, G. H. Kijak, M. Roederer, G. Levine, M. P. D'Souza,

M. Jaimes, R. Koup, T. Denny, J. Cox, and G. Ferrari. 2014. Establishment and maintenance of a PBMC repository for functional cellular studies in support of clinical vaccine trials. *J. Immunol. Methods* 409: 107–116.

177. Ducar, C., D. Smith, C. Pinzon, M. Stirewalt, C. Cooper, M. J. McElrath, J. Hural, and NIAID HIV Vaccine Trials Network. 2014. Benefits of a comprehensive quality program for cryopreserved PBMC covering 28 clinical trials sites utilizing an integrated, analytical web-based portal. *J. Immunol. Methods* 409: 9–20.

178. Trellakis, S., K. Bruderek, J. Hütte, M. Elian, T. K. Hoffmann, S. Lang, and S. Brandau. 2013. Granulocytic myeloid-derived suppressor cells are cryosensitive and their frequency does not correlate with serum concentrations of colony-stimulating factors in head and neck cancer. *Innate Immun.* 19: 328–336.

179. Wagner, A., E. Garner-Spitzer, J. Jasinska, H. Kollaritsch, K. Stiasny, M. Kundi, and U. Wiedermann. 2018. Age-related differences in humoral and cellular immune responses after primary immunisation: indications for stratified vaccination schedules. *Sci. Rep.* 8: 9825.

180. Kovaiou, R. D., D. Herndler-Brandstetter, and B. Grubeck-Loebenstein. 2007. Age-related changes in immunity: implications for vaccination in the elderly. *Expert Rev. Mol. Med.* 9: 1–17.

181. Weiskopf, D., B. Weinberger, and B. Grubeck-Loebenstein. 2009. The aging of the immune system. *Transpl. Int.* 22: 1041–1050.

182. Ciabattini, A., C. Nardini, F. Santoro, P. Garagnani, C. Franceschi, and D. Medaglini. 2018. Vaccination in the elderly: The challenge of immune changes with aging. *Semin. Immunol.* 40: 83–94.

183. Thompson, T. W., A. B. Kim, P. J. Li, J. Wang, B. T. Jackson, K. T. H. Huang, L. Zhang, and D. H. Raulet. 2017. Endothelial cells express NKG2D ligands and desensitize antitumor NK responses. *Elife* 6.

184. Sanchez-Correa, B., I. Gayoso, J. M. Bergua, J. G. Casado, S. Morgado, R. Solana, and R. Tarazona. 2012. Decreased expression of DNAM-1 on NK cells from acute myeloid leukemia patients. *Immunol. Cell Biol.* 90: 109–115.

7. CONTRIBUTIONS OF COLLABORATORS

I would like to take a moment to acknowledge the work and assistance of a few specific collaborators. Firstly, the Sx-MDSC cell surface proteomic screen was completed prior to the start of my Master's project by our collaborator Dr. Kislinger. The results from this screen were an important piece to formulate my rationale and hypothesis, as explained in the introduction. Christiano T. de Souza played an instrumental role in the planning and completion of my murine experiments. He administered the anti-CD155 IP and B16F10 IV injections, and although he taught me the technique of operating on mice, most of the surgeries were completed by Christiano to ensure consistency between experiments. He also performed the murine euthanasia by lethal buprenorphine injections and cervical dislocation. During larger murine endpoint experiments, Leonard Angka often helped me process murine samples when I had to complete flow phenotyping and *ex vivo* killing assays in parallel. Additionally, it is important to note that half of the biological replicates for the Sx-MDSC and granulocyte populations in Figure 8 are from experiments completed by Leonard. I decided to combine them with my own experiments to increase numbers and help visualize the postoperative changes in these populations. All other figures are results entirely from my own experiments. Lastly, I would like to acknowledge collaborators in Australia Dr. Liam Town, manager, and Dr. Mark Smyth, principal investigator, for donating the B16F10-CD155 KO and parental B16F10-WT cell lines, as well as their guidance on maintaining these cells.

8. APPENDIX

APPENDIX A: ANTIBODY TABLE

HUMAN MDSC ANTIBODIES	
1. PE-Cy7 – CD33 (Clone P67.6)	Biolegend 366618
2. APC-Cy7 – CD14 (Clone MφP9)	BD Biosciences 557831
3. AF700 – CD11b (Clone ICRF44)	R&D Systems FAB1699N
4. e450 – CD15 (Clone MMA)	Life Technologies 48-0158-42
5. APC – HLA/DR (Clone L243)	Biolegend 307610
6. PE – CD155 (Clone SKII.4)	Biolegend 337610
7. PE – IgG1 k Isotype (Clone MOPC-21)	Biolegend 400114
8. PE - CD155 (Clone PV404.19)	Miltenyi 130-105-846
9. PE - IgG1 k Isotype (Clone IS5-21F5)	130-113-200
10. FITC – CD19 (Clone HIB19)	Biolegend 302206
11. FITC – CD56 (Clone NCAM16.2)	BD Bioscience 340410
12. FITC – CD3 (Clone HIT3a)	Thermo Fisher 11-0039-42
MURINE MDSC ANTIBODIES	
1. BV786 – CD45 Rat IgG2b (Clone 30-F11)	BD Bioscience 564225
2. AF700 – CD3 Hamster IgG2 (Clone 500A2)	BD Bioscience 557984
3. APC-Cy7 – CD11b Rat IgG2b (Clone M1/70)	BD Bioscience 561039
4. FITC – GR1 Rat IgG2b (Clone RB6-8C5)	Biolegend 108405
5. APC – CD155 Rat IgG2a (Clone TX56)	Biolegend 131510
6. APC – IgG2a Isotype (Clone RTK2758)	Biolegend 400512
MURINE NK CELL ANTIBODIES	
1. BV786 – CD45 (Clone 30-F11)	BD Bioscience 564225

2. AF700 – CD3 (Clone 500A2)	BD Bioscience 557984
3. PE – CD49b (Clone DX5)	BD Bioscience 553858
4. PE-Cy7 – CD122 (Clone TM-beta1)	Thermo Fisher 25-1222-82
5. BV421 – DNAM (Clone TX42.1)	Biolegend 133615
6. BV421 – IgG2a k Isotype (Clone RTK2758)	Biolegend 400549
7. FITC – NKG2D CD314 (Clone C7)	Biolegend 115711
8. FITC – Armenian Hamster Isotype (Clone HTK888)	Biolegend 400905
BLOCKING ANTIBODIES	
1. Purified anti-human CD155 (Clone SKII.4)	Biolegend 337602
2. Purified mouse IgG1 k isotype control (Clone MOPC-21)	Biolegend 400102
3. Purified anti-mouse CD155 – Low Endotoxin Functional Formulation, GOLD (Clone 4.24.1)	Leinco Tech C2833

APPENDIX B: HUMAN CD155 ANTIBODY SELECTION

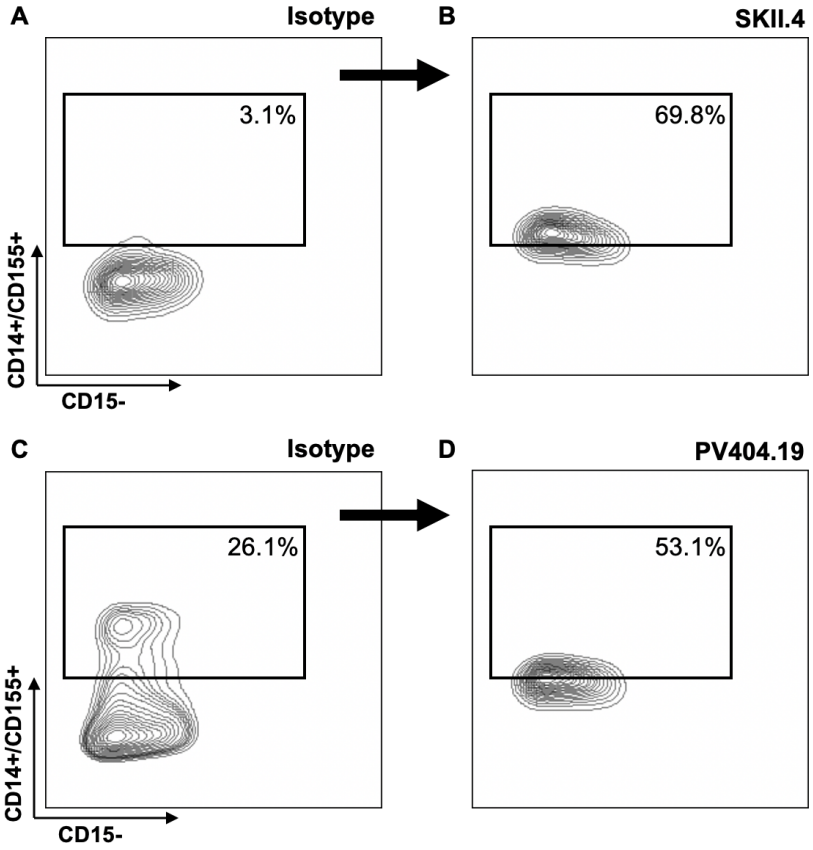

Appendix B. Selection of Human CD155 Antibody Clone.
Representative smooth plots of a cancer patient for CD155 expression on Sx-MDSC, gated $Lin^{-}/CD33^{+}/CD14^{+}/CD15^{lo}$. Isotypes are compared to their samples for titrated antibodies SKII.4 (**A-B**) and PV404.19 (**C-D**).

APPENDIX C: DETAILED FLOW CYTOMETRY GATING OF HUMAN SX-MSDC

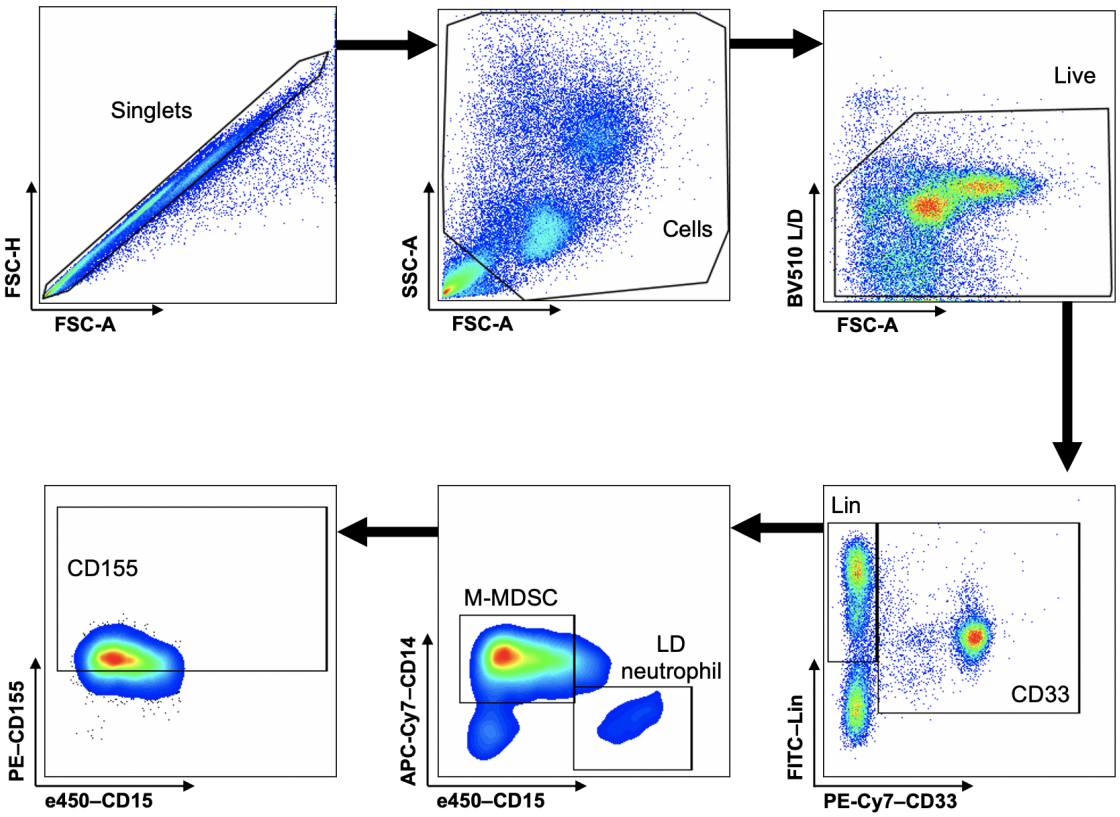

Appendix C. Detailed Flow Cytometry Gating Strategy for Human Sx-MDSC.
Representative gating for a POD1 cancer patient. After excluding doublets, debris and dead cells, Lin(CD3, CD56,CD19) cells are removed. Of the $CD33^{+}$ myeloid cells, M-MDSC are gated $CD14^{+}/CD15^{lo}$ while the LD neutrophils are $CD14^{-}/CD15^{+}$. CD155 is gated based on its corresponding isotype control.

APPENDIX D: NON-CANCER Sx-MDSC CD155

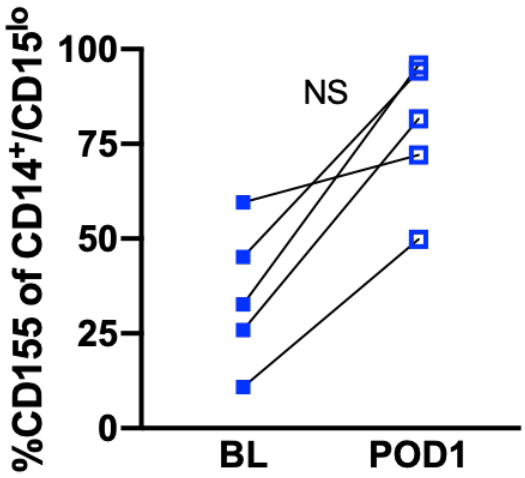

Appendix D. Sx-MDSC CD155 Expression in Non-Cancer Patients.
Percentage CD155+ of Sx-MDSCs (gated $CD33^{+}/CD14^{+}/CD15^{lo}$) for 5 non-cancer patients, comparing baseline (BL) to POD1. Matched POD1 compared to BL by Wilcoxon matched rank test. NS p=0.06.

APPENDIX E: FLOW CYTOMETRY GATING FOR HUMAN *EX VIVO* SUPPRESSION ASSAY

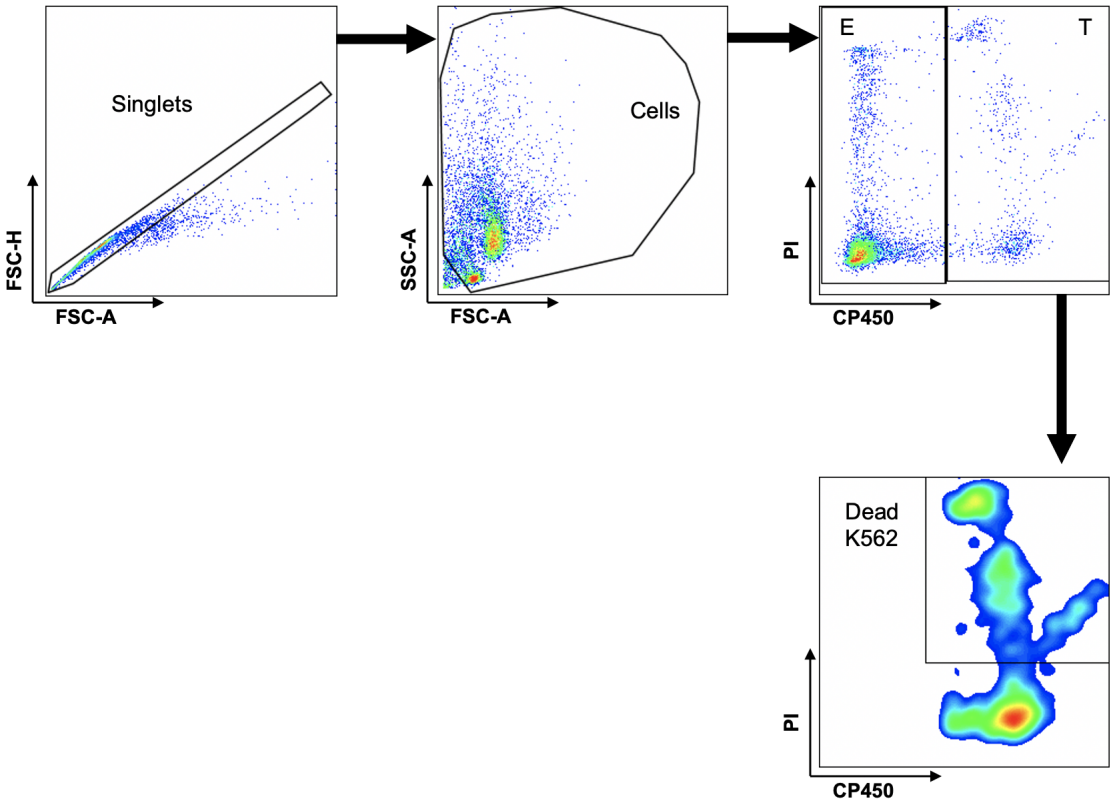

Appendix E. Flow Cytometry Gating Strategy for *Ex Vivo* Human Suppression Assay. Representative gating for a POD1 cancer patient. After excluding doublets and debris, effector cells (E) are separated from K562 target cells (T) based on CP450 expression. Proportion of dead K562 gated $CP450^{+}/PI^{+}$.

9. CURRICULUM VITAE

EDUCATION

2016-2023	General Surgery Resident, University of Ottawa
2018-2020	Master of Science (MSc) in Cancer Immunology, University of Ottawa
2018-2020	Surgeon-Scientist, Clinician Investigator Program (CIP), University of Ottawa
2018	Surgical Foundations Examination, Royal College of Physicians & Surgeons
2017	Licentiate of the Medical Council of Canada (LMCC) Parts I & II, Canada
2015-2016	Family Medicine Resident, Western University
2011-2015	Doctor of Medicine (MD), University of Ottawa
2007-2011	Bachelor of Science (BSc), Biopharmaceutical Sciences, University of Ottawa

SELECT ACADEMIC AWARDS

2020	**First Place Podium Presentation Award**, General Surgery Annual Research Day (GSRD) 2020, Ottawa, Ontario
2020	**Best Presentation**, Cancer Therapy and Cancer Pathogenesis, Department of BMI Seminar day 2020, Faculty of Medicine, Ottawa, Ontario
2019-2020	**Ontario Graduate Scholarship (OGS) Recipient**, University of Ottawa, Canada
2019	**First Place Podium Presentation Award**, General Surgery Annual Research Day (GSRD) 2019, Ottawa, Ontario
2018-2019	**Canada Graduate Scholarship (CGS) Recipient**, Canadian Institute of Health Research (CIHR), Canada
2018	**Resident/Fellow Award**, Best Basic Science/Translational Research Paper and Presentation, Society of Surgical Oncology (SSO), 2018, Chicago, Illinois
2018	**JP Collins Award** for Best Translational Research Presentation, Collin's Department of Surgery Research Day 2018, Ottawa, Ontario
2018	**First Place Podium Presentation**, Canadian Society of Surgical Oncology (CSSO), 2018 Annual Spring Meeting, Toronto, Ontario
2018	**CACSR Nomination for Golden Scalpel** Award Best National Oral Presentation, Canadian Surgery Forum 2018, St. John's, Newfoundland
2011	**Ontario Graduate Scholarship (OGS) and NSERC Scholarship** – Offered both scholarships to pursue graduate studies in biochemistry.

2014 **RBC Students Leading Change National Scholarship Recipient**, Canada – Selected for various leadership and extracurricular activities in the field of surgery

2011 **Undergraduate Research Excellence Award**, Faculty of Science, University of Ottawa, ON

MANUSCRIPT PUBLICATIONS

1. Market M & Angka L, **Martel AB**, Bastin D, Olanubi O, Tennakoon G, Boucher D, Ng J, Ardolino M & Auer RC. 2020. Flattening the COVID-19 Curve with Natural Killer Cell Based Immunotherapies. *Frontiers Immunology. Accepted.*

2. Gawad N, Tran A, **Martel AB**, Baxter NN, Allen M, Manhas N & Balaa FK. 2020. Co-Second Author. Gender and academic promotion of Canadian general surgeons: a cross-sectional study. *CMAJ Open.* DOI:10.9778/cmajo.20190090

3. Baker L, Park L, Gilbert R, **Martel A**, Ahn H, Davies A, Saidenberg E, Fergusson D & Martel G. 2019. Guidelines on the intraoperative transfusion of red blood cells: a protocol for systematic review. *BMJ Open*. 17;9(6):e029684. DOI:10.1136/bmjopen-2019-029684

4. Tran A, Gawad N, **Martel AB**, Manhas N, Allen M, Hameed M & Balaa FK. 2019. Co-Second Author. The Changing Face of Academic General Surgery in Canada: A Cross-Sectional Cohort Study. *Canadian Journal of Surgery (CJS).* 23;62(6):016418. DOI: 10.1503/cjs.016418

5. Angka L and **Martel AB**, Kilgour M, Jeong A, Sadiq M, Tanese de Souza C, Baker L, Kennedy MA & Auer RC. 2018. Co-first author. Natural Killer Cell IFN gamma secretion is profoundly suppressed following colorectal cancer surgery. *Annals of Surgical Oncology.* DOI.org/10.1245/s10434-018-6691-3

6. Gilbert S, **Martel AB**, Seely AJ, Maziak DE, Shamji FM, Sundaresan SR, Villeneuve PJ. 2015. Second Author. Prognostic Significance of a Positive Radial Margin after Esophageal Cancer Resection. *Journal of Thoracic and Cardiovascular Surgery (JTCVS).* 149(2):548-55

7. Adamczyk A, **Martel AB**, Stokl A & Ramnanan CJ. 2014. Co-First Author. Minding the Gap: Student-Led, Surgically-Oriented Anatomy Electives. *Medical Education*. 48(11):1108-09. doi: 10.1111/medu.1256

8. Liu Y, Nandi S, **Martel A**, Antoun A, Ioshikhes I & Blais A. 2012. Co-Second Author. Discovery, Optimization and Validation of an Optimal DNA-Binding Sequence for the Six1 Homeodomain Transcription Factor. *Nucleic Acids Research*. 40(17):8227-39.

ORAL PRESENTATIONS

1. **Martel AB,** Angka L, Tanese de Souza C, Ng J, Market M, Tennakoon G, Kennedy MA & Auer RC. **Targeting CD155 Poliovirus Receptor: A Novel Strategy to Prevent Postoperative Immunosuppression in Cancer Patients.**
   - May 2020 – Annual Seminar Day, Department of BMI, Ottawa, Ontario
   - April 2020 – General Surgery Annual Research Day (GSRD), Ottawa, Ontario

2. **Martel AB,** Angka L, Tanese de Souza C, Ng J, Kennedy MA & Auer RC. **Targeting CD155 on Myeloid Derived Suppressor Cells to Prevent Post-Operative Immune Suppression in Cancer Patients**.
   - September 2019 – Canadian Surgery Forum, Resident Research Retreat, Montreal, Quebec
   - April 2019 – General Surgery Annual Research Day (GSRD), Ottawa, Ontario

3. **Martel AB**, Angka L, Jeong A, Sadiq M, Kilgour M, Tanese De Souza C, Kennedy M & Auer RC. **Surgical Stress Suppresses Natural Killer Cell IFNγ Release in Colorectal Cancer Patients.**
   - September 2018 – CSSO Session, Canadian Surgery Forum (CSF), St. John's, Newfoundland
   - September 2018 – CACSR Session, Canadian Surgery Forum, St. John's, Newfoundland
   - May 2018 – Collin's Department of Surgery Research Day, Ottawa, Ontario
   - April 2018 – CSSO 27th Annual Meeting, Toronto, Ontario
   - April 2018 – General Surgery Annual Research Day, Ottawa, Ontario
   - March 2018 – Society of Surgical Oncology (SSO) 71st Annual Meeting, Chicago, Illinois

LEADERSHIP AND FACULTY INVOLVEMENT

2020 **Grant reviewer,** Resident Research Grant Competition, Department of Surgery, The Ottawa Hospital, Ottawa, Ontario

2019-2020 **Chief Resident, Clinician Investigator Program (CIP), University of Ottawa**
- Elected to represent CIP residents from all departments at TOH
- Attended quarterly CIP RPC committee meetings
- Led residents through a successful accreditation internal review

2019 – **Medical Examiner** for NAC and Undergraduate OSCE, Medical Council of Canada (MCC), University of Ottawa, Ontario

2018-2019 Lecturer and CBL Instructor for Undergraduate Medical Education (UGME), Gastroenterology and General Surgery Block, Faculty of Medicine, University of Ottawa

2018-2020 Teacher for Clerkship Core General Surgery Lecture, Faculty of Medicine, University of Ottawa

2016 – **General Surgery CaRMS Committee, Resident Representative**
- Improved the CaRMS review process and updated interview scoring criteria
- Involved in the file review stage and participated as CaRMS interviewer

2016 – **General Surgery Residency Program Committee (RPC), Resident Representative**
- Responsible to represent PGY cohort in the RPC committee
- Attended quarterly RPC meetings to address program issues, improve curriculum development and solicit resident feedback

2016-2019 Copy Editor, University of Ottawa Journal of Medicine (UOJM)

2013-2014 Advanced Surgical Anatomy Interest Group, ASAIG (Co-founder)
- Created the group to address deficiencies in surgical anatomy content
- Integrated common clinical encounters with the relevant operative anatomy during peer-led sessions

2012-2013 **Editor-in-Chief, University of Ottawa Journal of Medicine (UOJM)**
- Oversaw the entire developmental process and involved in every decision-making aspect
- Responsible for sponsorship and budget decisions
- Created and led editing workshops for editorial team
- Ensured the quality control of manuscripts at the final stage of editing
- Managed the publication stage, including copy-editing, layout editing and distribution

WORK EXPERIENCE

2016 – General Surgery Resident, The Ottawa Hospital, Ottawa, ON
2015-2016 Family Medicine Resident, London Health Sciences Centre, London, ON
2010-2013 Bilingual On-call Crisis Line Worker, Distress Centre Ottawa, Ottawa, ON
2013 Research assistant, Department of Pathology, CHEO, Ottawa, ON
2010-2011 Research assistant, Department of Biochemistry, University of Ottawa, ON
2006-2011 Level 3 Hockey Referee, ODMHA, EOJHL, NCJHL, Embrun, ON
2007-2010 Science Store Clerk, University of Ottawa Faculty of Science, Ottawa, ON
2004-2007 Assistant Golf Professional, Casselview Golf & Country Club, Casselman, ON

MEMBERSHIPS & AFFILIATIONS

2018 – SSO – Society of Surgical Oncology
2018 – CSSO – Canadian Society of Surgical Oncology
2017 – ACS – American College of Surgeons
2016 – OAGS – Ontario Association of General Surgeons
2015 – CATS – Canadian Association of Thoracic Surgeons

2015 – PARO – Professional Association of Residents of Ontario
2015 – TAC – Trauma Association of Canada
2015 – CHS – Canadian Hernia Society
2013 – CAGS – Canadian Association of General Surgeons
2011 – OMA – Ontario Medical Association & CMA – Canadian Medical Association

SELECT CONFERENCES

2020 General Surgery Research Day (GSRD) 2020, Ottawa, ON
2019 Ottawa Hospital (OHRI) Research Day 2019, Ottawa, ON
2019 Canadian Surgery Forum (CSF) 2019, Montreal, QC
2019 Collin's Surgical Research Day 2019, Ottawa, ON
2019 General Surgery Research Day (GSRD) 2019, Ottawa, ON
2018 Nanoscale Flow Cytometry for Cancer, Infection and Disease, Ottawa, ON
2018 Canadian Surgery Forum (CSF) 2018, St. John's, NF
2018 Collin's Surgical Research Day 2018, Ottawa, ON
2018 Canadian Society of Surgical Oncology (CSSO) 2018 Meeting, Toronto, ON
2018 General Surgery Annual Research Day (GSRD) 2018, Ottawa, ON
2018 Society of Surgical Oncology (SSO) 2018 Annual Conference, Chicago, IL

PROFESSIONAL DEVELOPMENT AND TRAINING

2018 Good Clinical Practice (GCP), OHRI, Ottawa, ON
2018 Flow Cytometry Training, Flow Core Facility, University of Ottawa, Ottawa, ON
2018 ACVS Animal Training, University of Ottawa, Ottawa, ON
2017 Laboratory and Safety Training, OHRI, Ottawa, ON
2016 Advanced Trauma Life Support (ATLS), University of Ottawa, ON
2016 Neonatal Resuscitation Program (NRP), Western University, ON
2014 Advanced Cardiac Life Support (ACLS), University of Ottawa, ON
2013 Clinical Research Course, Ottawa Hospital Research Institute (OHRI), Ottawa, ON
2012 TPCS-2 CORE: Ethics Course for Research Involving Humans, Ottawa, ON
2010 60-Hour Intensive Crisis Intervention Skills Training, Distress Centre, Ottawa, ON
2010 Applied Suicide Intervention Skills Training (ASIST), Distress Centre, Ottawa ON

LANGUAGES

French and English – fluently spoken and written